

UNCLASSIFIED

AD

427277

DEFENSE DOCUMENTATION CENTER

FOR

SCIENTIFIC AND TECHNICAL INFORMATION

CAMERON STATION, ALEXANDRIA, VIRGINIA



UNCLASSIFIED

NOTICE: When government or other drawings, specifications or other data are used for any purpose other than in connection with a definitely related government procurement operation, the U. S. Government thereby incurs no responsibility, nor any obligation whatsoever; and the fact that the Government may have formulated, furnished, or in any way supplied the said drawings, specifications, or other data is not to be regarded by implication or otherwise as in any manner licensing the holder or any other person or corporation, or conveying any rights or permission to manufacture, use or sell any patented invention that may in any way be related thereto.

AD No. ~~427277~~ 427277

DDC FILE COPY.

427277

#9.10

⑤ 127300

✓ 64-7

①

NP-13463

BOEING



DDC

JAN 22 1964

TISIA A

SEATTLE, WASHINGTON

5 127300

BOEING AIRPLANE COMPANY
SEATTLE 14, WASHINGTON

NP-13463

14 Document no ✓

6 TEST NO T2/2128

UNCLASSIFIED TITLE October, 1960, Godiva III

Minuteman Radiation Effects Tests,

MODEL NO WS-133A 15 CONTRACT NO AF 04(647)-289

ISSUE NO _____ ISSUED TO _____

CLASSIFIED TITLE _____
(STATE CLASSIFICATION)

AI

5-78105

2-7640-0

58089

WORK ORDER NO.

UNIT NO

ITEM NO

SPECIAL LIMITATIONS ON ASTIA DISTRIBUTION

ASTIA may distribute this report to requesting agencies subject to their security agreement, approved fields of interest, and the following:

UNLIMITED—To all agencies of the Department of Defense and their contractors.

LIMITED—To U. S. Military organizations only.

This report may be distributed to nonmilitary agencies not approved above subject to BAC approval of each request.

NOTE: The LIMITED category may be checked only because of actual or potential patent, proprietary, ethical, or similar implications.

Test

Conducted By H. B. Almond
H. B. Almond

Report

Prepared By H. J. Lubatti and H. W. Wicklein 12/30/60

TEST

CONDUCTED BY H. J. Lubatti
H. J. Lubatti

REPORT

PREPARED BY H. W. Wicklein 12/30/60

H. W. Wicklein 12/30/60
H. W. Wicklein

SUPERVISED BY

G. J. Keister 12/30/60

WITNESSED BY H. B. Almond 12/30/60
H. B. Almond

APPROVED BY

D. A. Hicks 12/30/60

CLASS & DISTR

APPROVED BY D. A. Hicks 12/30/60

(DATE)

(DATE)

NO. OF PAGES 105 (EXCLUDING TITLE AND REVISION AND ADDITION PAGES)

MODEL **WB-133A**

DOCUMENT NO. **T2-2128** ⁴⁴

TITLE **October, 1960, Godiva III Minuteman Radiation Effects Tests** ¹²

REVISIONS				ADDITIONS			
PAGE	DATE	PAGE	DATE	PAGE	DATE	PAGE	DATE
1	8/1/62						
53	8/1/62						
54	8/1/62						

FROM MS 45:60

TO: MS

ABSTRACT

Transient radiation effects tests on silicon controlled rectifiers, associated Minuteman circuits, and tantalum and aluminum electrolytic capacitors were performed at the Godiva III prompt critical assembly, Los Alamos, New Mexico, on Oct. 27 and 28, 1960. Fourteen out of 31 SCR's exhibited firing at gamma radiation rates between 6×10^5 ^A and 3×10^6 ^B r/sec. The gamma-induced SCR leakage current at firing generally exceeded twice the initial holding current of the device. A possible method for predicting gamma rates for firing SCR's is indicated. An empirical relationship for dependence of SCR leakage current (I_c in amperes) on gamma rate ($\dot{\phi}$ in r/sec) was determined, as $I_c = (6 \pm 3) \times 10^{-10}$ ^C $\dot{\phi}^{1.2 \pm 0.1}$ ^D. Leakage resistance change factors ($\frac{R - R_0}{R_0}$) as low as 3.6×10^{-8} ^E and 2.6×10^{-7} ^F for tantalum and aluminum electrolytic capacitors, respectively, were noted at gamma radiation rates up to 4.5×10^7 ^G r/sec. A relationship between capacitor leakage resistance (R in ohms), capacitance (C in farads), and gamma radiation rate ($\dot{\phi}$ in r/sec) was determined at $R = G/\dot{\phi}C$, where $C = 2.1 \times 10^5$ ^A for aluminum foil capacitors, 3.29×10^5 ^A for tantalum foil capacitors, and 1.81×10^5 ^A for tantalum solid electrolyte capacitors. This relationship does not apply for tantalum capacitors at times past the peak intensity of a radiation pulse due to long-time decay relationships which were determined. Charge generation effects due to gamma radiation were observed and interpreted for coaxial cables and uncharged capacitors.

- A 10 to the 5th power
- B 10 to the 6th power
- C 10 to the minus 10 power
- D ϕ to the 1.2 plus or minus 0.1 power
- E 10 to the minus 8 power
- F 10 to the minus 7 power
- G 10 to the 7th power

TABLE OF CONTENTS

	<u>PAGE</u>
ABSTRACT	1
NOMENCLATURE	6
PURPOSE	10
FACILITY	11
DOSIMETRY	12
TEST LAYOUT AND PROCEDURE	18
SCR AND CIRCUIT TEST	23
TEST SPECIMENS	23
TEST EQUIPMENT AND PROCEDURES	29
DATA ANALYSIS AND RESULTS	35
DISCUSSION OF RESULTS	49
CONCLUSIONS	54
RECOMMENDATIONS	55
CAPACITOR TESTS	56
TEST SPECIMENS	56
TEST EQUIPMENT AND PROCEDURES	59
DATA ANALYSIS AND RESULTS	67
Capacitance Test Results	67
Cable Test Results	67
Capacitor EMF Test Results	71
Leakage Test Analysis and Results	76
Permanent Effects Measurements	89
DISCUSSION OF RESULTS	89
Capacitor Leakage Tests	89
Cable Tests	93
Capacitor EMF Tests	95
CONCLUSIONS	99
RECOMMENDATIONS	102
ACKNOWLEDGMENTS	103
REFERENCES	104



LIST OF FIGURES

FIGURE	TITLE	PAGE
1	Representative Dosimetry Time Response (0-500 μ s)	13
2	Representative Dosimetry Time Response (500 μ s-100 μ s)	14
3	Equipment Layout at Kiva II	19
4	Test Specimen Mounting Arrangement	20
5	Squib Driver Circuit	24
6	SCR Power Buffer Amplifier Circuit	25
7	Block Diagram of Circuit Test Boards	26
8	Circuit Layout (Type A)	27
9	Cable Test Circuit Boards	28
10	SCR Device Test Box	30
11	Block Diagram of Circuit Test Instrumentation	32
12	Block Diagram of Device Test Instrumentation	33
13	SCR Gating Circuit used in Device Tests	33
14	General Type of Oscilloscope Traces for SCR Tests	41
15	Leakage Current vs Gamma Rate up to "Turn On"	44
16	Leakage Current vs Gamma Rate up to "Turn On"	45
17	Effect of Permanent Damage on Induced Leakage Current	46
18	Leakage Current at "Turn On" vs Holding Current	51
19	Typical Capacitor Test Specimens	58
20	Circuitry for Capacitor Test A - Leakage	60
21	Circuitry for Capacitor Test B-EMF	60
22	Circuitry for Capacitor Test C-Capacitance Change	62
23	Typical Capacitance Test Data	68
24	Typical Cable EMF Data	69
25	Rate Dependence of Generated Cable Current	72

LIST OF FIGURES (Continued)

FIGURE	TITLE	PAGE
26	Capacitor EMF Data	69
27	EMF Tests - Capacitor Charge vs Gamma Dose (to 300 μ s)	73
28	EMF Tests - Charging Current vs Gamma Rate	74
29	EMF Tests - Time Response After 200 μ s	75
30	Typical Capacitor Leakage Data	77
31	Rate Dependence of Conductivity for Aluminum Oxide (Al_2O_3)	81
32	Comparison of Conductivity and Gamma Rate Pulses for Tantalum Oxide	84
33	Breakdown of Conductivity for Tantalum Oxide (0-130 μ s)	87
34	Breakdown of Conductivity for Tantalum Oxide (130-510 μ s)	88



LIST OF TABLES

TABLE	TITLE	PAGE
I	Representative Godiva III Burst Characteristics	17
II	Summary of Device Tests	34
III	Summary of Circuit Tests	36
IV	Tabulation of Critical Parameters for SCR's used in Device and Circuit Tests	37
V	Results of Circuit Tests	42
VI	Gamma Rate and Integrated Neutron Flux at "Turn on" and "Turn Off"	47
VII	Effect of Permanent Neutron Damage on SCR Gamma Induced Leakage Current	48
VIII	Capacitor Test Parts	57
IX	Summary of Capacitor Tests	65
X	Capacitance Test Results	70
XI	Leakage Test Results for Aluminum Foil Electrolytic Capacitors	79
XII	Leakage Test Results for Tantalum Electrolytic Capacitors	80
XIII	Geometry and Relative Dosimetry Distribution for Aluminum Foil Capacitors	83

NOMENCLATURE

<u>Symbol</u>	<u>Definition</u>
Al	<u>Aluminum.</u>
C	<u>Capacitance value (farads).</u> <u>Dosimeter</u> - device used for measuring nuclear radiation dose, i.e., used in <u>dosimetry</u> .
E	<u>Particle energy (Kev or Mev).</u>
EMF	<u>Electromotive force</u> - used in this report to indicate voltage or current generation by nuclear radiation.
G	<u>Constant</u> $\left[\frac{(\text{farad})(r)(\text{ohm})}{\text{sec}} \right]$ - used in description of leakage resistance variation with gamma rate.
h	<u>Height (volts)</u> of radiation intensity dosimetry curves.
I_c	<u>SCR gamma-induced leakage current (ma or amp).</u>
I_g	<u>SCR gate current (ma)</u> - value of current flowing between gate and cathode.
I_H	<u>SCR holding current (ma)</u> - value of the anode-cathode current below which the SCR "turns off."
k	<u>Dielectric constant</u>
K	<u>Rate-dependence generation constant</u> $\left[\frac{\text{sec}}{(r)(\Omega - \text{cm})} \right]$ - i.e., multiplier of gamma rate in expression for radiation-induced dielectric conductivity.
K_α, K_β	<u>Rate-dependence generation constants</u> $\left[\frac{\text{sec}}{(r)(\Omega - \text{cm})} \right]$ for α and β components of tantalum oxide conductivity.
K'_α, K'_β	<u>Dose-dependence generation constant</u> $\left[(r)(\Omega - \text{cm}) \right]^{-1}$ for α and β components of tantalum oxide conductivity - i.e., multiplier of gamma dose in expression for radiation-induced dielectric conductivity.
Kev	<u>Particle energy unit</u> - thousands of electron volts; 1 Mev = 1.603×10^{-9} erg.

<u>Symbol</u>	<u>Definition</u>
Mev	<u>Particle energy unit</u> - millions of electron volts; 1 Mev = 1.603×10^{-6} erg.
	<u>Mozs spectrum</u> - an accepted energy distribution for gamma radiation produced by nuclear fission.
	<u>Permanent radiation effect</u> - any radiation effect which remains permanently after the radiation field is removed. In a broad sense, this term includes any effects which arise indirectly from a transient radiation pulse (i.e., breakdown or burn-out caused by a momentary transient radiation effect) and remain after irradiation; such effects might be termed <u>transient-induced permanent effects</u> .
Pol.	<u>Polarized</u> .
Pu nt	<u>Plutonium neutrons</u> - neutrons whose energies are greater than 4 Kev.
rad	<u>Radiation dose unit</u> - the amount of incident nuclear radiation which is required to deposit 100 ergs of energy per gram of material. This amount of radiation is dependent on type of material, type of radiation and energy spectrum of radiation.
r	<u>Roentgen</u> - a unit of radiation dose which represents the amount of incident X or gamma radiation required to produce one electrostatic unit of electricity, of either sign, (i.e., 2.08×10^{19} ion-pairs) in 1 cc of dry air at 0° C and standard atmospheric pressure.
$1/r^2$	<u>Dependence of radiation intensity on the inverse square of distance from a point source (or the equivalent of a point source)</u> . In this case r represents the distance from the point source to the point where radiation intensity is taken.
R	<u>Capacitor leakage resistance (ohms)</u> except when appearing in figures.
R	<u>Roentgen</u> - unit for radiation dose (i.e., r) in figures only.
$R_{min.}$	<u>Minimum capacitor leakage resistance (ohms)</u> observed during radiation burst.
R_0	<u>Capacitor leakage resistance (ohms)</u> before irradiation.
SCR	<u>Silicon controlled rectifier</u> .
S nt	<u>Sulfur neutrons</u> - neutrons whose energies are greater than 2.5 Mev.

SymbolDefinition

t	<u>Time (sec or μs).</u>
t_p	<u>Time at maximum intensity of radiation burst (μs).</u>
$\Delta t_{1/2}$	<u>Time interval (μs) between half-maximum points of radiation burst.</u>
ΔT	<u>Temperature rise ($^{\circ}$C) of fissionable material during burst.</u>
T_0	<u>Temperature ($^{\circ}$C) of fissionable material at beginning of burst.</u>
Ta	<u>Tantalum.</u>
	<u>Transient radiation effect</u> - any radiation effect which disappears within a limited time (i.e., seconds to minutes) after the radiation field is removed. Many transient radiation effects depend entirely on radiation rate and disappear immediately when the radiation is removed; such effects might be termed <u>rate effects</u> .
v	<u>Voltage change (mv) across capacitor during radiation burst.</u>
V_{BO}	<u>SCR breakover voltage (volts)</u> - The value of positive anode voltage at which a controlled rectifier switches into the conductive state with the gate circuit open.
α, β	<u>Exponential decay constants (sec^{-1})</u> for the decay of the very-rapidly-decaying and "slowly"-decaying portions of tantalum oxide gamma-induced conductivity, respectively.
γ	<u>Gamma radiation.</u>
ϵ_0	<u>Electrical permittivity of vacuum</u> = 8.85×10^{-14} farad/cm.
σ	<u>Electrical conductivity</u> [$(\text{ohm} - \text{cm})^{-1}$].
$\sigma_{\alpha}, \sigma_{\beta}$	<u>Electrical conductivity</u> [$(\text{ohm} - \text{cm})^{-1}$] for large and small components of tantalum oxide conductivity, respectively.
$\dot{\sigma}$	<u>Time rate of change of conductivity</u> [$(\text{ohm} - \text{cm})^{-1} (\text{sec})^{-1}$] = $d\sigma/dt$.
$T_{1/2}$	<u>Half-life (μs)</u> - time required for σ_{β} to decay to half of its initial value.
\int	<u>Total (or integrated) gamma dose (r)</u> - time integral of gamma rate during a radiation burst.
\int_0^t	<u>Integrated gamma dose (r)</u> from times 0 to t.
\int	<u>Total (or integrated) neutron flux (neutrons/cm²)</u> - total number of neutrons passing through a unit cross-sectional area of material during irradiation.

SymbolDefinition \int_t^N Integrated neutron flux (nt/cm²) from times 0 to t. $\int_t^N(t_o)$ Integrated neutron flux (nt/cm²) at SCR "turn on." $\int_t^N(t_o)$ Integrated neutron flux (nt/cm²) at SCR "turn off." $\dot{\gamma}$ Gamma radiation rate (r/sec) - the amount of gamma radiation incident upon a material per unit time, i.e., $\frac{d\phi}{dt}$. $\dot{\gamma}(b.o)$ Gamma radiation rate (r/sec) at SCR "turn on." $\dot{\gamma}_p$ Maximum gamma radiation rate (r/sec) during burst. $\dot{\gamma}(t_o)$ Gamma radiation rate (r/sec) at SCR "turn off."

PURPOSE

This report describes tests performed at the Godiva III prompt critical assembly on October 27 to 28, 1960. The purpose of these tests was to obtain data on the effect of short duration pulse of gamma radiation on silicon controlled rectifiers, Minuteman squib and relay driver circuits, tantalum solid electrolytic capacitors, and tantalum and aluminum foil electrolytic capacitors; the tests were designed to provide a maximum amount of data which would be useful in determining the effect of a gamma radiation pulse on Minuteman ground electronic systems.

FACILITY

The Godiva III prompt critical assembly is located in Kiva II at the Parajito Site of Los Alamos Scientific Laboratories. Coordination and operation of the facility for radiation effects testing by Department of Defense contractors is accomplished by Sandia Corporation personnel.

Godiva III provides the following transient nuclear radiation environment for each burst at the point of closest experimental approach (Ref. 1):

1. 2×10^{13} fast neutrons/cm² (neutron energy > 1 Kev)
2. 2×10^{17} fast neutrons/cm²-sec at peak intensity
3. 2000 to 5000 rads (water) of gamma radiation
4. 2 to 5×10^7 rads/sec gamma at peak intensity
5. An approximate Gaussian distribution of radiation intensity vs time with a minimum pulse width of 60 μ s at half intensity
6. Godiva III has a leakage neutron spectrum with slightly lower energies than a U₂₃₅ fission spectrum; the gamma spectrum is considered to be a Motz spectrum

Additional description concerning Godiva III is provided in References 1 and 2.

DOSIMETRY

The dosimetry required for the October 27 to 28 test series was:

1. Gamma radiation rate vs time
2. Integrated neutron flux and gamma dose vs time

The following measurements were required in order to provide this information:

1. Radiation intensity vs time during the radiation burst (i.e., pulse shape)
2. Total gamma radiation dose
3. Total neutron flux

Pulse shape information was taken by International Business Machines Corp. personnel who were utilizing half of the Godiva III facility during the October 27 to 28 tests. IBM recorded the output of a large plastic scintillator and phototube which were located near Godiva III. Three oscilloscope photographs were taken during each burst; these photographs show the radiation intensity variation during the time intervals 0 to 500 μ s, 500 μ s to 5 ms and 5 ms to 100 ms (Ref. 3 and 4). Figures 1 and 2 show a typical set of the oscilloscope traces.

Total gamma dose was measured by chemical dosimeters which were placed at the test specimen locations where gamma rate data were required. These dosimeters were purchased from Edgerton, Germeshausen and Grier, Inc. and were returned to them for reading after the radiation exposure. No correction was made for the relatively small contribution from thermal neutrons. The calibration of the chemical dosimeters is based on an ionization chamber calibrated for Co^{60} gamma radiation.

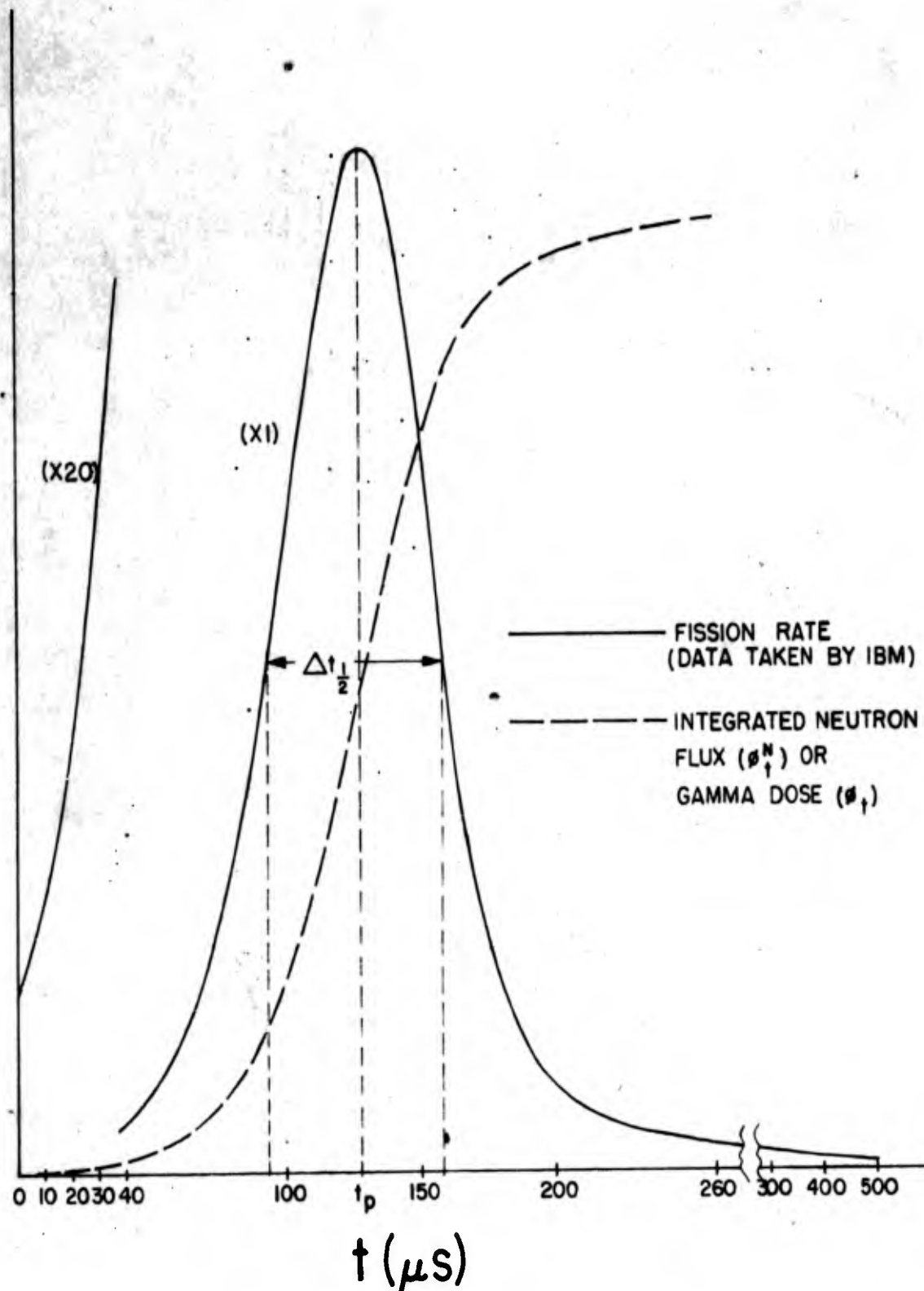


FIGURE 1
 REPRESENTATIVE DOSIMETRY TIME RESPONSE
 (0-500 μs)

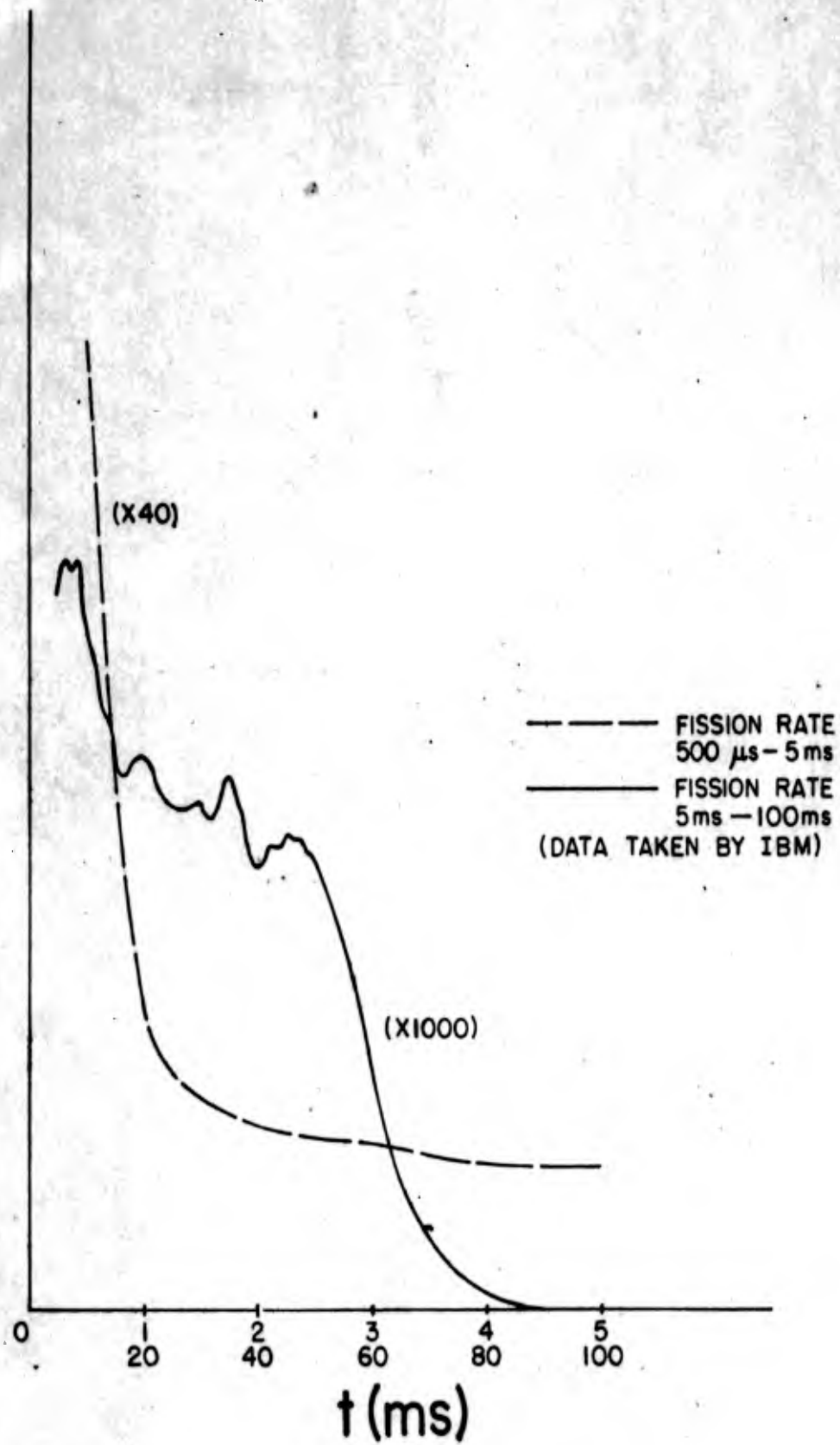


FIGURE 2

REPRESENTATIVE DOSIMETRY TIME RESPONSE (500 μ s-100ms)

Total neutron flux was measured by exposing sulfur pellets (cylinders 1/4 inch high by 1/2 inch diameter) at the test specimen positions. Induced phosphorus beta activity, produced by the $S^{32}(n,p)P^{32}$ reaction for neutrons of energy > 2.5 Mev, was counted with calibrated equipment in the Radiation Effects Laboratory at Boeing. Results are presented in Reference 5. Details of this procedure are given in Reference 6. The sulfur integrated neutron flux ($E > 2.5$ Mev) was converted to a total (plutonium) neutron flux ($E > 4$ Kev) using a multiplication factor of 5.4 (Ref. 7). Appreciable variations may result from neutron scattering by experimental equipment (Ref. 8).

Gamma radiation rates were obtained by the following procedure:

1. Graphical integration of the pulse shape curves obtained from IBM (0 to 100 ms)
2. Application of the relationship:

$$\dot{\phi} = \frac{0.7 \phi h}{\sum_0^{100 \text{ ms}} h \Delta t}$$

where: $\dot{\phi}$ = gamma rate at time t.

h = height of pulse shape curve at time t.

ϕ = total gamma dose received during the radiation burst and until ~20 minutes after the burst when the gamma dosimeters could be removed from the test position.

The factor 0.7 represents the portion of the total recorded gamma dose which occurs during the time interval 0 to 100 ms (Ref. 9). This factor was determined by IBM "mousetrap" experiments as described in References 3 and 4. Zero time occurs when the scintillator pulse height reaches the level required to cause operation of IBM's oscilloscope triggering system. A negligible fraction of the total dose arrives before this time.

Neutron integrated flux or gamma dose vs time were obtained from the following relationship:

$$\phi_t^N \text{ (or } \phi_t) = \phi^N \text{ (or } 0.7 \phi) \frac{\sum_0^t h \Delta t}{100 \text{ ms} \sum_0 h \Delta t}$$

where: ϕ_t^N = integrated neutron flux from times 0 to t.
 ϕ^N = total neutron flux determined from sulfur pellets.
 ϕ_t = gamma dose from times 0 to t.

Greater than 99 percent of the total neutron dose is received in the prompt pulse (Ref. 10). A representative integrated neutron flux or gamma dose curve is given in Figure 1.

Table 1 shows representative characteristics of the thirteen radiation bursts obtained during the two days of testing. Chemical and sulfur dosimeters used in these tests were mounted in the same horizontal plane and at the same radius as the test specimens, insofar as possible. Dosimeters were potted with the test specimens in order to provide similar shielding conditions.

TABLE I

Representative Godiva III Burst Characteristics

Burst No.	$\frac{T_0}{(o_G)}$	$\frac{T}{(o_G)}$	$\frac{t_p}{(\mu s)}$	$\frac{t_{1/2}}{(\mu s)}$	$\dot{\phi}_P^*$ (r/sec x 10^{-7})	ϕ^N (Pu Nt/cm ² x 10^{-12})
1	15.8	83.1	130	66	3.8	9.9
2	17.1	67.9	158	89	1.9	9.1
3	18.2	85.8	131	64	4.3	12.3
4	19.2	84.0	131	63	3.7	11.3
5	19.1	83.9	129	63	4.0	12.2
6	20.4	77.6	132	68	3.7	8.6
7	16.9	82.2	125	62	4.5	11.7
8	19.1	81.5	127	63	4.0	9.5
9	19.1	82.8	128	68	2.7	10.6
10	19.6	71.4	138	75	2.5	8.0
11	**20.0	78.3	(132)	(68)	(3.7)	9.6
12	20.8	80.0	125	65	3.2	9.5
13	18.5	80.4	129	68	2.9	10.6

* Values for position 5/8" from screen.

** The pulse shape for burst 11 was not available. Burst 6 was used as an approximation, since the ΔT 's were nearly equal.

TEST LAYOUT AND PROCEDURES

The test layout and procedures used in the October 27 to 28 radiation effects tests were designed to provide a maximum amount of useful data. Tests were expedited by:

1. Mounting of specimens on a retractable trolley in order to permit specimen changing in a low radiation field between bursts.
2. Adequate preparation of specimens, circuitry and dosimetry in advance so that a minimum of time was required for specimen changing and circuit adjustments between bursts.
3. Close coordination with IBM (who shared Godiva III) during the test series.

The equipment layout at Kiva II is presented in Figure 3. The specimen mounting trolley (Fig. 4) consisted of a superstructure mounted on a laboratory cart. A spring-loaded boom extended from the superstructure. A curved bracket was provided for mounting capacitor specimens on the boom; the boom was swung out from Godiva III by a rope and pulley arrangement during insertion or retraction of the trolley. Circuit test specimens were mounted on the superstructure next to the screen of Godiva III (position 1), and SCR test specimens were mounted on brackets which were attached to the superstructure at positions 1, 2, and 3 (Fig. 4). The grooved wheels of the specimen trolley rode along a track from Godiva III to the north door of Kiva II. The insertion or retraction of the trolley was accomplished by a rope and pulley arrangement. This method of specimen mounting, with specimen mounting geometry adjusted before the start of the test series, eliminated the need for personnel to enter the Kiva after a radiation burst. This allowed them to work at the north door of the Kiva within twenty minutes after a radiation burst and minimized their exposure to radiation.

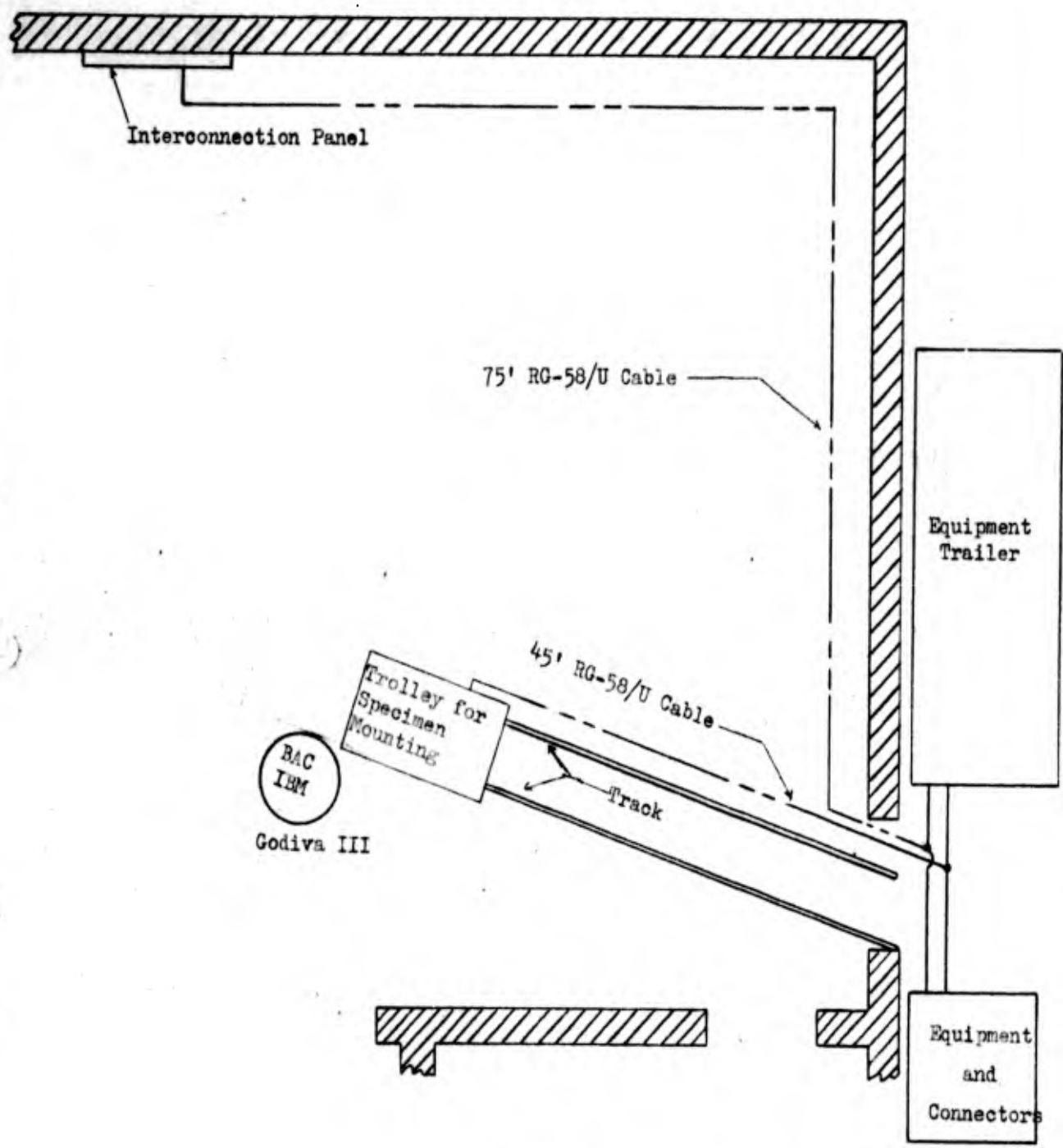


Figure 3
 Equipment Layout at Kiva II

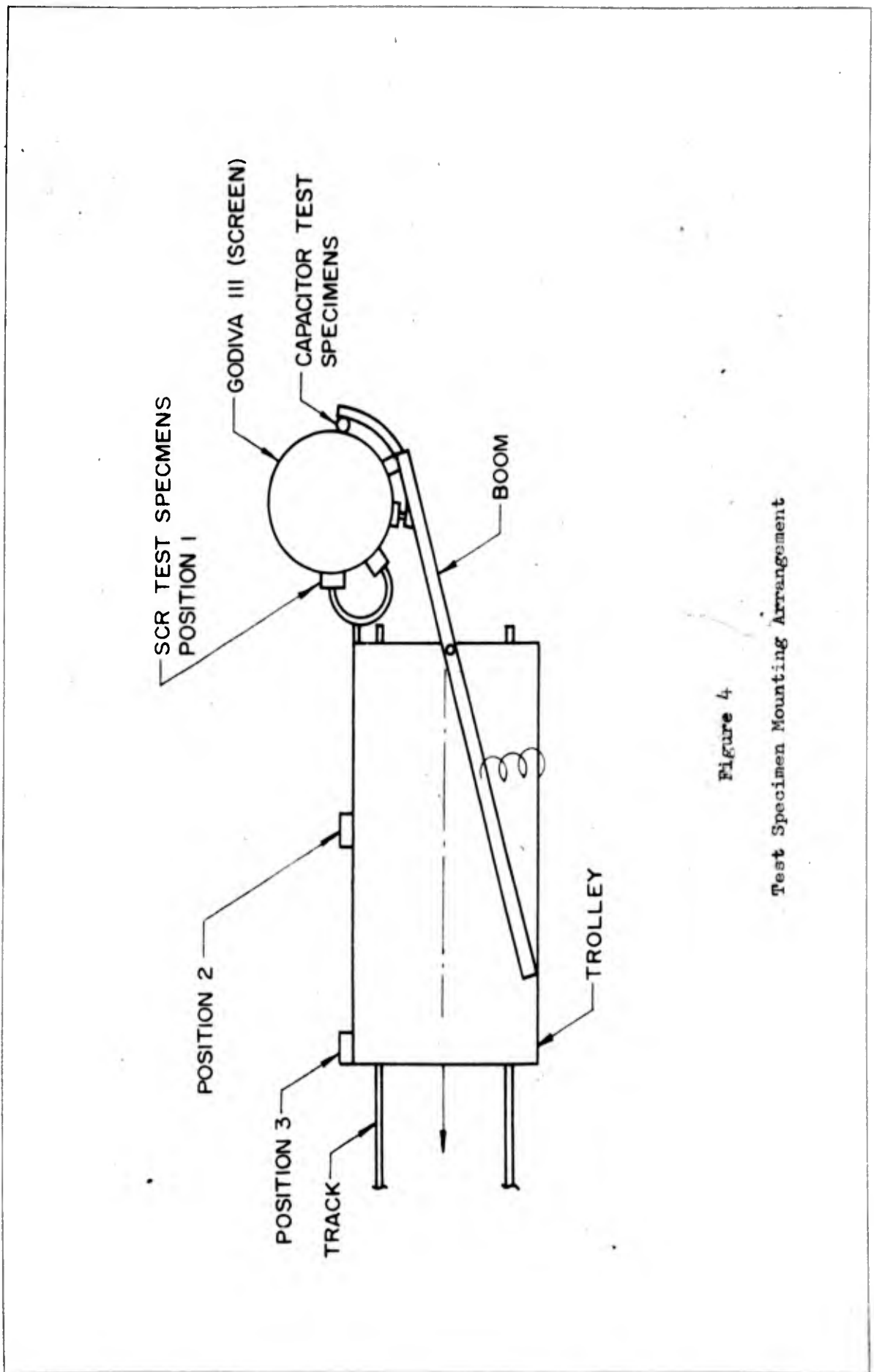


Figure 4
Test Specimen Mounting Arrangement

The 45 foot length of RG-58/U coaxial cable from the door to Godiva III formed an integral part of each test specimen; this portion of the cabling was new for each burst so that any persistent effects in cables were reduced. The 75 foot lengths of RG-58/U cable from the interconnection panel to the door remained throughout the test series but were laid near the Kiva wall so that radiation exposure was minimized. Interconnections between the 75 foot and 45 foot cables were made outside the door, thereby reducing radiation exposure of cable connectors. Battery power and control circuitry used in the SCR and circuit tests were located beside the door and shielded by the Kiva wall. The semi-trailer which was used for transporting equipment and as a portable laboratory was located as shown in Figure 2. Equipment for capacitance measurements was located in the trailer during the second day of testing.

The 75 foot lengths of RG-58/U cable were connected directly to existing 1265 foot lengths of RG-22/U coaxial cable. The RG-22/U cables, with center conductors paralleled, carried test signals back to the control building. The interconnection panel at Kiva II was by-passed in order to reduce ground loop and noise pickup problems. Forty foot lengths of RG-58/U cable were used to complete the signal path from the interconnection panel at the control building to the recording equipment located in the basement of the control building. Signals were displayed on five Tektronix 551 dual beam oscilloscopes and one Tektronix 545 oscilloscope. Recording was done with four Beattie-Coleman and two Dumont polaroid oscilloscope cameras. An oscilloscope and camera were located in the equipment trailer during the second day of tests.

The triggering signal for the oscilloscopes was obtained from IBM in order to provide the same time reference as the dosimetry information. This signal was

carried from IBM's equipment trailer to the oscilloscopes over two 200 foot lengths of RG-58/U cable. Sixty-cycle AC power and control leads were connected between the basement of the control building and Kiva II. In all cases care was taken to isolate connections sufficiently to eliminate ground loops.

Test specimens, in most cases, were completely potted in Silastic RTV. 882 or Silastic RTV 881 in order to reduce the possibility of air ionization effects. In all cases the electrical connections at the test specimens were potted. Dosimeters were potted at suitable locations with the test specimens where possible; this was done in order to provide more realistic dosimetry measurements and to facilitate dosimetry changes between bursts. In most instances the specimen and dosimetry changes between bursts required only a quick disconnect - connect process and minor checks and adjustments.

Six radiation bursts were obtained on October 27 and seven on October 28. The average cycling time was 80 minutes, divided as follows:

<u>Time (Minutes)</u>	<u>Procedure</u>
0	Firing of Godiva III
0 - 20	Study of data; re-check test specimens for next burst
20	Retraction of specimen trolley from Kiva
20 - 35	Specimen and dosimetry mounting in pre-set positions; adjustments and circuit checks at Kiva
35	Insert specimen trolley into Kiva
35 - 79	Oscilloscope and camera adjustment; circuit check and adjustment; check test specimens for next burst
79 - 80	Countdown and firing of Godiva III

SCR AND CIRCUIT TEST

TEST SPECIMENS

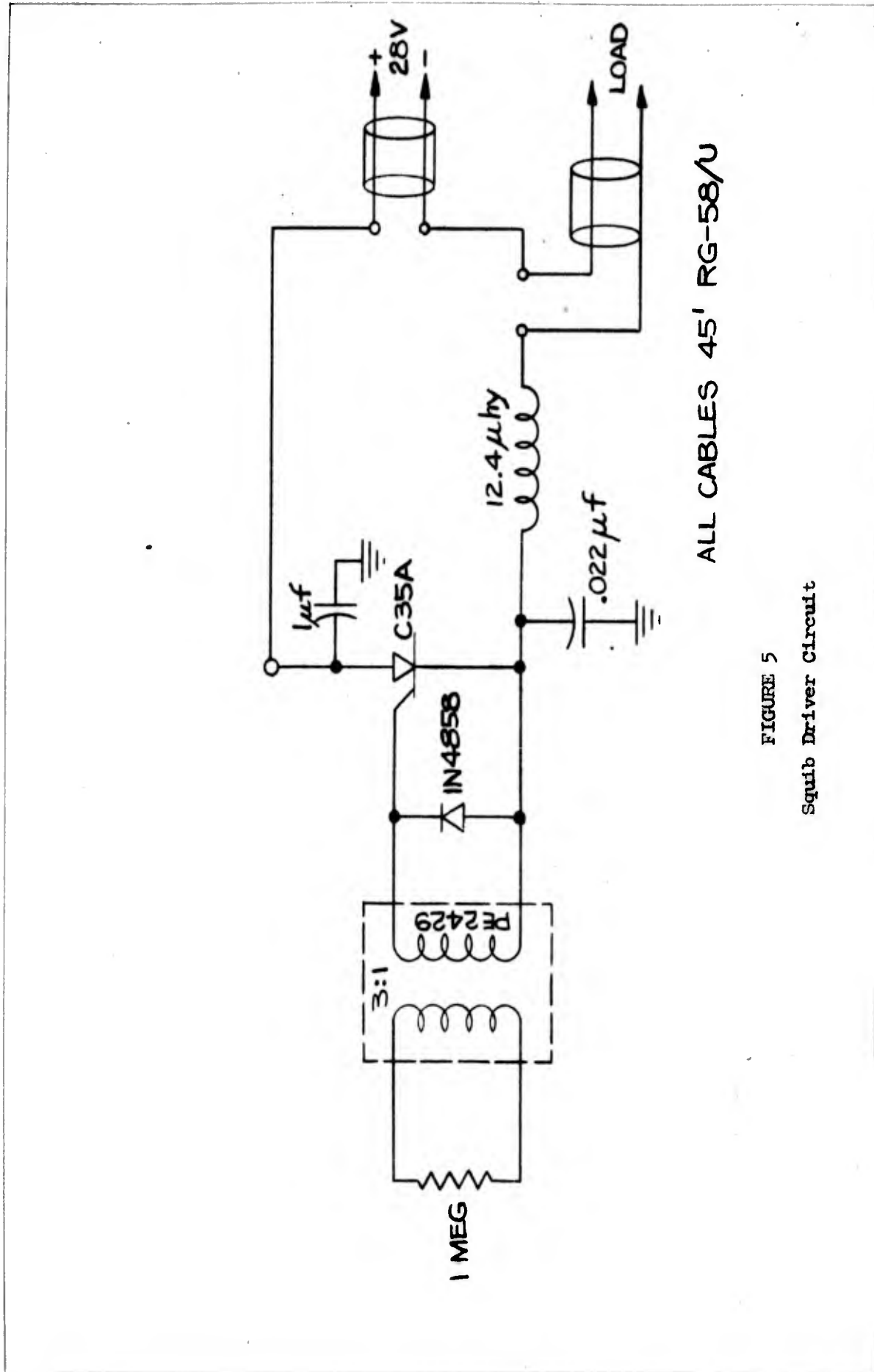
In order to determine the transient effects of gamma radiation on silicon controlled rectifier circuits the following items were tested:

1. The Minuteman squib driver circuit which contains an SCR (Fig. 5), (Ref. 11) - two bursts.
2. The Minuteman SCR power buffer amplifier circuit driving two squib driver circuits (Fig. 6), (Ref. 11). The SCR power buffer amplifier contains a transistor which could have sufficient transient increase in the leakage current during gamma radiation to put the SCR in the squib driver circuit into forward conduction - four bursts.
3. SCR's tested as separate entities in test circuits which would allow the effects of gamma radiation on SCR's to be closely studied - seven bursts.

Three types of circuits were constructed for the circuit tests (1 and 2 above); these circuits are shown in block diagram form in Figure 7. Two each of types A, B, and C circuits (Fig. 8) were constructed by mounting the circuit elements and dosimeters on 6" x 4" x 1/16" phenolic terminal boards in the configuration shown in Figure 8. Forty-five foot lengths of RG-58/U coaxial cable were fastened to terminals at T₁, T₂, T₃, T₄, T₅, T₆ and a ten foot length at T₇ (Fig. 6). Each circuit board was then potted with 1 1/2 inches of Silastic RTV 882 on the front and 3/4 inch on the back. This was done in order to cover all electrical connections which reduces air ionization effects.

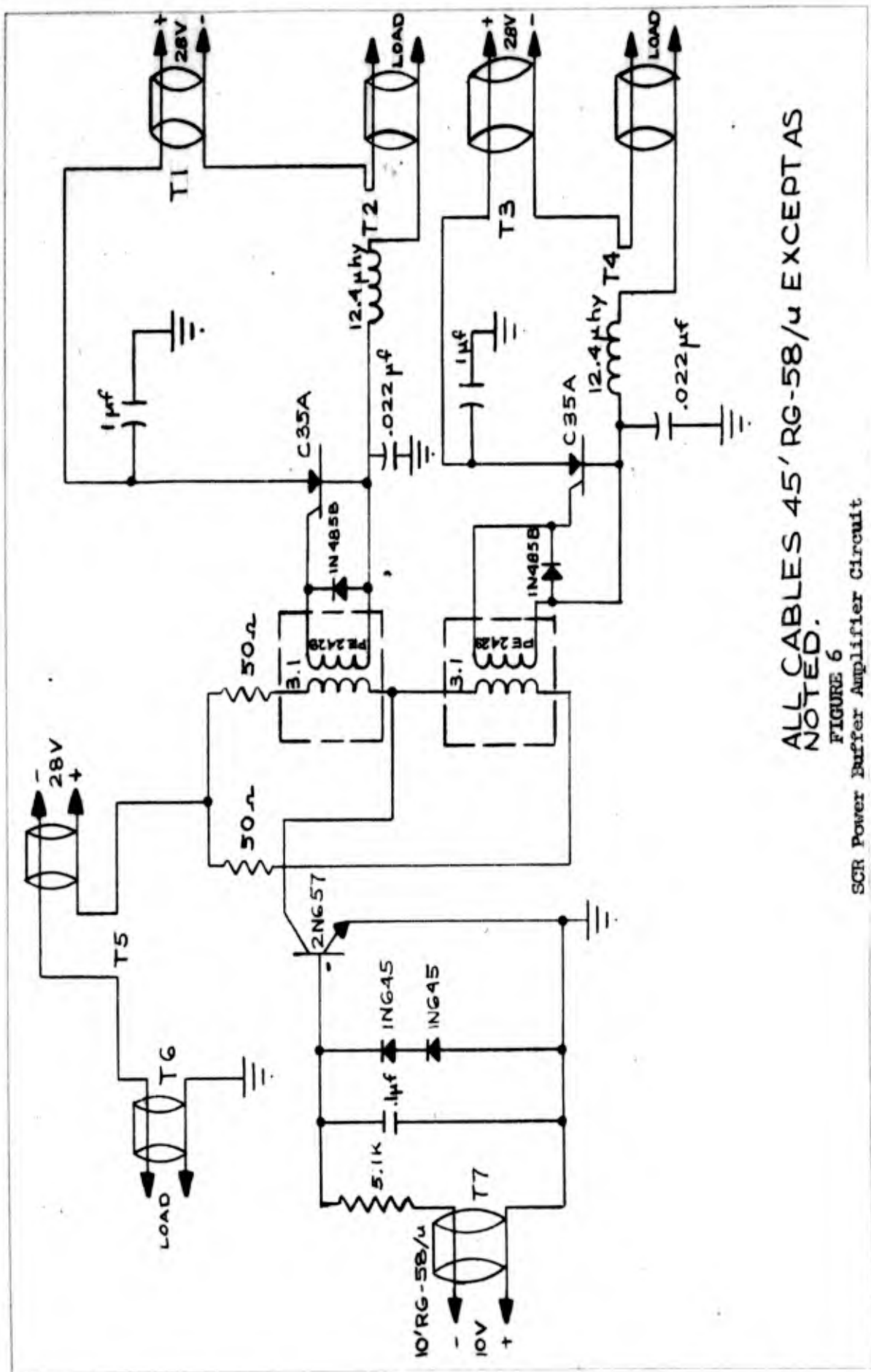
A cable effect test was performed with each circuit test. Three each of the two types of specimen shown in Figure 9 were constructed and potted in Silastic RTV 882 with the same thicknesses used on the circuit boards.

All parts used in the circuit tests except the 1 μ f and .022 μ f capacitors used in the filter were Minuteman standard parts or their commercial equivalents



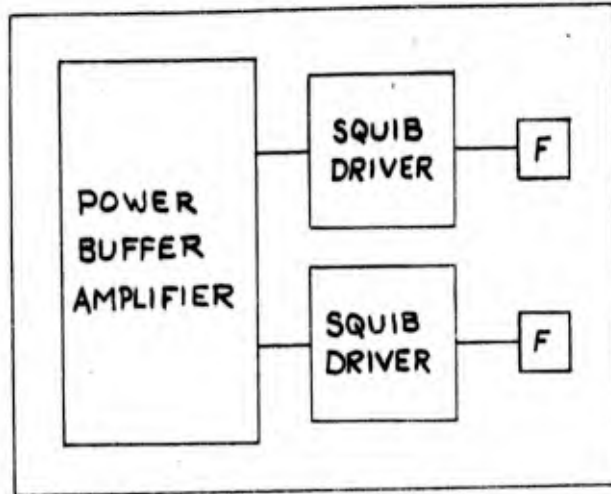
ALL CABLES 45' RG-58/U

FIGURE 5
Squib Driver Circuit



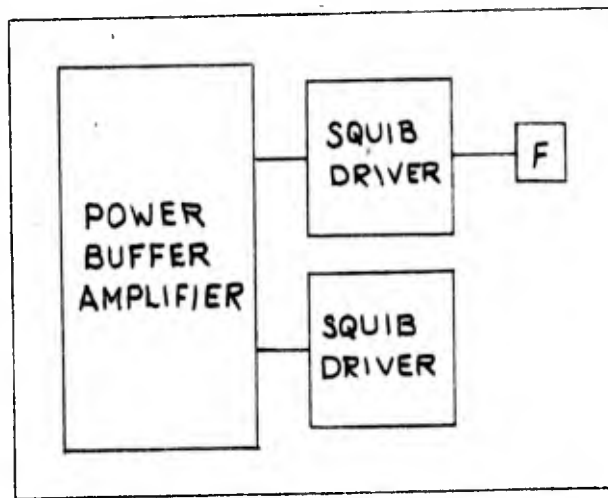
ALL CABLES 45' RG-58/u EXCEPT AS NOTED.

FIGURE 6
SCR Power Buffer Amplifier Circuit



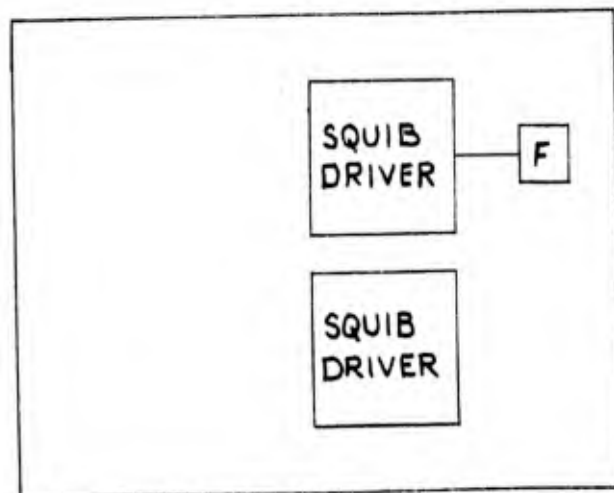
Type A Power buffer amplifier driving two squib drivers, each squib driver has a filter.

TYPE A



Type B: Power Buffer Amplifier driving two squib drivers, only one squib driver has a filter.

TYPE B



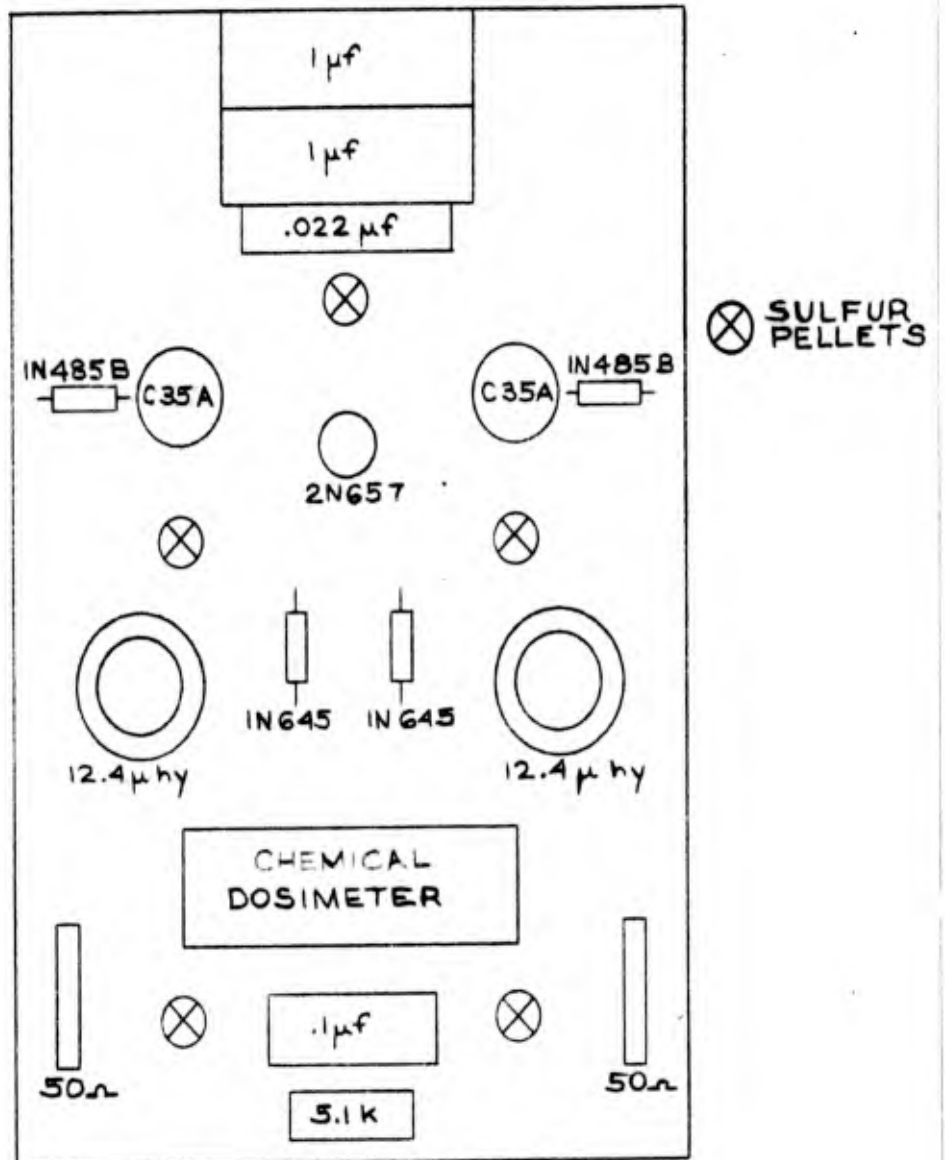
Type C: Two squib drivers; only one squib driver has a filter.

F indicates filter.

TYPE C

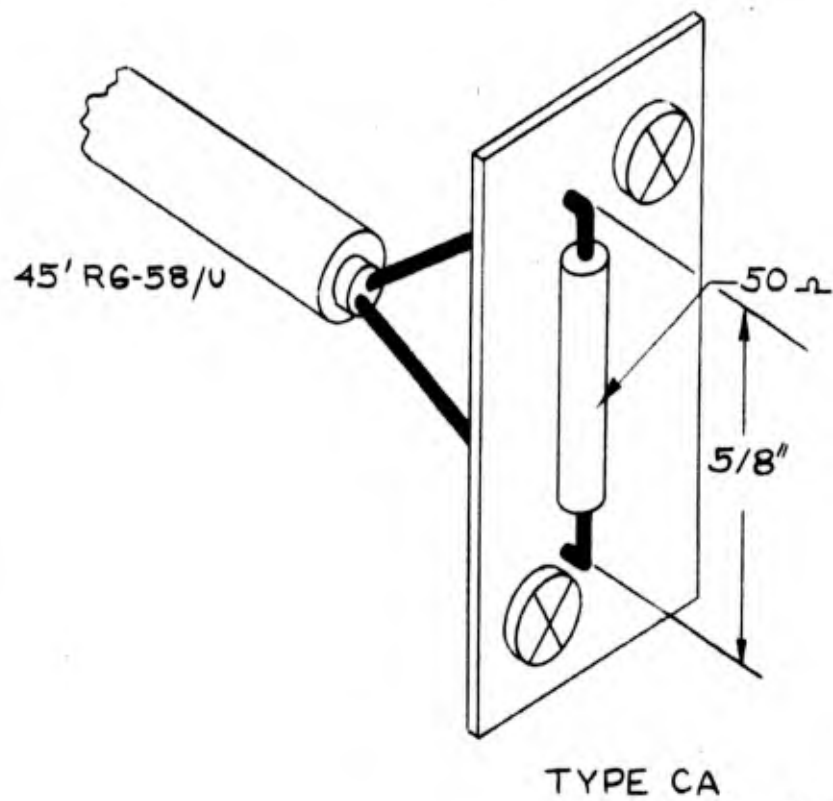
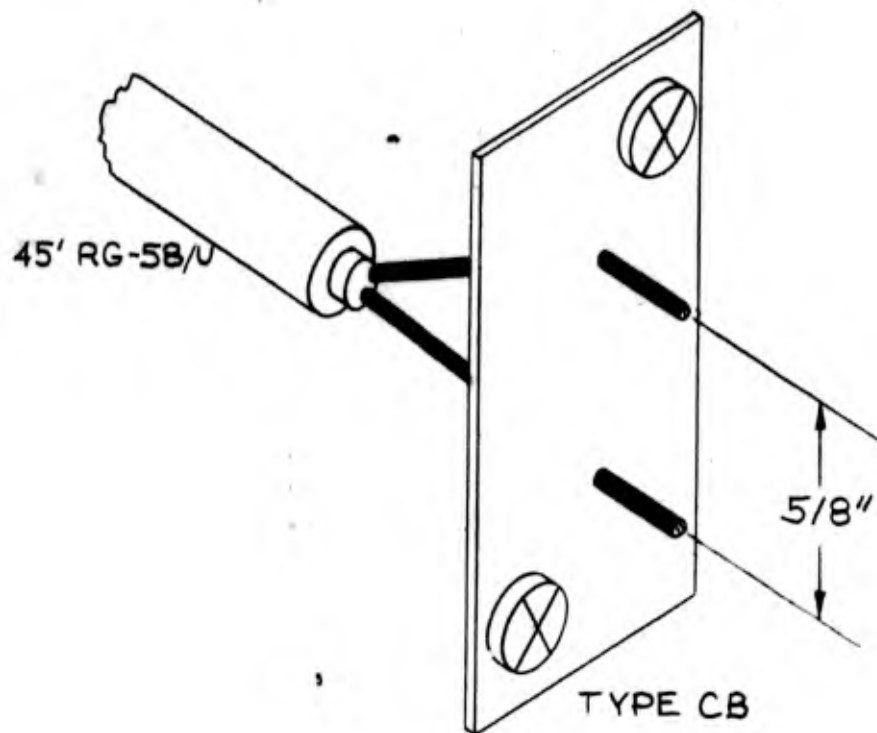
FIGURE 7

Block Diagram of Circuit Test Boards



Type B and C circuits have the same circuit configuration, with the exception that some of the above elements are not present.

FIGURE 8
Circuit Layout (Type A)




 SULFUR PELLETS

FIGURE 9
Cable Test Circuit Boards

(ref. 12). The filter was added to the squib driver circuitry a few days prior to the tests, and there was not sufficient time to obtain Minuteman standard parts. A 1 μ f, 400 VDC Sprague capacitor and a .022 μ f, 400 VDC Cornell Dublier capacitor were used.

All SCR's used in the device tests (Item 3 above) along with their dosimeters were placed in 3" x 3" x 2" aluminum containers as shown in Figure 10. Each can contained two SCR's, two sulfur pellets and one chemical dosimeter. The containers were filled with Silastic RTV 881 in order to cover all electrical connections which reduces air ionization effects. The SCR's used in both the circuit and device tests were manufactured by General Electric Co.

TEST EQUIPMENT AND PROCEDURES

In order to determine transient radiation effects on SCR's, two types of measurements were made:

1. The monitoring of the SCR cathode-anode current during irradiation.
2. The monitoring of transistor leakage current in the Minuteman power buffer amplifier during irradiation.

The first six bursts (Oct. 27) were devoted to circuit tests, and the remaining seven bursts (Oct. 28) to device tests. The tests were divided in this fashion because the mounting of the circuit boards differed from the mounting of the device cans, and unnecessary delays would otherwise result. The procedure followed was to preset and mark the mounting positions before the first burst each day.

In presetting the mounting positions for both the circuit and device tests, care was taken to insure that the SCR's would be vertically aligned with the center of the fissionable material ~~and that both the circuit boards and the cans~~

⊗ SULFUR

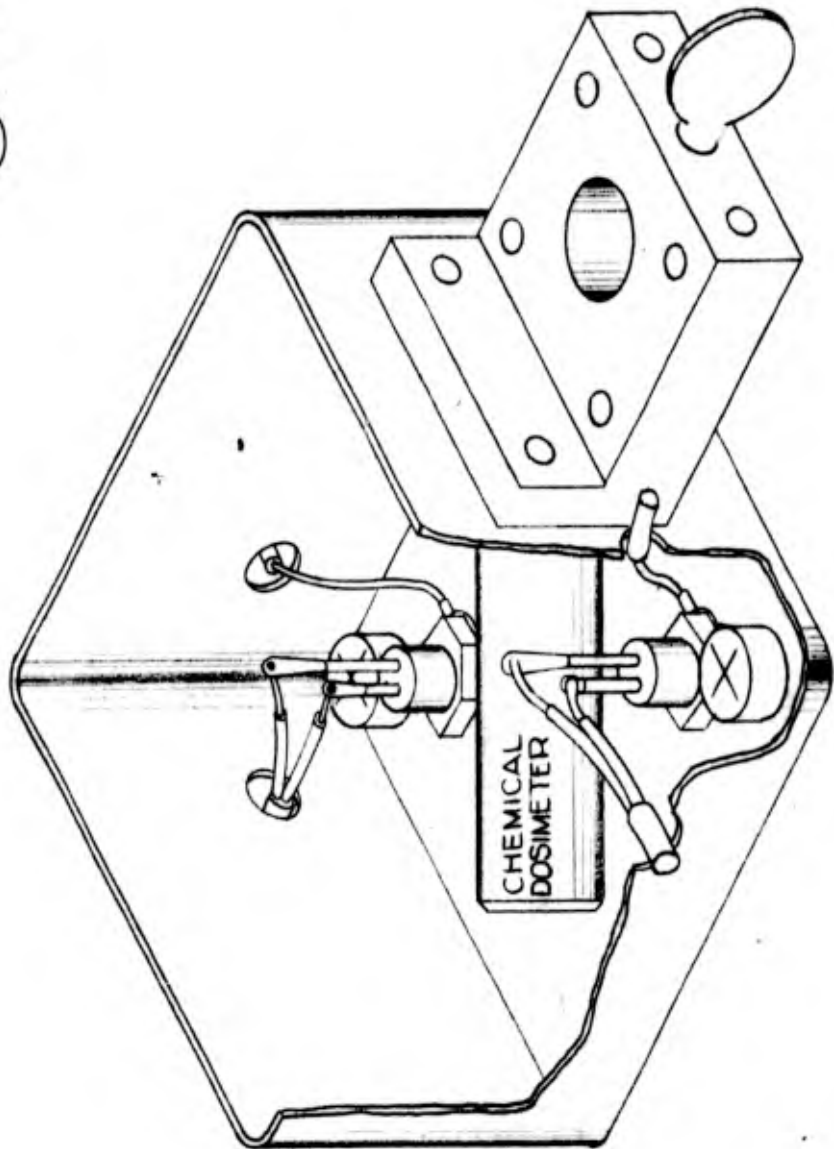


FIGURE 10

SCR Device Test Box

would be facing the protective screen. All circuit boards were mounted as close to the screen as possible. The device cans were placed at three different positions P_1 , P_2 and P_3 (Fig. 4). P_1 , P_2 and P_3 were zero, 20 inches and 60 inches from the screen, respectively. The distances were measured from the screen to the center of the cans and were chosen so that the intensity at P_2 and P_3 would be $1/10$ and $1/100$ of the intensity at the screen, respectively, assuming a $1/r^2$ relationship. Since each test item contained its own chemical dosimeter and sulfur pellets, exact distances from the screen were not important.

Figures 11 and 12 show in block diagram form the test setup from the Kiva which housed Godiva III to the control building where the oscilloscopes were placed. All leads coming out of the Kiva, all all loads and bias voltages with exception of a 10 volt supply (Fig. 11) were applied through a control box which was placed next to the Kiva door and was shielded by the Kiva wall. The control box also contained the SCR gating circuit shown in Figure 13. This circuit supplied gate bias during device tests. The current level in the gate was preset at the control box between bursts and turned on thirty seconds prior to burst by a relay operated from the control building. This sort of test would allow determination of the effect of gating current on the transient radiation response of the SCR. The pretest plan called for eight device tests with gating current; however, failure of the relay to function properly resulted in only four devices being tested in this fashion. In all other device tests the gating terminal was either left open or tied to ground through a load (Table II).

Both relay loads and noninductive resistive loads were used in device and circuit tests. The relay used had 50 ohms DC resistance and was a preprototype

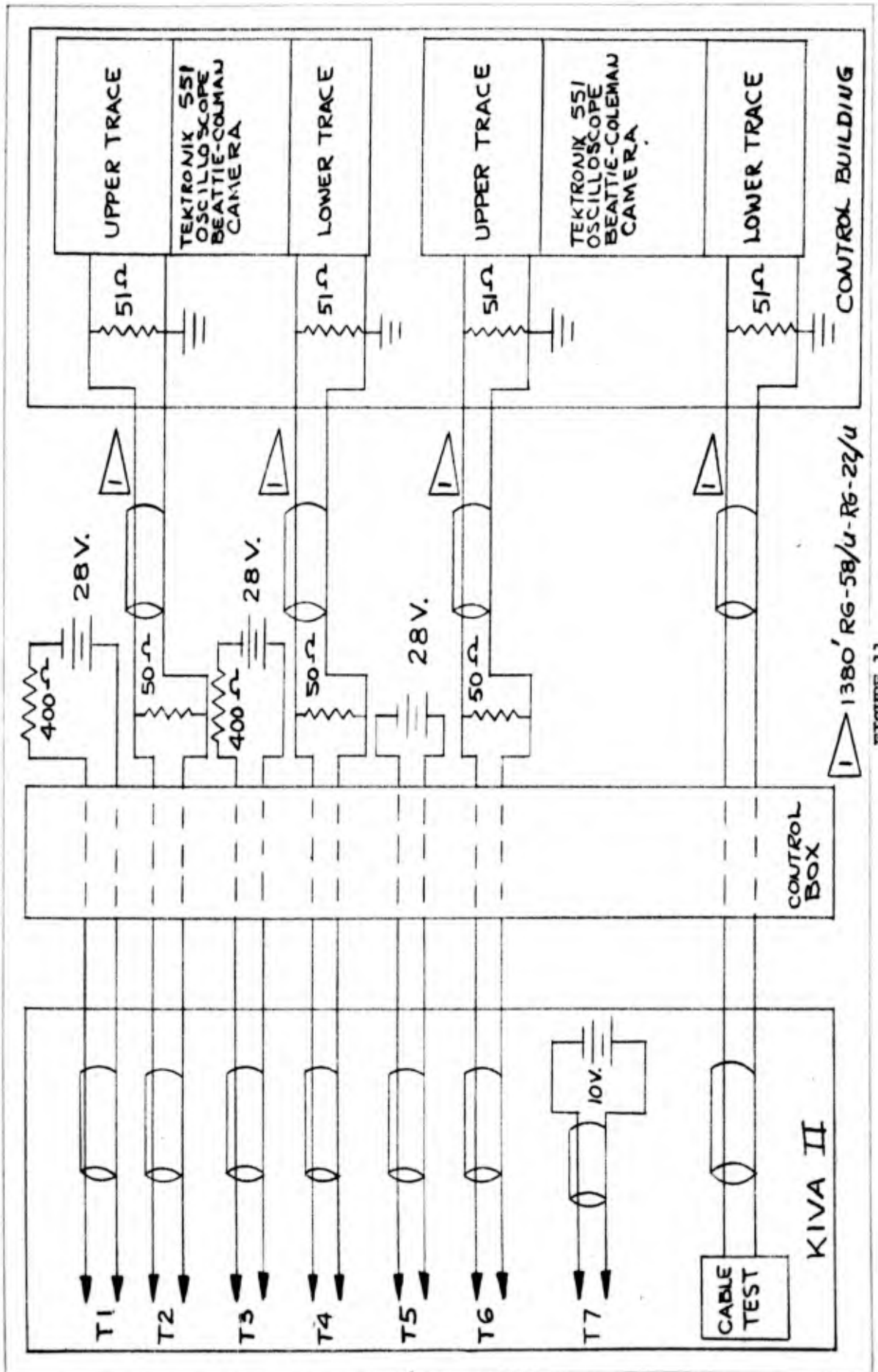


FIGURE 11
Block Diagram of Circuit Test Instrumentation

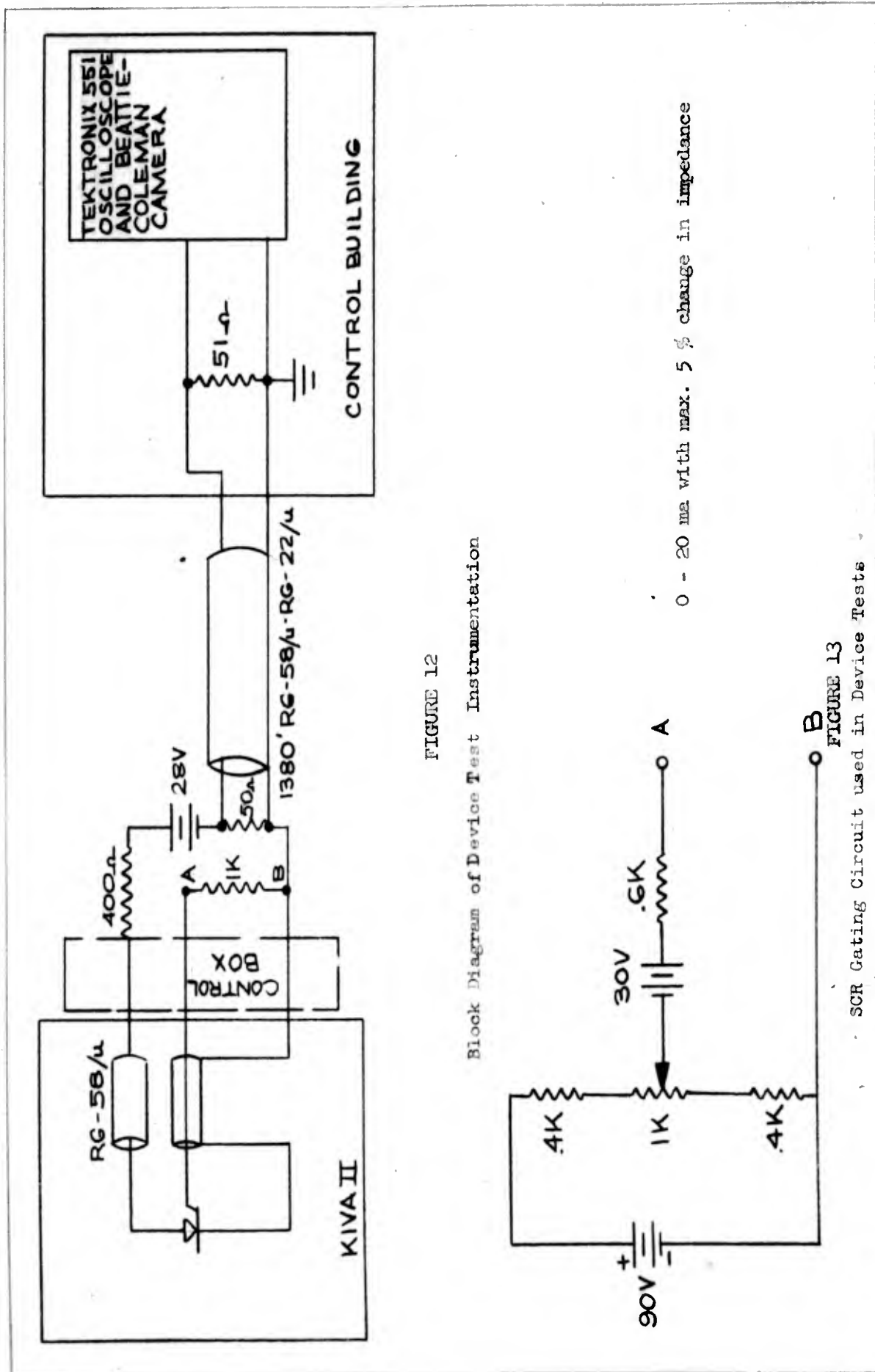


FIGURE 12

Block Diagram of Device Test Instrumentation

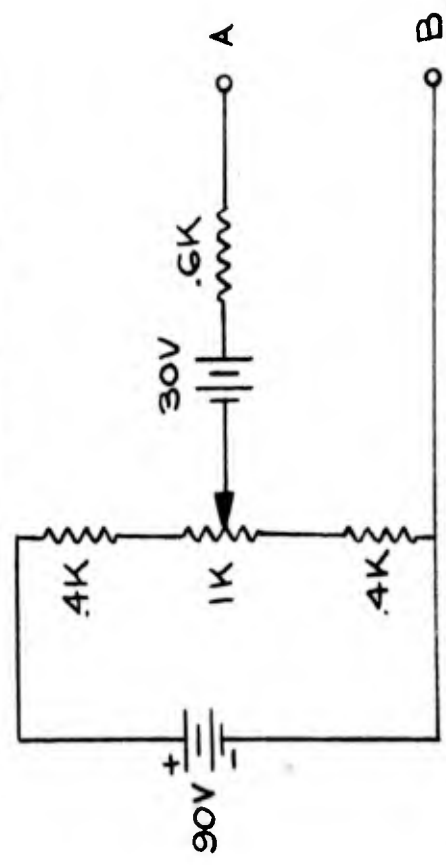


FIGURE 13
SCR Gating Circuit used in Device Tests

0 - 20 ma with max. 5 % change in impedance

TABLE II

Summary of Device Tests

Burst No.	Type of Measurement	Position in Kiva	Device	Device No.	Load	Gate
7	SCR Load Current ↑	P ₁	GE-C35A	1	50 ohms ⁺	*
		P ₁	GE-C35A	29	50 ohms ⁺	Open
		P ₁	GE-C35U	35	50 ohms ⁺	*
		P ₁	GE-C35D	36	50 ohms ⁺	*
8		P ₂	GE-C35A	2	50 ohms ⁺	*
		P ₂	GE-C35U	37	50 ohms ⁺	*
		P ₂	GE-C35D	38	10 ohms ⁺	*
		P ₁	GE-C35U	41	10 ohms ⁺	*
9		P ₁	GE-C35A	9	50 ohms ⁺	≠
		P ₁	GE-C35A	14	50 ohms ⁺	≠
		P ₂	GE-C35A	30	50 ohms ⁺	≠
		P ₂	GE-C35A	31	50 ohms ⁺	≠
10		P ₃	GE-C35A	17	50 ohms ⁺	1.2 ma
		P ₃	GE-C35A	19	50 ohms ⁺	1.9 ma
		P ₂	GE-C35A	22	50 ohms ⁺	6.0 ma
		P ₂	GE-C35A	27	50 ohms ⁺	12.0 ma
11		P ₁	GE-C35A	13	50 ohms ⁺	*
		P ₂	GE-C35A	18	50 ohms ⁺	*
		P ₂	GE-C35A	23	50 ohms ⁺	*
		P ₁	GE-C35A	32	50 ohms ⁺	*
12		P ₂	GE-C35A	7	50 ohms ⁺	*
		P ₁	GE-C35A	20	50 ohms ⁺	Open
		P ₂	GE-C35A	33	50 ohms ⁺	Open
		P ₁	GE-C35A	34	Relay	x
13	SCR Load Current ↓	P ₁	GE-C35A	10	Relay	*
		P ₁	GE-C35A	21	1 μf 400VDC	*

+ = non-inductive

≠ = open due to malfunction of relay

* = 1 K to ground

x = 1 μf 400 VDC to ground

BAC 1546 LR3

P₁ = at screen P₂ = 20" from screen

P₃ = 60" from screen

BOEING

NO. T2-2128

PAGE 34

27000

of a relay used in the Minuteman sequencer and monitor. In the sequencer and monitor the firing of an SCR energizes the relay. A 400 ohm current limiting resistance was placed in every SCR cathode-anode circuit, while the signals were observed across the loads listed in Table III. The RG-58/U cable used to bring the signal to the oscilloscope was terminated in a 51 ohm resistor.

Type D Tektronix oscilloscope preamplifiers were used for the cable and the transistor leakage current measurements in order to obtain maximum sensitivity. The SCR cathode-anode current was monitored with a Type K Tektronix preamplifier, as large (1-2 volts) changes in DC level were anticipated.

All applied voltages in both circuit and device tests are consistent with operating voltages in the Minuteman sequencer and monitor (Ref. 11).

A summary of the device and circuit tests performed is given in Tables II and III. The device number listed in the tables refers to the numbers which were assigned to the devices in order to make pre-test and post-test characterization measurements of the devices. Presence of 60 cps electrical noise, equipment failure, and other anomalies resulted in useless data or no data for some bursts. This will be discussed in more detail in the following section.

Pre-test and post-test static measurements of I_g , I_H and V_{BO} were made (Table IV). In the case of I_g , the gate-cathode current was slowly increased until the SCR "turned on"; then the SCR cathode-anode current was decreased by means of a variable resistor until the device "turned off" giving a measurement of I_H . V_{BO} was measured by conventional techniques.

DATA ANALYSIS AND RESULTS

The monitoring of the SCR cathode-anode current gave four general types of

* = See Fig. 7 and Fig. 9

+ = non-inductive

TABLE III

Summary of Circuit Tests

Burst No.	Test Item	Type*	Position in Five	Type of Measurement	Device	Device No.	Load
1	Circuit Bd.	B	P ₁	{ SCR Load Current SCR Load Current Transistor Leakage Leakage	GE-C35A	24	50 ohms ⁺
	Cable	CA	P ₁		TI 2N657	4	50 ohms ⁺
2	Circuit Bd.	B	P ₁	{ SCR Load Current SCR Load Current Transistor Leakage Leakage	GE-C35A	28	50 ohms ⁺
	Cable	CB	P ₁		TI 2N657	3	50 ohms ⁺
3	Circuit Bd.	A	P ₁	{ SCR Load Current SCR Load Current Transistor Leakage Leakage	GE-C35A	16	50 ohms ⁺
	Cable	CA	P ₁		TI 2N657	1	50 ohms ⁺
4	Circuit Bd.	A	P ₁	{ SCR Load Current SCR Load Current Transistor Leakage Leakage	GE-C35A	25	Relay
	Cable	CB	P ₁		TI 2N657	2	50 ohms ⁺
5	Circuit Bd.	C	P ₁	{ SCR Load Current SCR Load Current Leakage	GE-C35A	8	Relay
	Cable	CA	P ₁		GE-C35A	6	50 ohms ⁺
6	Circuit Bd.	C	P ₁	{ SCR Load Current SCR Load Current Leakage	GE-C35A	15	50 ohms ⁺
	Cable	CB	P ₁		GE-C35A	26	Relay



TABLE IV
 Tabulation of Critical Parameters for SCR's Used in Circuit and Device Tests

Burst	Device	Oscilloscope Trace	$V_{BO(B)}$ (Volts)	$V_{BO(A)}$ (Volts)	$I_G(B)$ (ma)	$I_G(A)$ (ma)	$I_H(B)$ (ma)	$I_H(A)$ (ma)	Neutron Flux (Neutrons/cm ² x 10 ¹²)	Max. γ Rate (r/sec x 10 ⁶)
1	24	No Signal	N.B.	N.B.	14.4	>100ma	--	--	5.01 +	19.5
1	12	No Signal	N.B.	N.B.	6.2	22.0	13.0	60.0	5.01 +	19.5
2	28	No Signal	N.B.	N.B.	11.1	26.0	16.0	38.0	4.11 +	13.2
2	5	Type b	N.B.	N.B.	7.6	2.8	4.8	8.4	4.11 +	13.2
3	16	No Data	327	405	3.2	8.4	5.2	10.8	4.04 +	31.9
3	3	Type a	380	382	4.0	18.0	4.4	<4	4.04 +	31.9
4	25	Type c	275	355	4.6	14.4	7.0	17.2	4.50 +	37.1
4	11	Type c	277	++	1.2	++	<100ua	++	4.50 +	37.1
5	8	No Signal	440	429	8.8	21.0	7.4	17.8	4.31 +	17.7
5	6	No Signal	400	415	26.0	41.0	16.0	12.0	4.31 +	17.7
6	15	Type a	292	396	26.0	55.0	4.2	18.0	4.46 +	23.2
6	26	Type a	198	N.B.	10.0	36.0	4.0	9.6	4.46 +	23.2
7	1	Type b	285	365	2.4	4.1	5.2	10.2	3.18	20.3
7	29	Type b	N.B.	N.B.	26.0	48.0	11.4	None	3.31	25.2
7	35	Type a	142	175	3.2	12.2	5.4	13.0	4.16	20.3
7	36	Type a	N.B.	N.B.	25.0	34.0	8.0	30.0	4.16	20.3

TABLE IV
 Tabulation of Critical Parameters for SCR's Used in Circuit and
 Device Tests (Continued)

Burst	Device	Oscilloscope Trace	V _{BO} (B) (Volts)	V _{BO} (A) (Volts)	I _G (B) (ma)	I _G (A) (ma)	I _H (B) (ma)	I _H (A) (ma)	Neutron Flux (Neutrons/cm ² x10 ¹²)	Max Y Rate (r/sec x 10 ⁶)
8	2	Type a	N.B.	N.B.	2.3	3.8	11.2	1.8	2.87	12.9
8	37	Type a	282	375	2.2	4.3	3.6	6.4	2.46	12.9
8	38	Type b	N.B.	N.B.	17.0	24.0	15.4	52.0	2.46	12.9
8	41	Type b	230	260	7.4	12.4	5.1	18.0	3.59	16.2
9	9	Type a	350	385	2.4	4.4	2.2	6.2	3.70	15.4
9	14	Type a	350	387	2.6	5.5	3.8	7.1	3.70	15.4
9	30	Type c	225	246	2.8	3.2	4.4	4.9	0.325	1.1
9	31	*No Signal	440	454	2.4	3.1	3.8	4.4	0.332	1.1
10	17	Type b	225	230	3.4	4.2	4.9	5.4	0.013	< 0.02**
10	19	Type b	392	346	2.6	3.2	4.0	4.9	0.013	< 0.02**
10	22	Type b	N.B.	N.B.	18.0	21.8	<100µa	28.0	0.277	0.82
10	27	Type b	390	360	18.0	19.5	<100µa	34.0	0.262	0.82
11	13	Type d	385	N.B.	16.0	36.0	11.0	32.0	3.34	20.42
11	18	Type b	320	302	10.0	12.6	11.6	13.4	0.029	1.23
11	23	Type b	335	352	10.8	13.2	2.8	4.8	0.270	1.23
11	32	Type a	395	420	1.9	4.5	3.9	9.6	3.34	20.4

TABLE IV
 Tabulation of Critical Parameters for SCR's Used in Circuit and Device Tests (Continued)

Burst	Device	Oscilloscope Trace	$V_{BO}(B)$ (Volts)	$V_{BO}(A)$ (Volts)	$I_{S(B)}$ (ma)	$I_{S(A)}$ (ma)	$I_{R(B)}$ (ma)	$I_{R(A)}$ (ma)	Neutron Flux (Neutrons/cm ² x 10 ¹²)	Max. γ Rate (r/sec x 10 ⁶)
12	7	Type c	280	297	26.0	21.0	<100 μ a	0.7	0.288	1.21
12	20	Type d	160	174	18.0	34.0	6.4	1.7	3.49	19.20
12	33	*No Signal	317	317	4.1	4.6	3.2	4.4	0.312	1.21
12	34	Type d	175	271	14.0	33.8	16.5	82.0	3.81	19.2
13	10	Type a	495	486	5.0	11.2	9.7	26.0	3.46	19.2
13	21	Type b	355	N.B.	7.2	22.0	12.8	50.0	3.46	19.2

+ = Represents average of the two sulfur tablets nearest the SCR's (see Fig. 8)

++ = Device destroyed, could not make post irradiation measurements.

(A), (B) = Pre-test and post-test respectively

* = Equipment Failure

** = Total gamma dose <50 roentgen (Chemical dosimeters used would not read this low.)

† = Dosimeter reading not available - screen value of burst 12 used since bursts 12 and 13 were similar.

N.B. = Did not break over at 500 volts.

oscilloscope traces (Fig. 14).

Case a: The device "turns on" and goes into forward conduction (reaches saturation) for approximately 100 μ s.

Case b: A current pulse having a shape similar to the Godiva pulse and peaking at approximately the same time as the Godiva pulse is observed.

Case c: The device "turns on" and remains on.

Case d: The device does not "turn on" but saturates the test instrumentation.

The results of monitoring the SCR cathode-anode current in the device and circuit tests are listed in Tables IV and V. Types of oscilloscope traces, values of V_{BO} , I_g and I_H , integrated neutron flux (neutron/cm²), and peak gamma rates (r/sec) are listed for each SCR tested. Table V also gives the results of the cable tests and transistor leakage current measurements.

Most of the data from the cable tests and transistor leakage current measurements were lost because of 60 cps electrical noise pickup at the high gain settings (1 mv/cm) used for these particular measurements. The noise came from the controls of a second prompt critical assembly (Godiva II). When Godiva II was shut down the noise generated by the firing of the SCR's was picked up at the high gain settings.

The data obtained by monitoring the SCR cathode-anode current for the SCR's used in the circuit tests were not as conclusive as that obtained from the SCR's used in the device tests. This is due to the fact that the circuit tests were performed on the first day of testing, and at that time the sweep speed and gain settings which would yield maximum information had not been well established; however, the SCR data from the first day's testing are consistent with the data from the second day's testing. With the exception of SCR No. 16, all SCR cathode-anode current data obtained during the circuit tests can be interpreted.

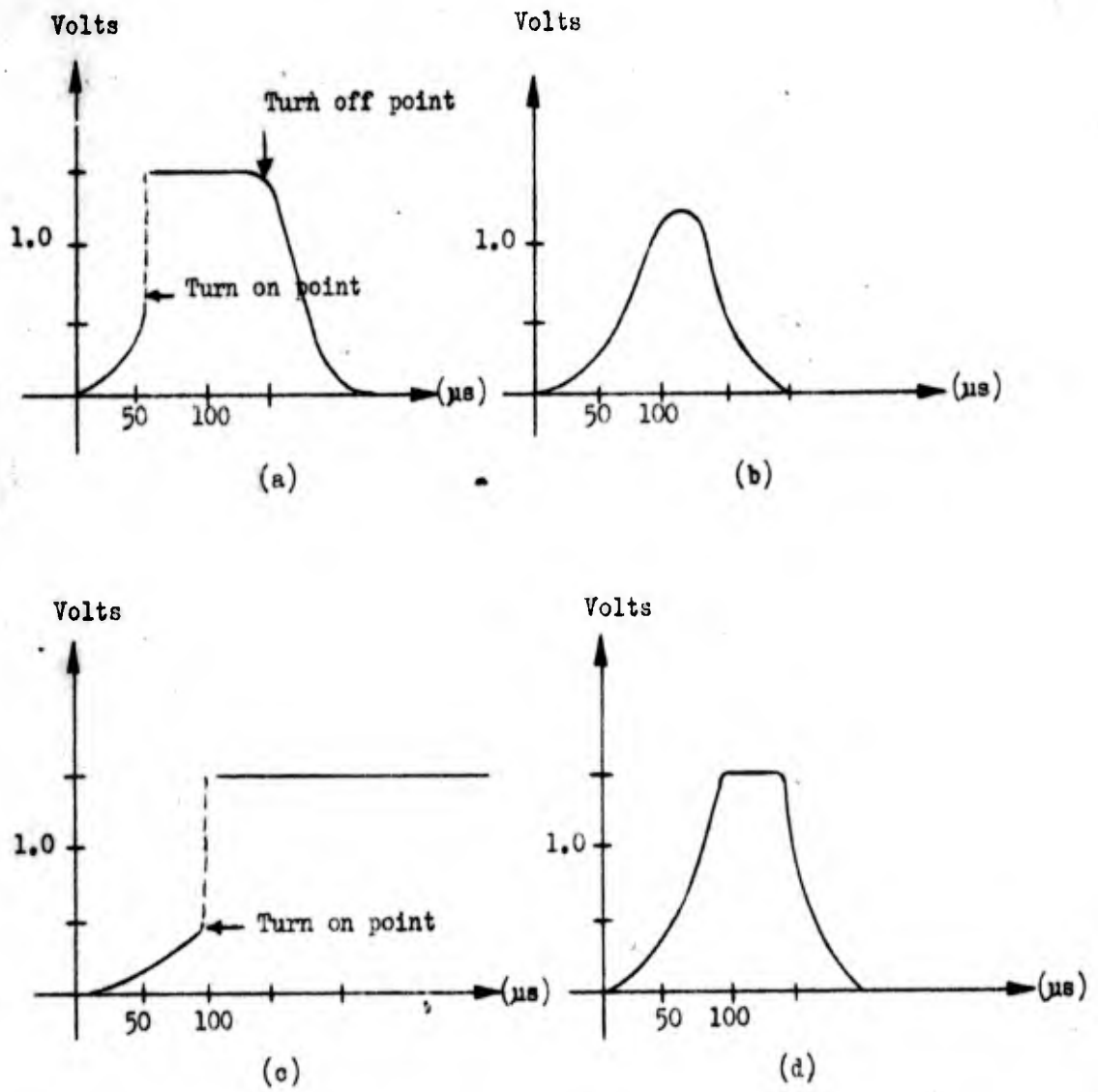


FIGURE 14

General Types of Oscilloscope Traces for SCR Tests

TABLE V
Results of Circuit Tests

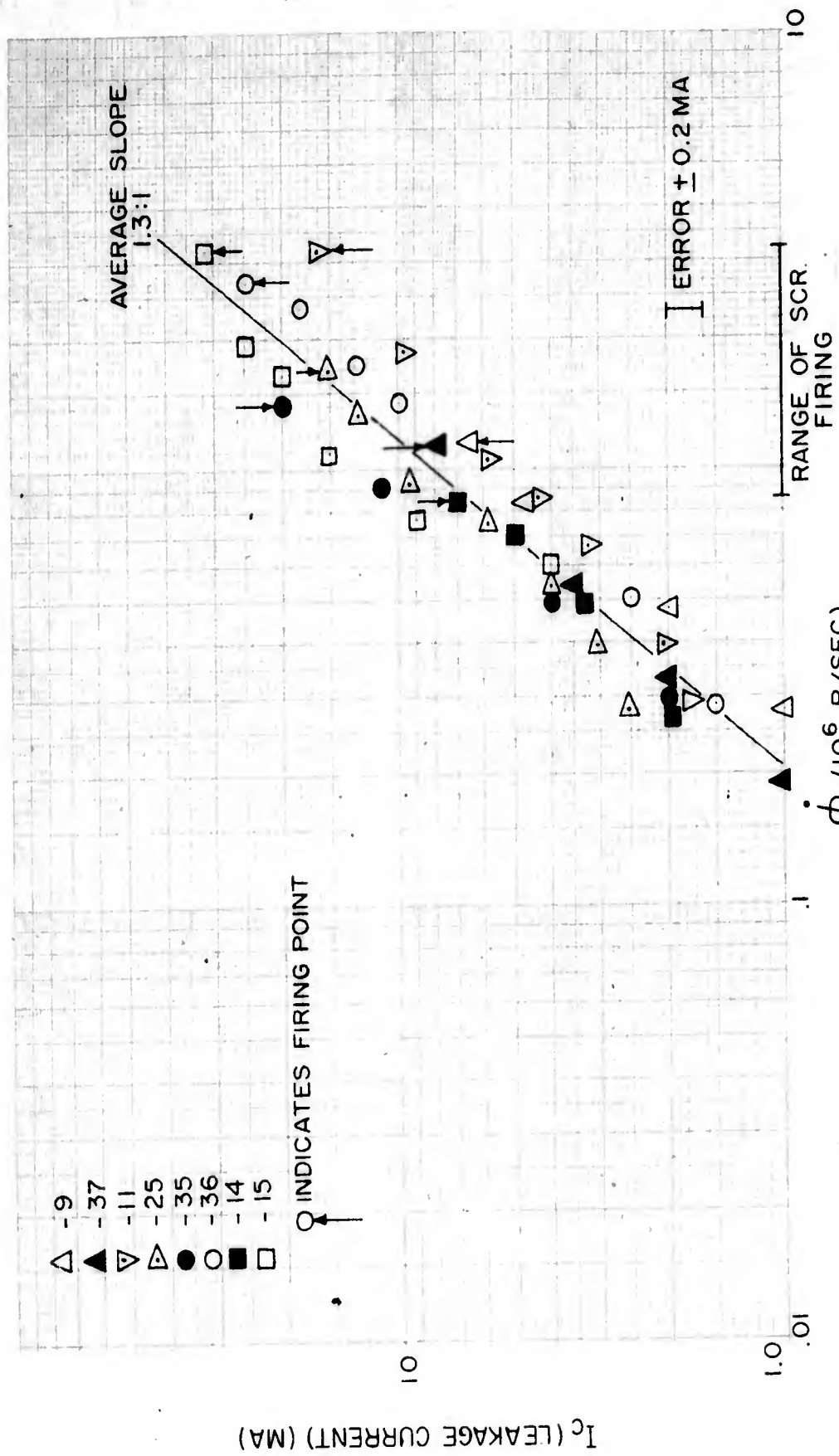
Test Item	Burst No.	Oscilloscope Traces	Remarks	Neutron Flux (Pu nt/cm ² x10 ¹²)	Max. Gamma Rate (r/sec x 10 ⁶)
SCR No. 24 SCR No. 12 Transistor No. 4 Cable No. CA ₁	1	No Signal Current Buildup No Signal 5 mv pos. signal	Equipment Failure Sweep Speed too Low Equipment Failure	5.01 ⁺	19.52
SCR No. 28 SCR No. 5 Transistor No. 3 Cable No. CB ₁	2	No Signal Type b Good Signal No Signal	Equipment Failure * Couldn't Use High Enough Gain Because of 60 cps Pickup	4.11 ⁺	13.15
SCR No. 16		No Data	Gain Set Too High Giving Signal Which Went Off Trace: Results Inconclusive * Camera Improperly Triggered	4.04 ⁺	31.90
SCR No. 3 Transistor No. 1 Cable No. CA ₂	3	Type a No Data No Data	Get Sharp Rise Then Off Trace; Signal Does Not Return in 250 μsec; Which Means Device Probably Turned On and Re- mained on* 60 cps 60 cps	4.50 ⁺	37.10
SCR No. 25 SCR No. 11	4	Type c Type c	Equipment Failure Equipment Failure	4.31 ⁺	17.71
Transistor No. 2 Cable CB ₂	5	No Signal No Signal 2 mv neg. signal	Good Signal " " Pickup from Firing of SCR's	4.46 ⁺	23.21
SCR No. 8 SCR No. 6 Cable No. CA ₃	6	Type a Type a Noise			

* - See Figure 14

+ - Represents avg. of the two pellets nearest the SCR's (See Fig. 8)

The oscilloscope traces of SCR load voltage as a function of time during each burst were converted first to current as a function of time and then to current as a function of gamma rate (r/sec). Leakage current (I_c) versus gamma rate ($\dot{\phi}$) is plotted in Figures 15 and 16 for those devices which "turned on" while a representative plot of I_c versus $\dot{\phi}$ for those devices which did not "turn on" is made in Figure 17. The gamma rates and integrated fluxes at "turn on" and "turn off" are listed in Table VI for those devices which went into forward conduction. Table VII lists the gamma rates necessary to produce one milliamperere of leakage current before irradiation and after irradiation for devices that did not "turn on." These gamma rate values are found by extrapolating curves similar to Figure 17.

Devices 10, 25, 8, 34, and 26 had a relay load which presented a DC impedance of 50 ohms and an impedance of 10^4 ohms to a 50 μ s pulse. In these cases the 51 ohm cable termination became the transient load for the SCR devices. The relay caused no unusual circuit effects in the case of the radiation-induced leakage currents.



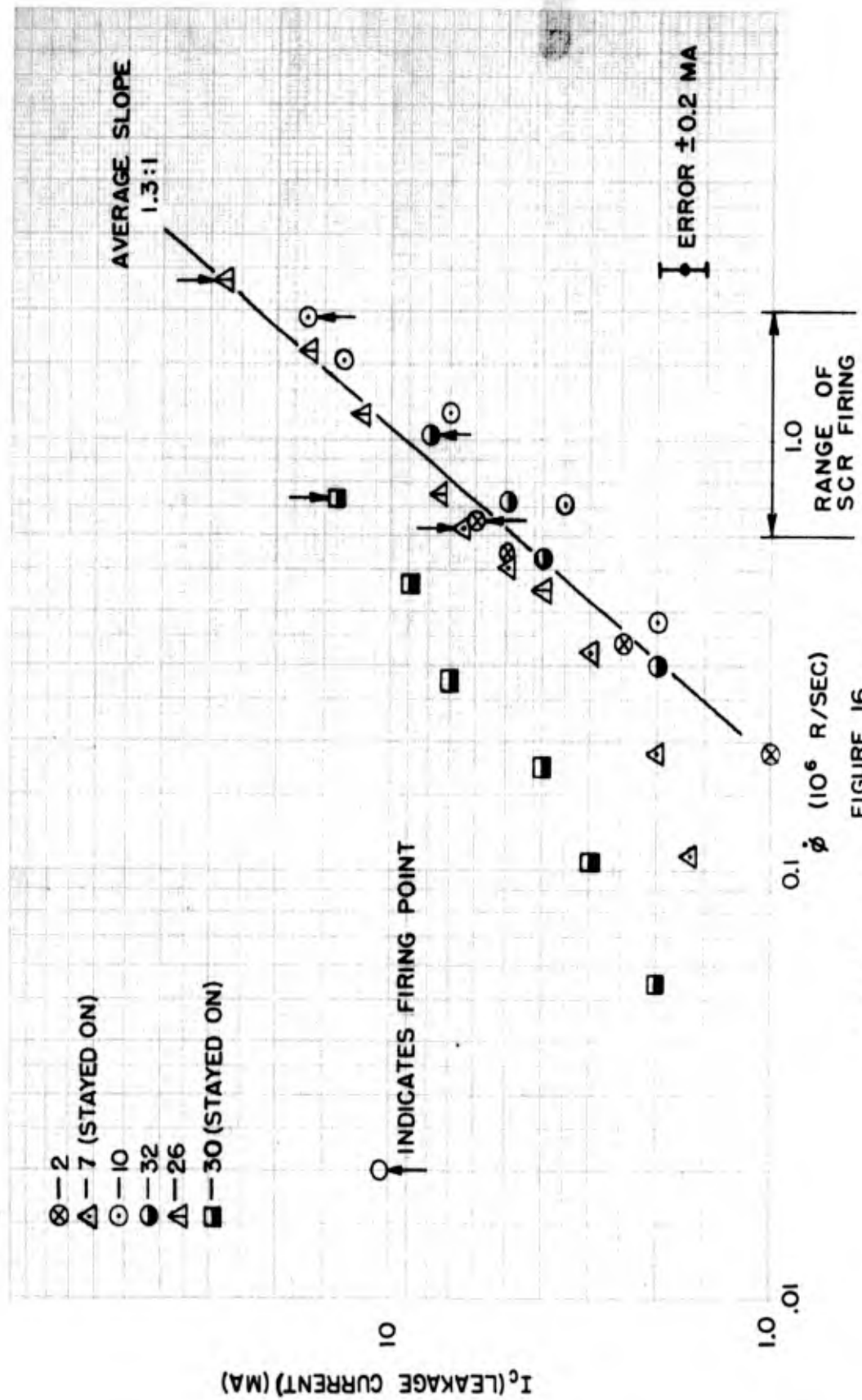
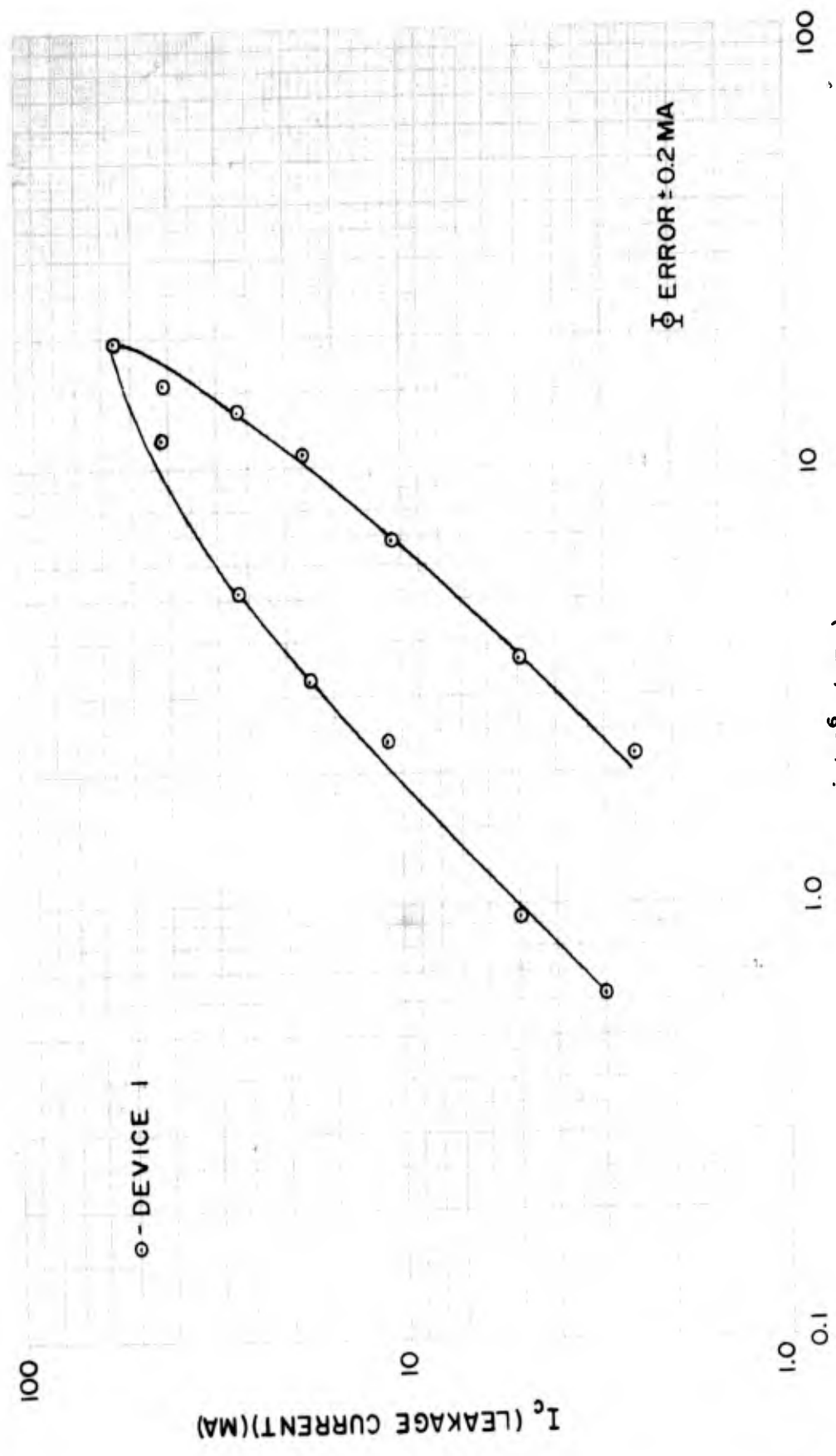


FIGURE 16

LEAKAGE CURRENT VS. γ -RATE UP TO 'TURN ON'



ϕ (10^6 R/SEC)

FIGURE 17

EFFECT OF PERMANENT DAMAGE ON INDUCED LEAKAGE CURRENT

TABLE VI

Gamma Rate and Integrated Neutron Flux at "Turn-On" and "Turn-Off"

Device	$\dot{\phi}_{(b.o)}$ (10^6 r/sec)	$\dot{\phi}_{(t.o)}$ (10^6 r/sec)	$\phi_{t(b.o)}^N$ (10^{12} Pu nt/cm ²)	$\phi_{t(t.o)}^N$ (10^{12} Pu nt/cm ²)
2	.647	9.80	.038	2.18
7	.626	Stays on	.076	Stays on
9	1.15	13.5	.079	2.56
10	1.96	15.7	.157	2.44
14	.819	13.5	.046	2.56
30	.720	Stays on	.098	Stays on
32	1.02	18.6	.072	2.26
35	1.40	20.5	.092	2.58
36	2.66	17.3	.204	2.54
37	1.17	11.8	.129	1.85
15 ⁺	3.21	10.54	.230	3.36
26 ⁺	2.36	13.0	.142	3.36
11 ⁺	3.20	Stays on	--	Stays on
25 ⁺	1.62	Stays on	--	Stays on

+ = SCR's in circuit tests

 $\dot{\phi}_{(b.o)}$ = Y-rate at which device "turned on" $\phi_{t(b.o)}^N$ = integrated neutron flux at "turn on" $\dot{\phi}_{(t.o)}$ = Y-rate at which device "turned off" $\phi_{t(t.o)}^N$ = integrated neutron flux at "turn off"

TABLE VII

EFFECT OF PERMANENT NEUTRON DAMAGE ON
SCR GAMMA INDUCED LEAKAGE CURRENT

Device	ϕ Required to Produce 1 ma of Leakage Current (10^6 r/sec)	
	Beginning of Burst	End of Burst
1	.21	.93
13	.16	1.87
18	.08	.30
20	.18	.95
22	.23	.30
23	.11	.54
27	.14	.16
29	.12	1.00
34	.17	1.58
38	.08	.50
41	.34	1.08



DISCUSSION OF RESULTS

The results obtained may be divided into two categories:

1. SCR's which "turned on."
2. SCR's which did not "turn on."

If we examine the first category in detail, we find that only four of the devices which "turned on" remained on; all others turned off at some time during the burst. The rates at which "turn on" occurs are lower than the gamma rates at which "turn off" occurs by approximately an order of magnitude (See Table VII). On the other hand, the integrated neutron flux at "turn off" is about the same for each device and about two orders of magnitude greater than that at "turn on." In fact, if devices 15 and 26 are neglected (the "turn off" point occurred off trace for these devices and had to be inferred), the average integrated neutron flux at which "turn off" occurs is:

$$\frac{\phi^N}{t_{(to)}} = 2.37 \times 10^{12} \text{ Pu nt/cm}^2$$

and the mean square deviation is $.058 \times 10^{12}$ which indicates that "turn off" is due to permanent neutron damage. Neutron damage causes I_H to increase.

It is assumed that the holding current (I_H) increases until it is larger than the induced leakage current, and when this occurs, the device "turns off." The two devices which remained on did not experience a high neutron flux since they were placed 20 inches from the screen. The increase in I_H resulting from neutron permanent damage was not sufficient to cause the device to turn off.

An attempt was made to correlate the "turn on" characteristics of the SCR with known parameters of the device. Since the holding current of the SCR is a measure of the minimum current which will sustain saturation, it was felt that this parameter might correlate with the radiation induced leakage current of the SCR at time of "turn on." Figure 18 is a plot of the leakage current at time of "turn on" versus the initial value of the holding current. It is seen that all devices that "turned on" except one lie above a line of slope two. The device that falls below the line did not exhibit normal characteristics in other respects (i.e., I_H decreased with neutron dose).

It is interesting to consider the devices that did not "turn on" to see if they exhibit similar characteristics on a I_C versus I_H plot. It is difficult to apply this test directly to the devices that did not break over due to changes in I_H with neutron flux. An attempt was made to correct for changes in I_H due to neutron permanent damage by applying the following relation:

$$I_H(t_0) = Be^{a\phi_{t_0}^N}$$

where $I_H(t_0)$ = value of holding current at time t_0 after burst

$\phi_{t_0}^N$ = integrated neutron flux at t_0

a, B = empirically determined constants, using pre- and post-irradiation measurements (Table IV)

M. M. Weiss of Bell Telephone Laboratories (Ref. 13) has irradiated two GE-C35's at the Brookhaven National Laboratory reactor, and indications are that the exponential fit may not be good below 10^{13} nt/cm²; however, his data are not sufficient to allow any concrete conclusions to be made. Since there were only two points (pre- and post-irradiation values) for I_H versus ϕ_t^N taken for devices

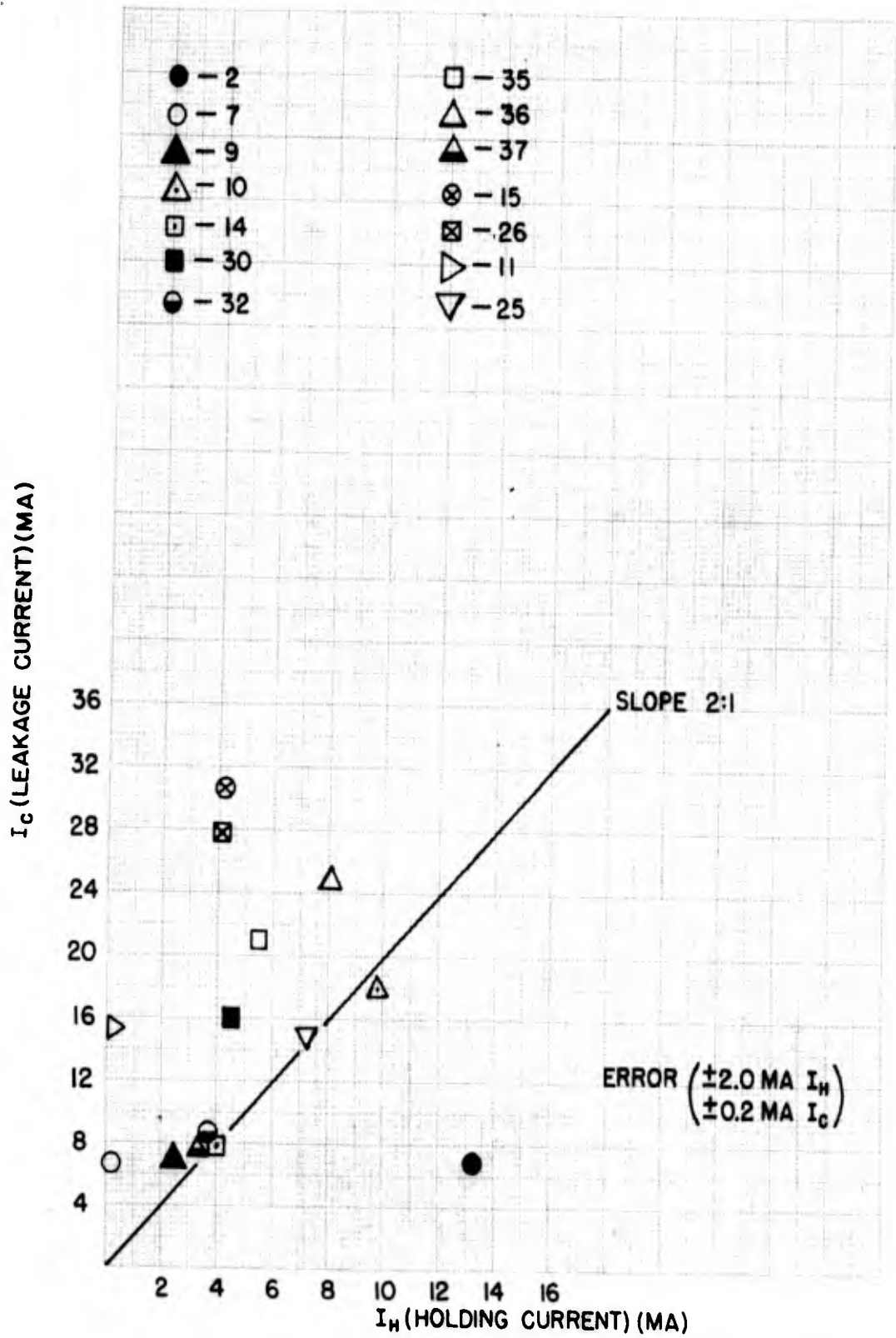


FIGURE 18
LEAKAGE CURRENT AT TURN ON VS. HOLDING CURRENT

tested at Godiva, it was impossible to try anything but an exponential fit for I_H versus ϕ_t^N .

Values of I_C versus I_H for these cases generally tended toward large values of I_H and for the most part fell below a line of slope two in the $I_H \leq 10$ ma region.

Although there is not complete agreement in the correlation of I_C and I_H , there is sufficient agreement to indicate a possible method of predicting when the SCR device will fire when exposed to Godiva type radiation. Further testing in a neutron-free environment will be required in order to determine if the slope of two relation holds for all devices.

As in the case of I_H , the post-irradiation values of I_g and V_{BO} are greater than their pre-irradiation values (Table IV). This effect is assumed to be caused by neutron damage; however, as only two points were available, no definite conclusions could be made.

The leakage current through the SCR is shown in Figure 15 to be proportional to the gamma rate to the 1.3 power. Transistors and diodes have been found to exhibit direct proportionality between leakage current and gamma rate. The power relation indicates that an amplification effect is occurring in the SCR. This is entirely reasonable since it is a four region device and amplification can occur through avalanche multiplication.

The plot of I_C versus gamma rate for the devices that did not "turn on" shown in Figure 17 indicates a reduction in the effective junction volume due to permanent neutron damage. The leakage current in semiconductor devices has been shown to be proportional to the effective volume which is defined by the

area of the junction and the junction width or base material diffusion length, whichever is shorter. The reduction in this volume due to neutron induced changes in the diffusion length has been observed for silicon diodes.

The average leakage current of the SCR can be expressed as follows:

$$I_c = (6 \pm 3) \times 10^{-10} \dot{\phi}^{1.2 \pm .1} \text{ amperes}$$

where I_c is the cathode leakage current with 28 volts applied
 $\dot{\phi}$ is the gamma rate in r/sec

The tests to determine the effect of a combination of partial gating current and radiation were inconclusive due to experimental difficulties. However, the result of circuit and device tests indicate that the SCR devices will fire due to radiation before they can be turned on by transistor leakage current. Transistor induced leakage currents for 10^6 r/sec range from 1-10 μ a.



CONCLUSIONS

These tests indicate that SCR devices and circuits are affected by transient gamma radiation and are also subject to the usual permanent damage neutron effects present in all semiconductor devices that depend on transistor action. Specific conclusions are:

1. The leakage current in SCR devices increases under exposure to gamma radiation according to:

$$I_c = (6 \pm 3) \times 10^{-10} \dot{\phi}^{1.2 \pm .1} \text{ amperes}$$

where $\dot{\phi}$ is in r/sec.

2. As the leakage current increases in the SCR it reaches a value which causes the device to fire. This value is generally more than twice the holding current. Fourteen out of 31 devices on which usable data were obtained exhibited this effect. The rates at which these devices fired were between 6×10^5 and 3×10^6 r/sec.
3. Parameters of the device which experienced permanent neutron damage were V_{BO} , I_g , and I_H . The threshold of these permanent damage effects are consistent with silicon power transistors. This is approximately 10^{12} nt/cm².
4. Due to permanent neutron damage, the analysis of gamma rate effects was not possible in all cases.
5. Minuteman circuitry using SCR devices can be triggered by radiation rates of 10^6 r/sec.



RECOMMENDATIONS

Since it has been definitely established that the SCR devices can be triggered by a gamma radiation pulse having an amplitude of 10^6 r./sec., it is recommended that more information be obtained to determine the seriousness of this effect to the Minuteman system. Specifically, information is needed to:

1. Determine the effect of the radiation pulse width on the firing of the device. This will allow a more realistic evaluation to be made on the effect of a nuclear weapon burst on the device operation. Shorter pulse widths may not fire the device. A preliminary test at the BAC flash X-ray indicated that three devices did not fire when exposed to a rate of 10^6 r./sec. for 0.2 μ sec.
2. Attempts should be made to determine if it is possible to establish a criterion which will allow one to select devices which will not trigger in a given environment, or to predict when a specific device will be triggered.

The above items, and in particular Item 1, should be investigated in a neutron free environment. Such an environment is available either using the Applied Physics Section flash X-ray facility which can provide up to 10^6 r/sec. with a 0.2 μ sec pulse width or using the General Atomic linear accelerator which can provide up to 10^8 r/sec. with pulse widths ranging from 0.5 μ sec to 10 μ sec.

CAPACITOR TESTS

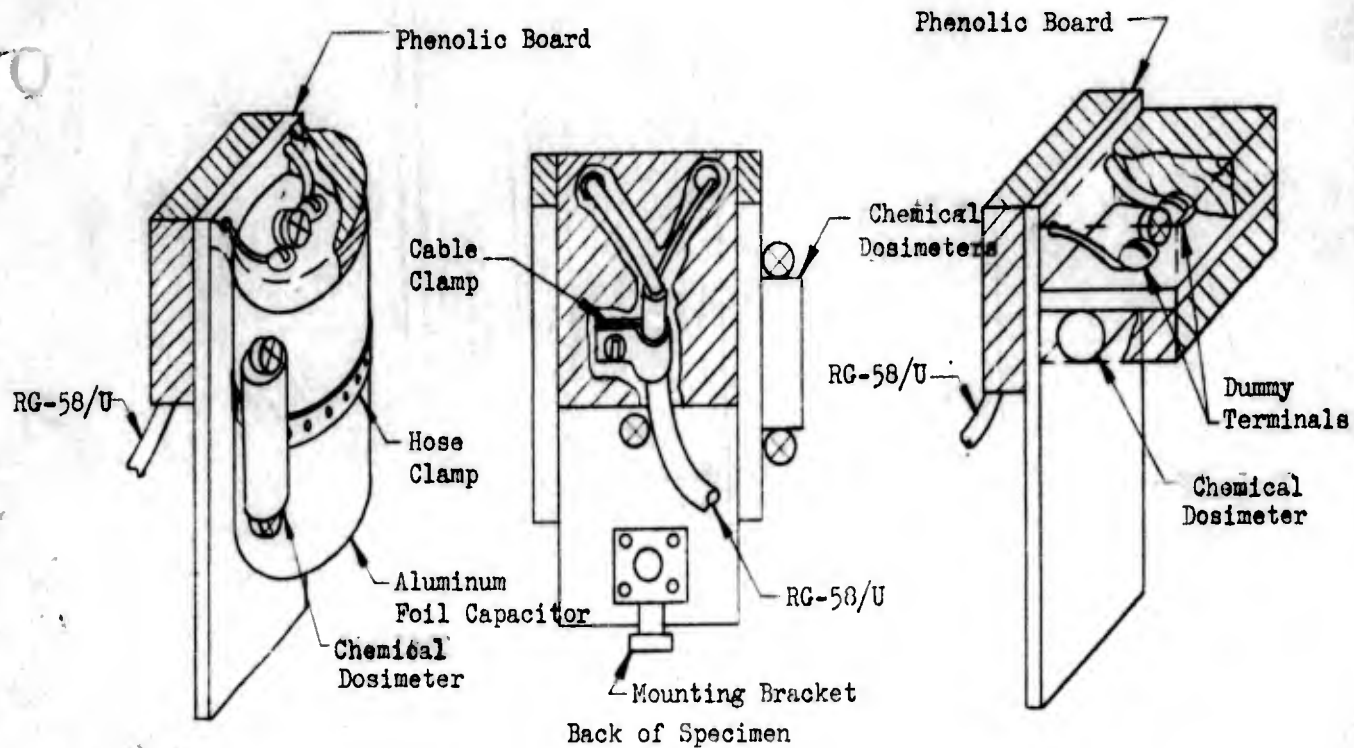
TEST SPECIMENS



Representative types and sizes of tantalum and aluminum electrolytic capacitors were chosen for these tests. The listing of test parts (Table VIII) includes (a) tantalum solid polarized, (b) tantalum plain foil polarized and non-polarized, (c) tantalum etched foil polarized and (d) aluminum etched foil polarized electrolytic capacitors. The test parts are similar to Minuteman standard parts and represent the range of capacitance and voltage rating values used in Minuteman for these capacitor types (Ref. 12).

All capacitors were mounted on 2" x 5 1/2" x 1/16" phenolic terminal boards; tantalum capacitors were mounted on 3/8 inch high terminals, and aluminum capacitors were fastened to the boards with hose clamps (Fig. 19). RG-58/U coaxial cable was connected directly to the capacitor terminals and fastened securely to the mounting board with cable clamps. Each specimen was provided with a mounting bracket which was well-insulated from the electrical connections. Tantalum capacitor test specimens, with dosimetry in place, were potted with 3/4 inch thick Silastic RTV 882 on the front, and with 1/2 inch thickness on the back. Aluminum capacitor test specimens were potted with 1/2 inch thickness of Silastic RTV 882 on the top of the capacitor and on the top half of the back of the specimen in order to cover all electrical connections. Dosimetry at the top and back of these specimens was potted in place, but dosimetry used at the side and bottom of the aluminum capacitors was added between bursts. Dummy specimens for cable tests were exactly

TABLE VIII
Capacitor Test Parts

	Capacitance (μ f)	Voltage Rating (Volts)	Manufacturer's Identification
a.	Tantalum	Solid, Polarized	Sprague Electric Co.
	0.22	35	150D225x0035A0
	2.2	20	150D225x0020A0
	22	35	150D226x0035R0
b.	Tantalum	Plain Foil, Polarized	General Electric Co.
	4.5	50	29F1561G2
	40	50	29F1564G2
	100	15	29F1643G2
c.	Tantalum	Plain Foil, Non-Polarized	General Electric Co.
	3	30	29F1662G2
	10	10	29F1632G2
	10	15	29F558
	100	10	29F1514G2
d.	Tantalum	Etched Foil, Polarized	General Electric Co.
	70	65	29F1681G2
	480	75	29F1090
d.	Aluminum	Etched Foil, Polarized	General Electric Co.
	1900	100	43F939CA3
	5000	75	43F1107CA1
	15000	50	43F878CA3



-  Silastic RTV682
-  Sulfur Pellets

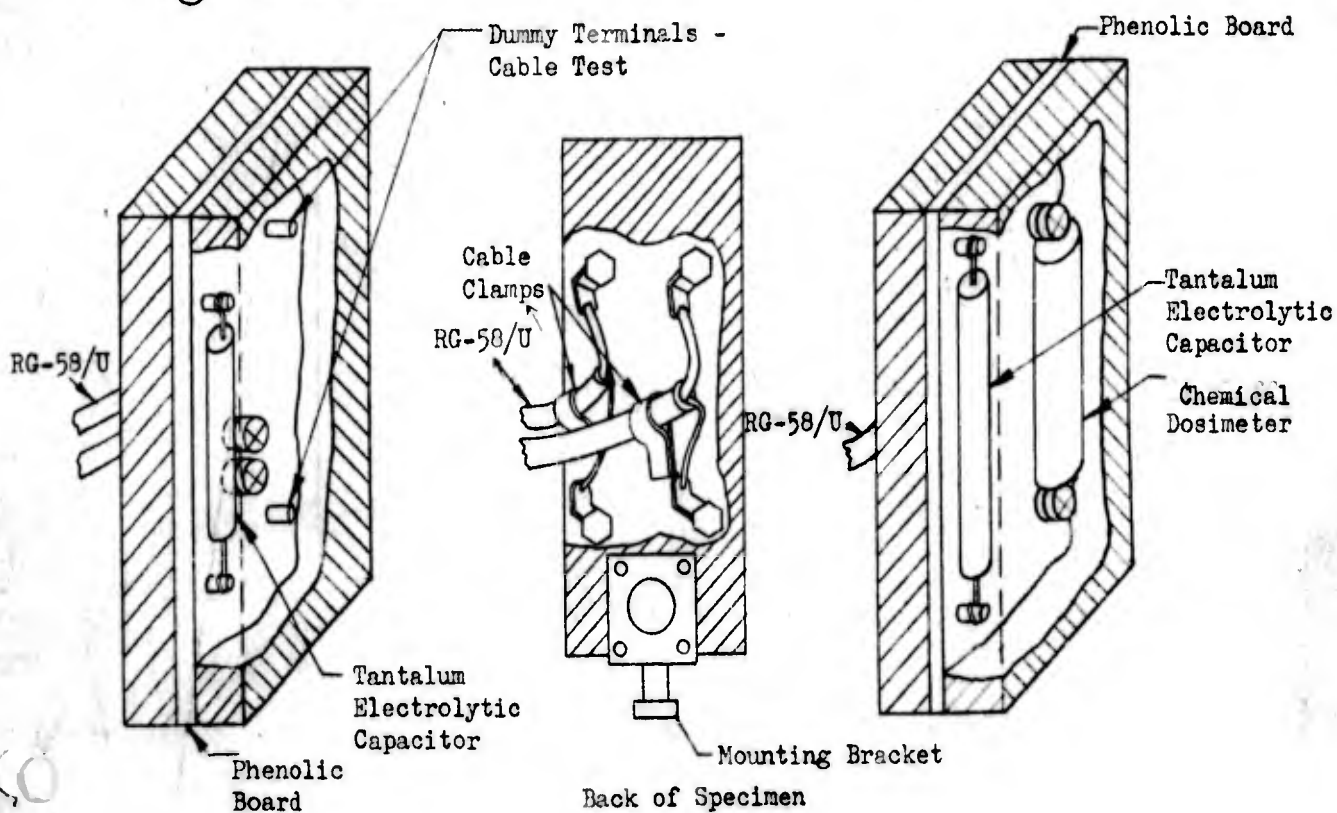


Figure 19

Typical Capacitor Test Specimens

the same except that capacitors were not connected between terminals. Various test specimen arrangements are shown in Figure 19. Distribution and placement of capacitors and dummy terminals on the specimen boards was dictated by the overall test plan, physical size of capacitors, dosimetry requirements, space allotted at Godiva III, requirements for electrical isolation and need for comparison of data taken during a single burst.

TEST EQUIPMENT AND PROCEDURES

Three types of tests were planned to determine transient effects on the capacitors due to the gamma radiation pulse from Godiva III. These tests were:

Test A	Capacitor leakage
Test B	EMF generation
Test C	Capacitance change

These tests were designed to yield a clear picture of the transient effects of gamma radiation on the capacitor dielectric materials and provide generalized data which could be applied to any tantalum or aluminum electrolytic capacitor in a gamma radiation field.

Figures 20 and 21 show the test equipment layout and circuitry for the leakage and EMF tests. The 51 ohm resistor provides a reasonable termination for the RG-58/U, RG-22/U cable. Leakage test specimens were allowed ample time to charge to the continuously applied 9.3 volt level before each test. The transient voltage change



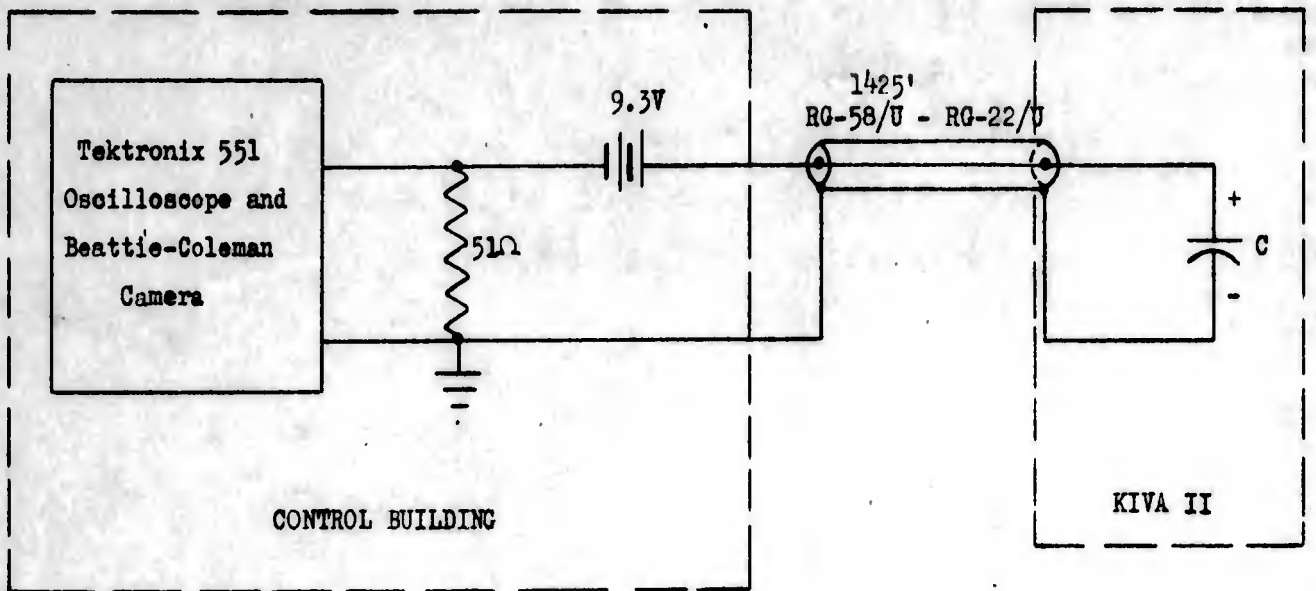


Figure 20

Circuitry for Capacitor Test A
Leakage

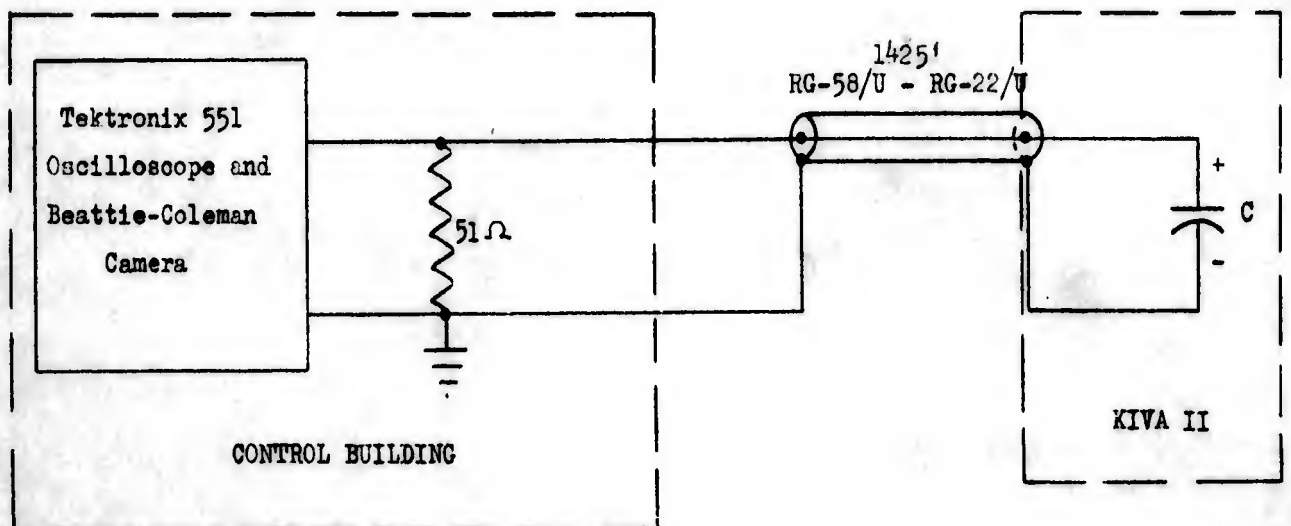


Figure 21

Circuitry for Capacitor Test B
EMF

across the capacitor due to gamma-induced leakage was monitored during the burst in Test A, and combined capacitor and cable current and voltage changes generated by gamma radiation were monitored during Test B. Cable tests with the dummy test specimens were performed in order to provide information which would permit separation of capacitor and cable effects in Tests A and B. The battery voltage was checked periodically during the test series.

Figure 22 shows the test equipment layout and circuitry for the capacitance tests. Fifty kilocycle AC voltage was supplied to a nearly constant matched load to provide a "constant-current" test for capacitance. A 9.3 volt bias was provided for the electrolytic capacitor test specimens. The AC voltage across the capacitor was adjusted to a suitable level before each burst; the oscilloscope gain was increased in order to increase measurement sensitivity, and both the top and bottom of the AC signal across the capacitor were monitored on the two oscilloscope channels during the burst. The applied AC voltage was checked after each burst. The oscillator, amplifier and oscilloscope were operated in the equipment trailer at the Kiva during these tests; a satisfactory impedance-matching system was not available to permit operation over the 1425 ft. of cable from the control room. The shielded bunker outside the Kiva was in use so that it was necessary to operate the equipment in the trailer at the risk of observing transient signal changes due to radiation exposure of equipment. The observed signal changes represented not only AC changes which would indicate changes in capacitive reactance of the test specimen, but also any AC and DC level changes caused by radiation effects in the test equipment. The oscilloscope trigger was generated by the "gate" output

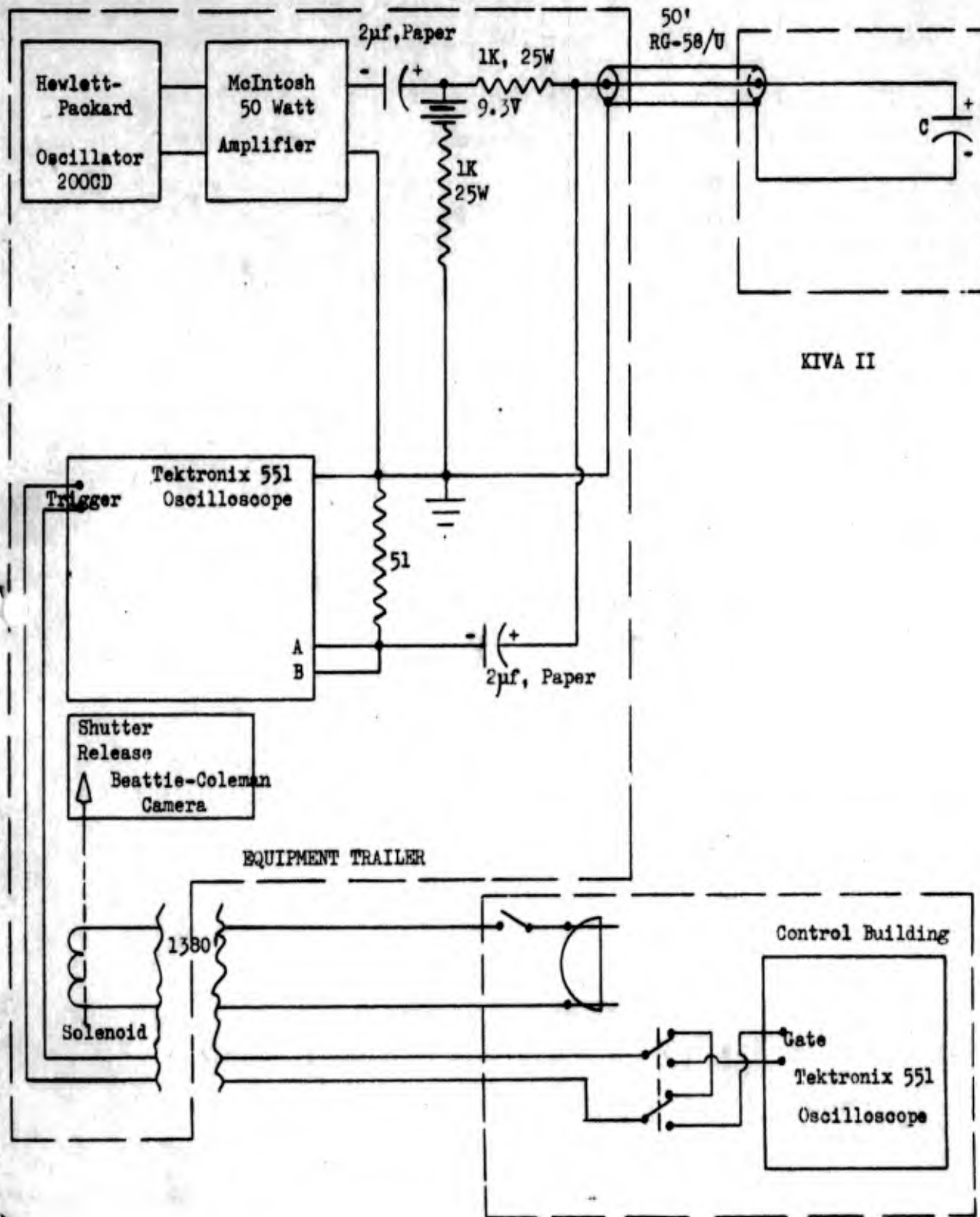


Figure 22

T2-2128

62

Circuitry for Capacitor Test C
- Capacitance Change

of an oscilloscope at the control building; this trigger input was shorted at the control building until the instant before burst in order to avoid premature single-sweep operation of the oscilloscope at the Kiva. The camera shutter was opened by an AC solenoid which was actuated from the control building before unshorting the trigger. The camera was closed immediately after burst.

The applied voltage levels used in all tests are consistent with those used in Minuteman circuitry. All test specimens were mounted as near to the Godiva III protective screen as possible in order to attain the maximum available radiation levels. The centers of all specimens except the aluminum capacitors and their dummy counterparts were $5/8$ inch (average) from the screen. The centers of the aluminum specimens and dummies were $1\ 1/4$ inches and $1\ 3/4$ inches from the screen. All specimens were centered vertically about a horizontal mid-plane through the fissionable material. These average positions were pre-set and marked before the first burst, and then maintained throughout the test series. Type D Tektronix oscilloscope plug-in units were used for all tests in order to obtain optimum sensitivity for signal observation.

Capacitance and dissipation factor were measured for each capacitor before and after the tests with a General Radio 60 ops impedance bridge. The DC leakage resistance of each capacitor was measured before and after the tests with a Keithley Model 200B electrometer and Model 2008 decade shunt; a voltage of 9-11 volts was used for these measurements.

A summary of the capacitor tests is presented in Table IX. Tests performed, initial data and dosimetry are given. Specimens did not receive radiation exposure prior to test except in the three cases given in Table IX; in these cases it was necessary to re-run capacitors where unirradiated specimens were not available. Table IX does not list tests for which data was unusable. Difficulties were experienced due to 60 cps electrical noise pickup at high gain settings (i.e. 1-10 mv/cm), radiation-induced "fogging" of the high speed film which was used in the equipment trailer at the Kiva, electronics failures and other causes. Some of the data were ineffective or unusable due to these causes.



TABLE IX
Summary of Capacitor Tests
Initial Measurements

Burst No.	Specimen Type	Initial Measurements					Conductivity ($\Omega\text{-cm}^{-1}$) $\times 10^{17}$	Test Type	Neutron Flux (Pu nt/cm^2) $\times 10^{-12}$	Max. Gamma Rate (r/sec) $\times 10^{-6}$
		Capacitance (μf)	Dissipation Factor ($60\sim$) (%)	Leakage Resistance ($\text{M}\Omega$)	Resistance ($\text{M}\Omega$)	Capacitance (μf)				
1	Al Foil, Pol., Etched, 75V	5,530	15.4	8.6		1.30	A	3.6	17.3	
1	Ta Foil, Pol., Etched, 50V	528	3.7	35.4		11.8	A	9.4	38.0	
2	Al Foil, Pol., Etched, 50V	15,000	--	2.14		1.93	A	3.3	8.7	
2	Ta Foil, Pol., Etched, 65V	78.9	2.38	≥ 2350		≤ 1.19	A	7.8	19.1	
3	Ta Foil, Non-Pol., Plain, 10V	9.88	1.7	≥ 2250		≤ 9.95	A	12.3	42.5	
3	Ta Foil, Non-Pol., Plain, 10V	96	2.22	≥ 229		≤ 10.0	A	12.3	42.5	
3	Ta Sol., Pol., 35V	20.4	3.53	84		129	A	10.4	42.5	
4	Ta Foil, Pol., Plain, 15V	103	2.93	≥ 990		≤ 2.16	A	11.3	37.0	
4	Ta Foil, Non-Pol., Plain, 30V	5.15	1.50	3030		2.31	A	11.3	37.0	
4	Al Foil, Pol., Etched, 100V	2,290	7.86	4.00		6.75	A	6.15	23.5	
5	Potted Terminals, 4.0" Spacing						A	12.2	40.3	
5	Potted Terminals, 2.0" Spacing						A	12.2	40.3	
6	Ta Foil, Pol., Etched, 65V	63.2	2.38	5550		0.63	A	7.35	37.2	
6	Ta Foil, Pol., Plain	39	1.27	895		6.33	A	(9.07)* 17.67	37.2	
7	Simulated Terminals for 5000 μf Al Foil Capacitor (1.4" Spacing)						A	3.22	16.3	
7	Potted Terminals, 0.8" Spacing						A	11.1	44.6	
7	Ta Foil, Pol., Plain, 50V	4.49	1.9	≥ 370		≤ 11.3	C	11.7	44.6	

* Capacitor Re-run. Parenthesis indicated prior flux. Accumulated flux is given

Table IX Cont'd.

Burst No.	Specimen Type	Initial Measurements					Neutron Flux (Pu nt/cm ²) x 10 ⁻¹²	Max. Gamma Rate (r/sec) x 10 ⁻⁶
		Capacitance (60~) (μf)	Dissipation Factor (60~) (%)	Leakage Resistance (MΩ)	Conductivity (Ω-cm) ⁻¹ x 10 ⁻¹⁷	Test Type		
8	Simulated Terminals for 1900 μf Al Foil Capacitor (0.85" Spacing)							
8	Potted Terminals, 0.8" Spacing							
9	Ta Foil, Pol., Plain, 15V	102.1	2.82	≥1090	≤ 1.98	A	4.5	16.5
9	Potted Terminals, 2.0" Spacing					A	9.45	40.3
9	Ta Foil, Non-Pol., Plain, 15V	10.4	4.67	400	53.1	B	10.6	27.1
10	Ta Foil, Non-Pol., Plain, 10V	95.5	2.28	385	6.00	B	10.6	27.1
10	Potted Terminals, 2.0" Spacing					C	9.45	27.1
11	Al Foil, Pol., Etched, 75V	5390	14.3	9.1	1.26	B	8.03	25.1
11	Ta Sol., Pol., 35V	0.213	2.55	≥5,500	≤29.2	B	8.03	25.1
12	Ta Foil, Pol., Etched, 50V	503	3.97	≥141	≤ 3.12	A	3.5	16.6
12	Ta Sol., Pol., 20V	2.085	10.75	3080	34.4	B	9.62	36.6
13	Ta Sol., Pol., 35V	23.3	3.69	146	65	B	8.05	31.8
13	Ta Foil, Pol., Etched, 50V	528	3.7	35.4	11.8	A	9.45	31.8
13	Ta Sol., Pol., 20V	2.085	10.75	3080	34.4	B	10.1	29.3
						A	(9.4)*	29.3
						C	18.15	
							(9.45)*	29.3
							20.05	

* Capacitor Re-run. Parenthesis indicates prior flux. Accumulated flux is given.

DATA ANALYSIS AND RESULTS

Throughout this analysis it is assumed that all transient radiation effects are caused by gamma radiation. Radiation effects tests to date have indicated that neutrons have little effect insofar as transients are concerned. It is also assumed that the cable termination (51 ohms) was nearly ideal so that no signal changes occurred in the transmission lines.

All usable data were projected to about 7X to 8X magnification, and the best fit curves were traced in order to enhance accuracy and ease of analysis.

Capacitance Test Results

Typical data obtained in capacitance change tests are shown in Figure 23. It will be noted that large AC and DC level changes occurred in the observed signal (Table X), however these changes were of a duration much longer than the radiation pulse and reached a maximum at 500-1000 μ s. There were no appreciable additional changes observed specifically at the time of the burst peak which could be attributed to the capacitors being tested within accuracies given in Table X. This result is in agreement with leakage test results. A large capacitive reactance change in the test specimen would cause a proportional DC voltage change in the leakage tests since the circuit time constants are long. Such changes were not indicated. The changes observed are attributed to gamma effects in the oscillator, amplifier and oscilloscope at estimated peak rates ≤ 300 r/sec in the equipment trailer.

Cable Test Results

Typical cable test data are shown in Figure 24. The observed signals were similar to the radiation pulse in shape for both zero and 9.3 volts applied. Average curves of current generated in the 51 ohm terminating resistor by the



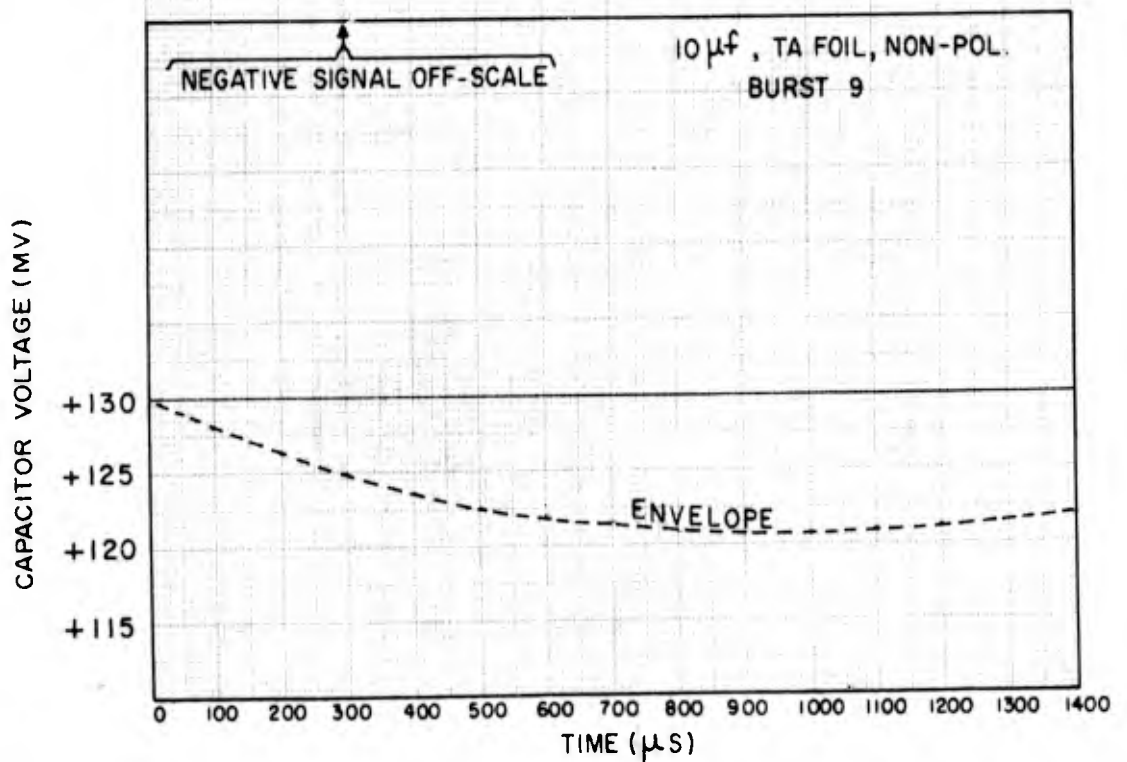
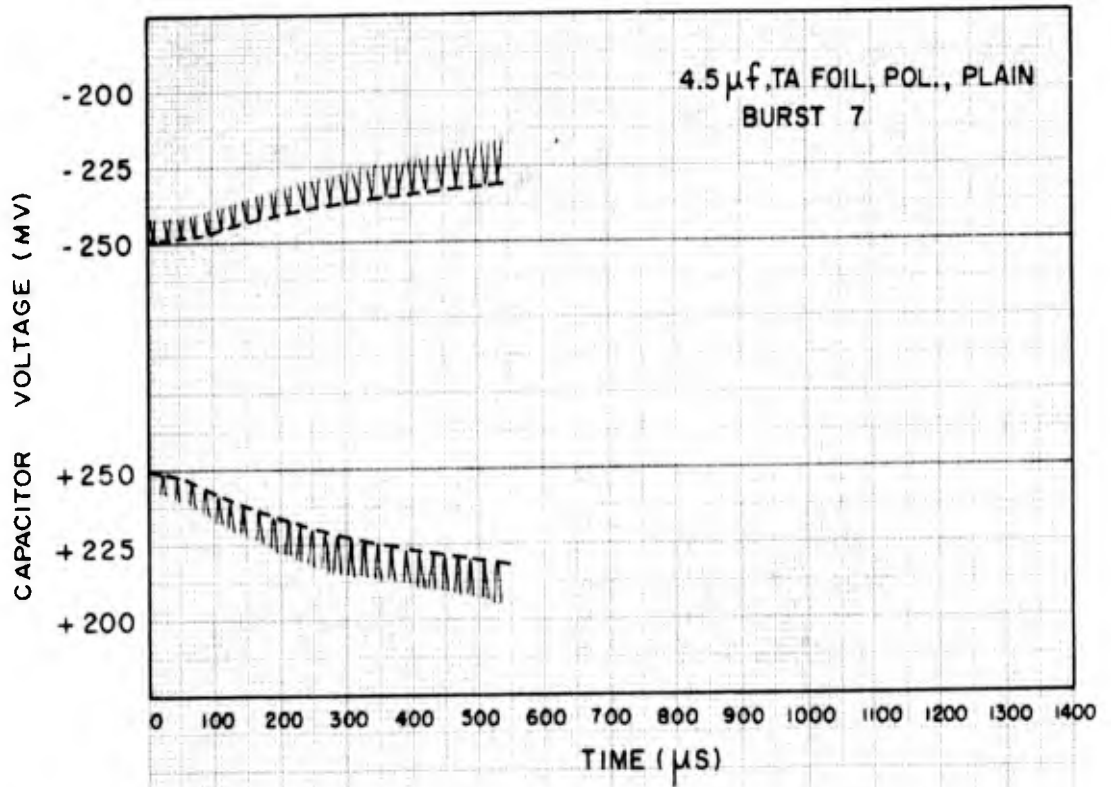


FIGURE 23
TYPICAL CAPACITANCE TEST DATA

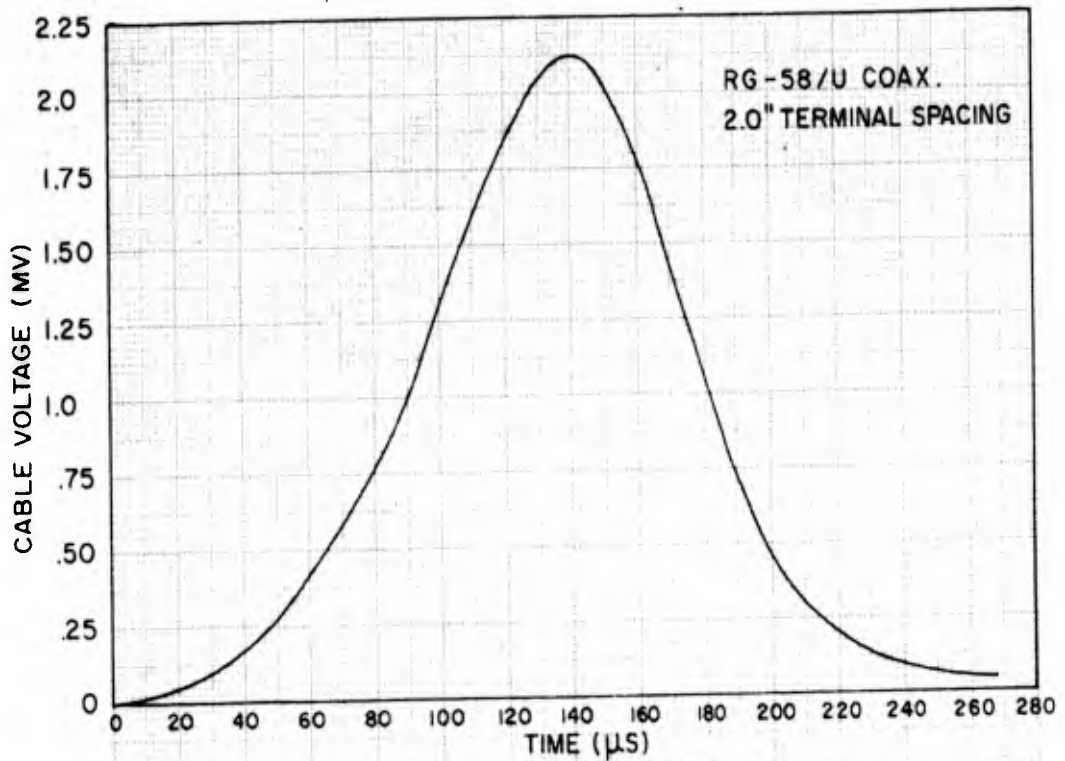


FIGURE 24
TYPICAL CABLE EMF DATA

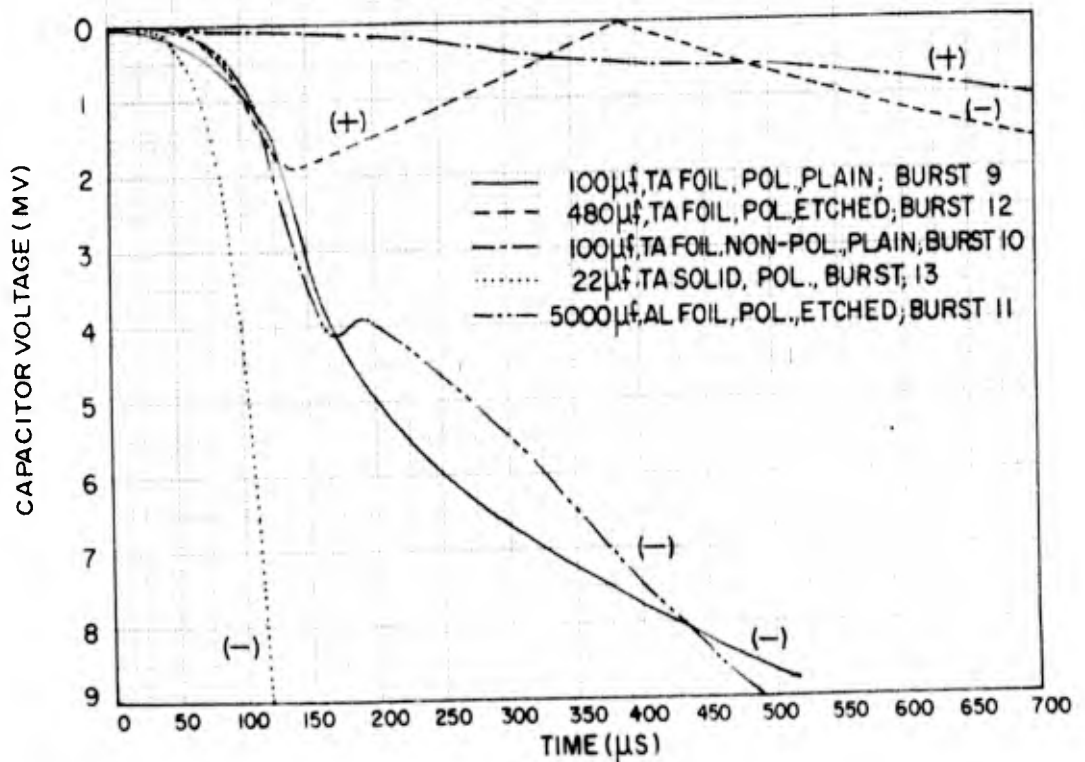


FIGURE 26
CAPACITOR EMF DATA

TABLE X

Capacitance Change Test Results

<u>Burst No.</u>	<u>Capacitor Tested</u>	<u>Capacitance Change</u>	<u>Oscillator Max. Change</u>
7	4.5 μ f, 50V, Ta Foil, Pol., Plain	0 \pm 1%	-(\sim 9.8%) at 500 μ s
9	10 μ f, 15V, Ta Foil, Non-Pol., Plain	0 \pm 1%	-(\sim 5.5%) at 990 μ s
13	2.2 μ f, 20V, Ta Solid, Pol.	0 \pm 0.5%	-(\sim 8.2%) at 670 μ s



RG-58/U coaxial cable are shown in Figure 25 as a function of gamma rate for two cases with zero volts applied and six cases with 9.3 volts applied. The generated cable voltage and current was positive from center conductor to shield, and the applied voltage was positive on the center conductor. Gamma rates are those at the position of the dummy terminals. There were no trends noted due to differences in spacing of the dummy terminals. It is noted that the generated current decreases as the applied voltage increases, and the current shows saturation tendencies at higher gamma rates.

Capacitor EMF Test Results

Capacitor EMF test data are shown in Figure 26. The results for the five capacitors tested are presented in Figures 27, 28, and 29 in the form of capacitor generated charge versus gamma dose to 300 μ s, capacitor equivalent charging current (i.e. charge generation rate) versus gamma rate through the burst peak, and capacitor generated charge versus time after 200 μ s respectively. The generated charge was obtained by multiplying capacitance at 60 cps by the observed capacitor voltage at the gamma dose of interest; this charge is defined as positive when the positive terminal of the capacitor (or center conductor of the cable) shows a positive voltage. The charging current was obtained by multiplying capacitance at 60 cps by the observed time rate of change of capacitor voltage at the gamma rate of interest; this current is defined as positive when the positive capacitor terminal (center conductor of cable) exhibits an increasing voltage (i.e. negative charge flowing away from the terminal).

The non-polarized capacitor exhibits a very small effect when compared with the polarized types. The charge generation rate and accumulated charge for

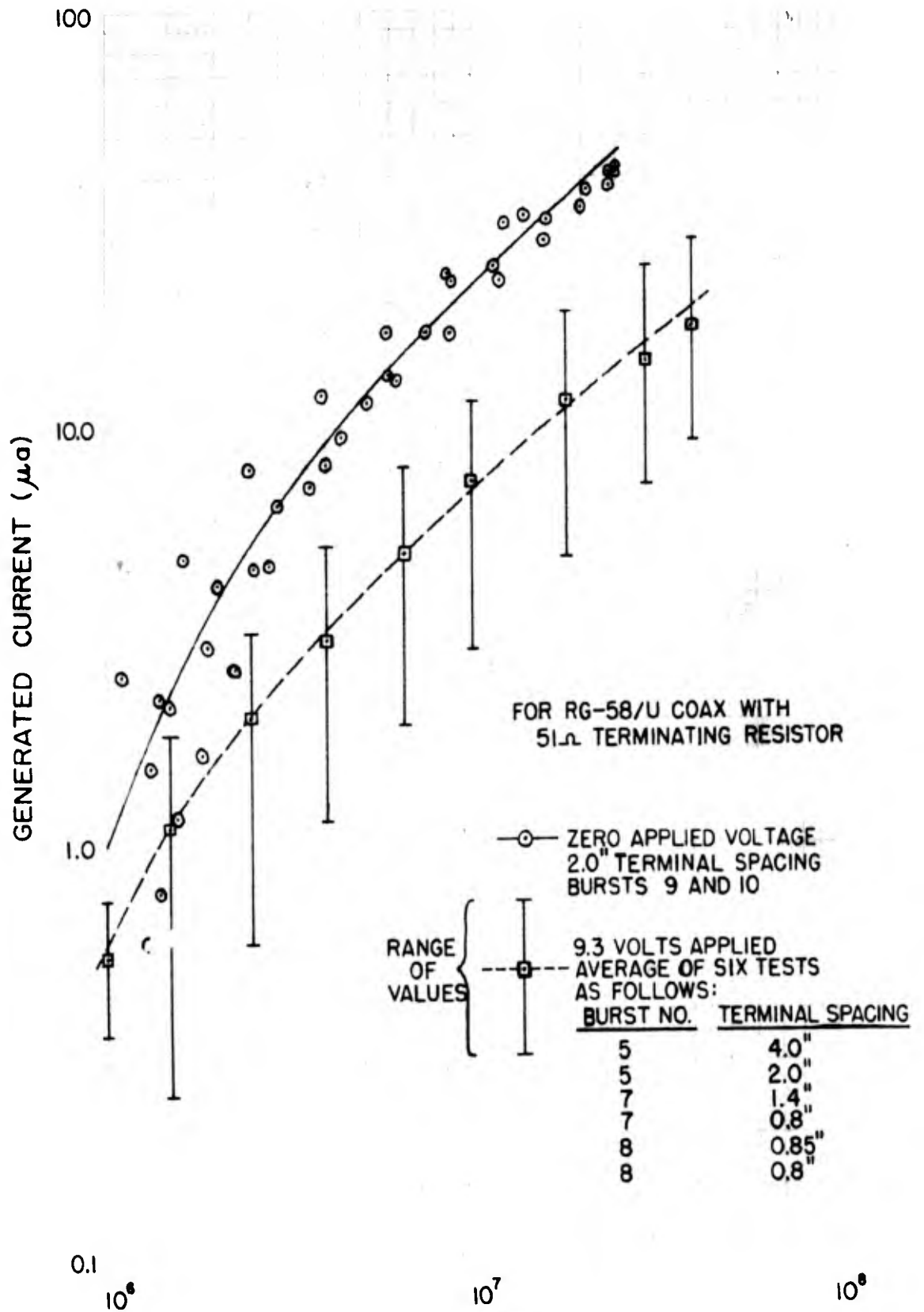
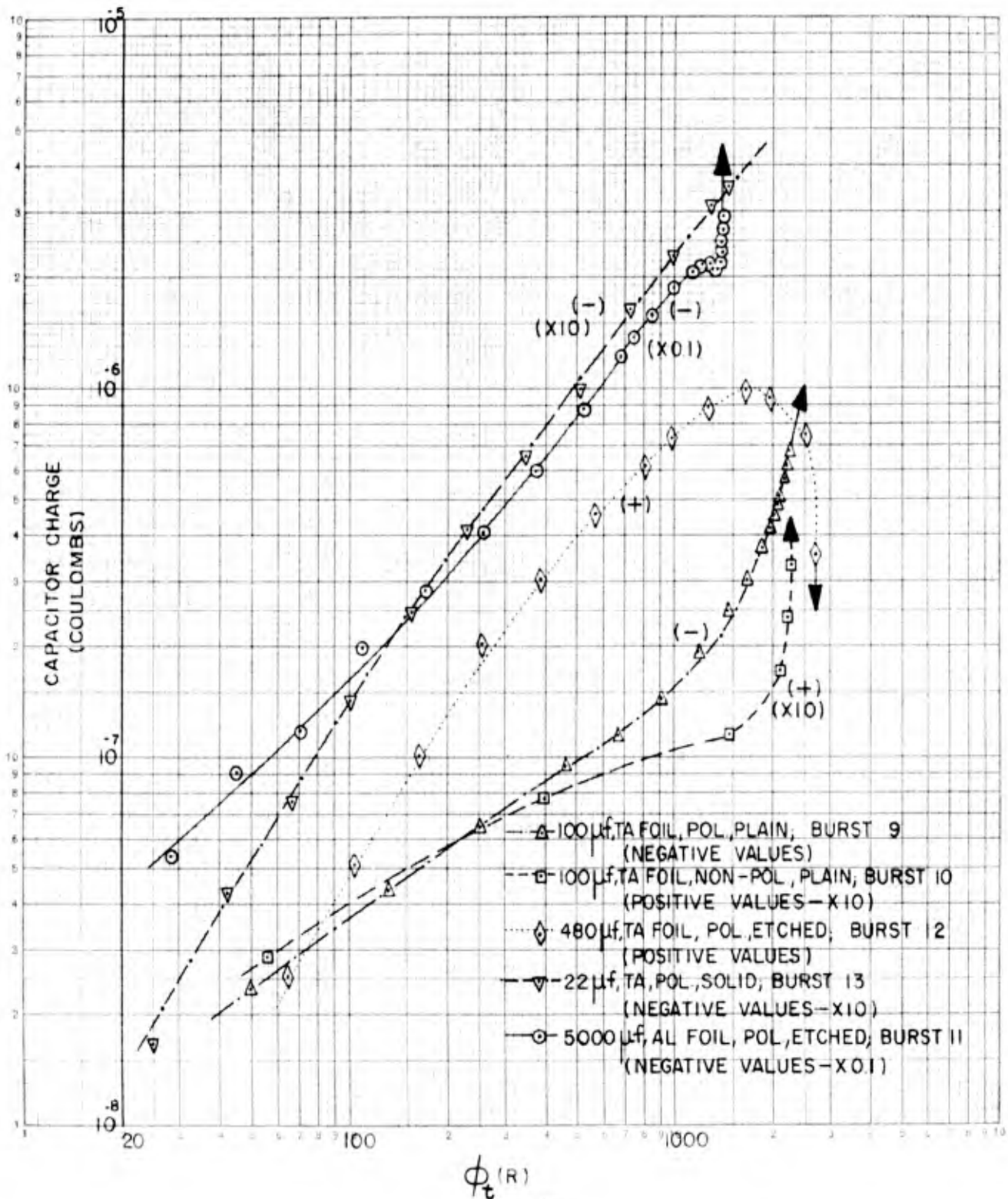


FIGURE 25
RATE DEPENDENCE OF GENERATED CABLE CURRENT

K₀E LOGARITMIC 359-120
 KRUPPEL & EBERHOLD MAPPE 1.1
 1/3 COPIES



EMF TESTS - CAPACITOR CHARGE VS GAMMA DOSE
 (TO 300 μ S)

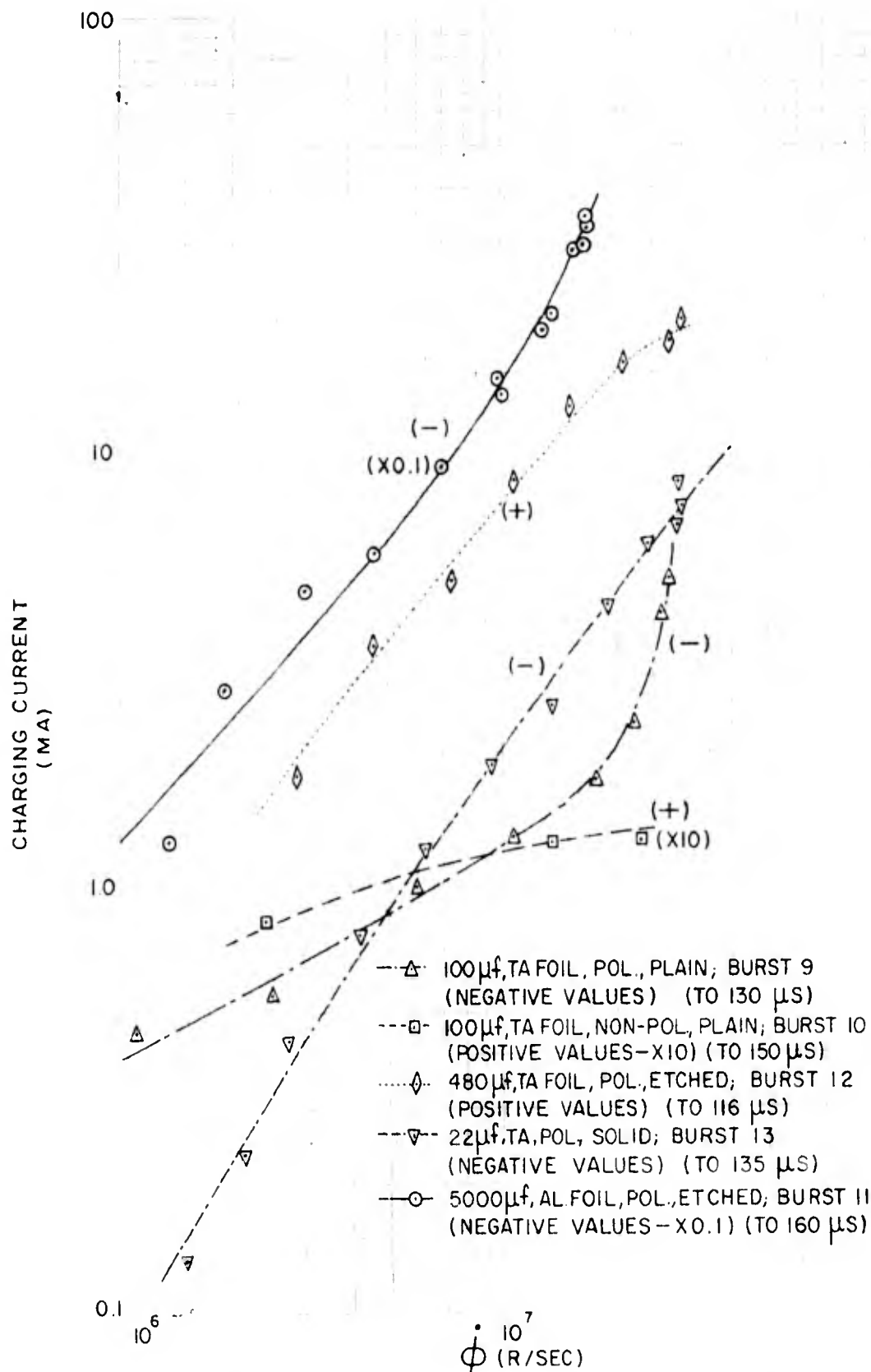
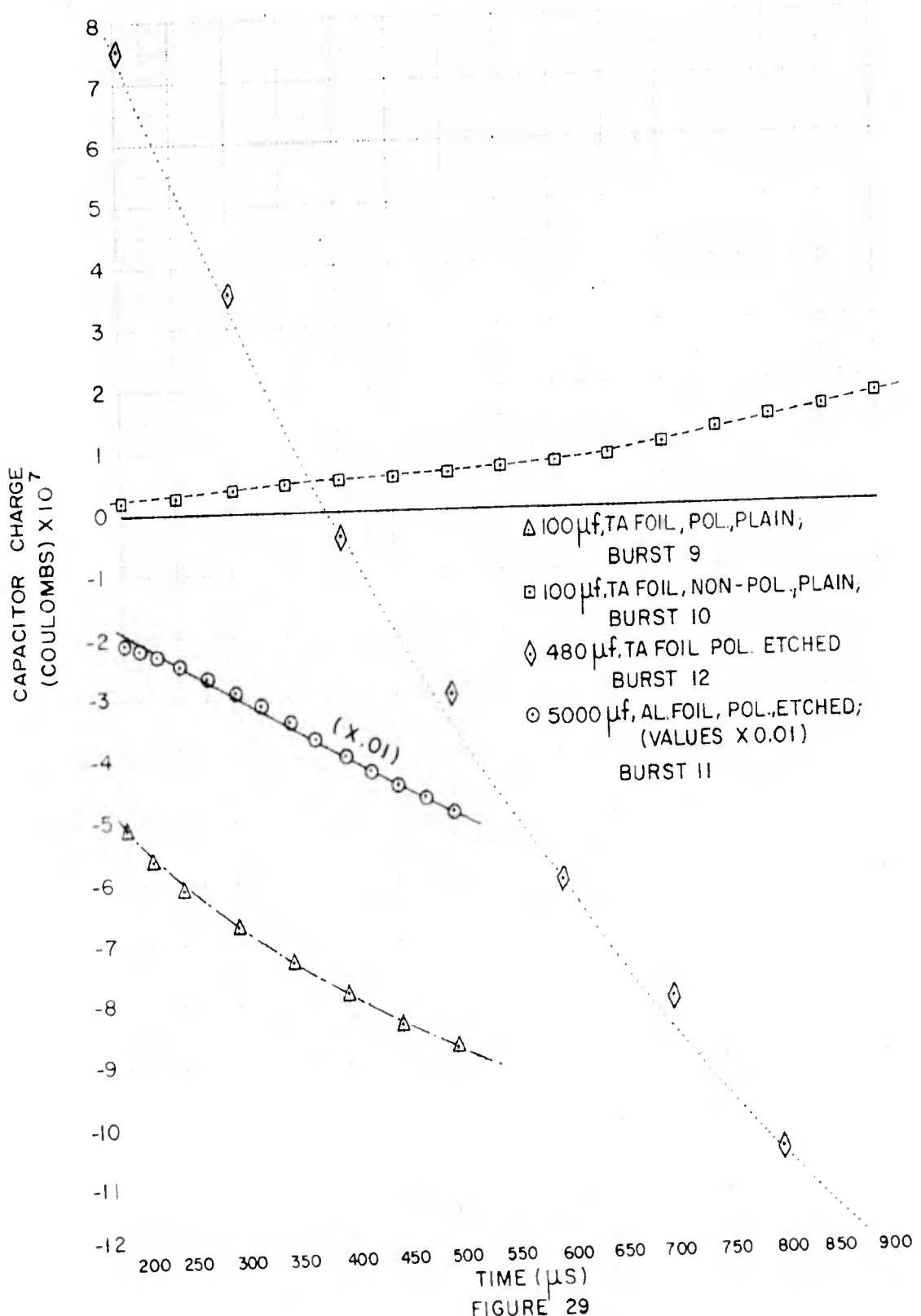


FIGURE 28
EMF TESTS-CHARGING CURRENT VS GAMMA RATE



EMF TESTS — TIME RESPONSE AFTER 200 μ S

the polarized capacitor increases with capacitance value (i.e. effective area of electrodes and dielectric material). The polarized capacitors exhibit similar behavior during the rising portion of the radiation pulse except that the 480 μ f foil capacitor shows a positive charge rather than negative. The later portion of the signals shows similar behavior for all polarized capacitors. The accuracy of these data is questionable due to superimposed electrical noise of the same magnitudes as the signals.

Leakage Test Analysis and Results

Typical leakage test signals are shown in Figure 30. The data for the 3 μ f capacitor represents a case where the measuring circuit time constant permits re-charging of the capacitor during the recorded time interval; the 1900 μ f capacitor data represents a long time constant with no re-charging.

The following assumptions were made in analyzing the leakage data:

1. Capacitance value at 60 cps is representative throughout the radiation pulse.
2. Capacitance does not change during the radiation burst.
3. Generated cable and capacitor effects are negligible compared with leakage signals. No adjustment of data was attempted.

Capacitor leakage resistance values were computed for 20-40 times during the voltage pulse for each test. The relationship used is:

$$R = \frac{(9.3 \text{ volts} - v)}{v/51\Omega + C \frac{dv}{dt}}$$

where:

R = leakage resistance in ohms

v = capacitor voltage change (as shown in Figure 30) in volts

C = capacitance value at 60 cps in farads

$\frac{dv}{dt}$ = time rate of change of capacitor voltage (as shown in Figure 30) in volts/sec



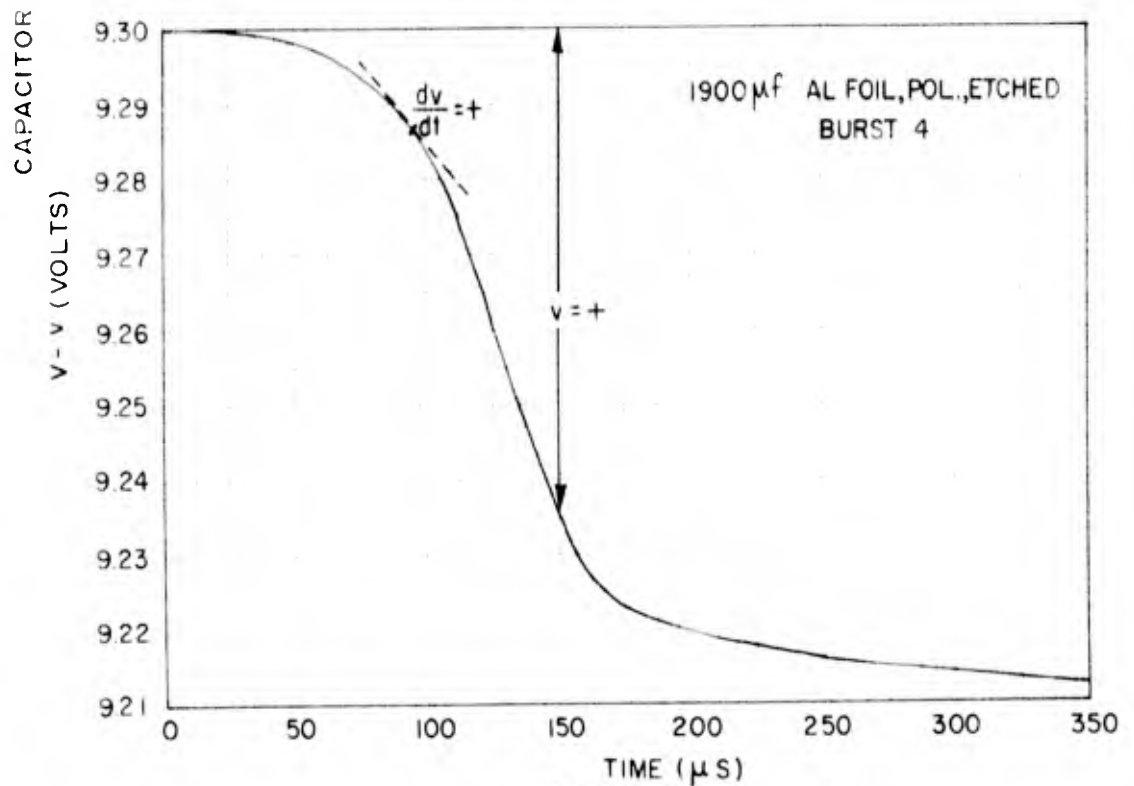
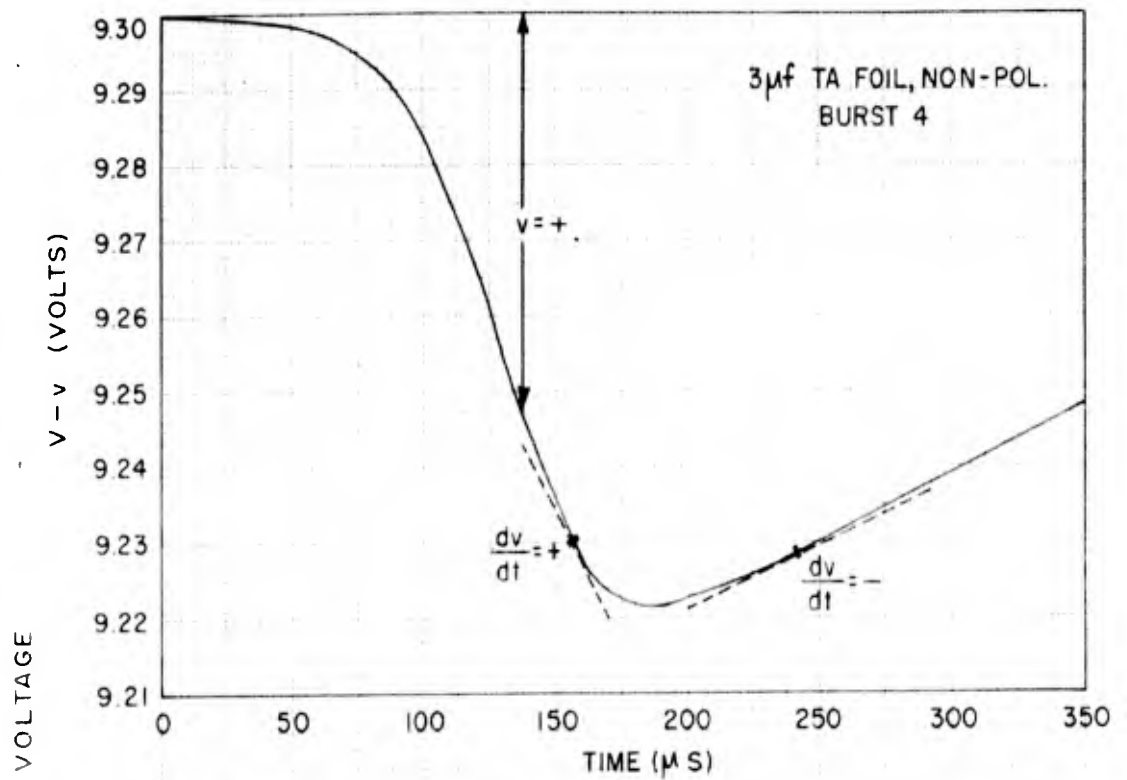


FIGURE 30
TYPICAL CAPACITOR LEAKAGE DATA

It is assumed that other measuring circuit resistances are small compared with the 51 ohms terminating resistance. This relationship accounts for both capacitor discharge and re-charging. Measured minimum values of leakage resistance (R_{\min}) and maximum values for ν are tabulated in Tables XI and XII. Values of the leakage resistance change factor R_{\min}/R_0 are also given. These values are representative but will vary with radiation pulse size and shape.

The resistance values were converted to electrical conductivity values for the dielectric materials with the relationship:

$$\sigma = \frac{k \epsilon_0}{R C}$$

where:

- σ = conductivity in (ohm-cm)⁻¹
- k = dielectric constant
- ϵ_0 = electrical permittivity of vacuum = 8.85×10^{-14} farad/cm

This equation is strictly true only for a parallel plate geometry; however it is thought to be a good approximation here since dielectric thicknesses are $\sim 10^{-5}$ cm so that deviations from parallelism of anode and cathode due to capacitor geometry are relatively small. Uniformity of dielectric film thickness is also a consideration in the validity of this approximation. The values of dielectric constant used in this analysis were 25 for tantalum oxide (Ta_2O_5) and 7.0 for aluminum oxide (Al_2O_3) (Ref. 14).

The conductivity values for aluminum oxide followed the radiation pulse shape. These values are displayed as a function of radiation rate in Figure 31. A best visual fit of the data yields the relationship $\sigma = K \dot{\phi}$, where $K = 2.95 \times 10^{-18} \frac{\text{sec}}{(\text{r}) (\Omega \text{-cm})}$ and $\dot{\phi}$ = gamma rate in r/sec. The radiation rate varies

TABLE XI

Leakage Test Results for Aluminum Foil Electrolytic Capacitors

Capacitor Value	Burst No.	Minimum Resistance (ohms)	R_{min}/R_o $\times 10^7$	Maximum Voltage Drop (%)
1900 μ f, 100V	4	3.64	9.1	~ 0.97
5000 μ f, 75V	1	2.2	2.6	~ 0.9
15,000 μ f, 50V	2	1.02	4.8	~ 0.8



TABLE XII

Leakage Test Results for Tantalum Electrolytic Capacitors

Capacitor Type	Burst No.	Minimum Resistance (ohms)	$\frac{R_{min}}{R_0} \times 10^7$	Max. Voltage Drop (%)	$K_a \frac{\text{sec}}{(\Omega\text{-cm})(r)} \times 10^{18}$	$K'_\beta \frac{1}{[(\Omega\text{-cm})(r)]^{1.4}} \times 10^{14}$
<u>Solid, Polarized</u>						
0.22 uf, 35V	11	1.48×10^4	≤ 4.2	~ 0.34	15.1	9.84
2.2 uf, 20V	12	$\sim 3.19 \times 10^3$	~ 1.0	~ 0.5	9.6	2.88
22 uf, 35V	3	134	16	~ 2	$\frac{11.9}{12.2 \text{ AV}}$	$\frac{8.94}{7.22 \text{ AV}}$
<u>Plain Foil, Polarized</u>						
40 uf, 50V	6	340	3.8	0.64	3.83	0.70
100 uf, 15V	4	46.6	≤ 0.47	~ 1.7	$\frac{10.8}{7.31 \text{ AV}}$	$\frac{1.21}{0.96 \text{ AV}}$
<u>Plain Foil, Non-Polarized</u>						
3 uf, 50V	4	2.04×10^3	6.8	0.84	8.0	3.38
10 uf, 10V	3	901	≤ 4.1	0.75	5.3	0.92
100 uf, 10V	3	73.7	≤ 3.2	1.1	$\frac{7.1}{6.8 \text{ AV}}$	$\frac{0.58}{1.62 \text{ AV}}$
<u>Etched Foil, Polarized</u>						
70 uf, 65V	2	210	≤ 0.90	~ 0.8	5.65	1.98
70 uf, 65V	6	199	0.36	~ 0.80	4.3	1.14
480 uf, 75V	1	15.8	4.5	~ 1.7	5.75	2.76
480 uf, 75V	13	9.5	2.7	~ 1.9	$\frac{9.7}{6.35 \text{ AV}}$	$\frac{3.39}{2.30 \text{ AV}}$
All Foil Types						



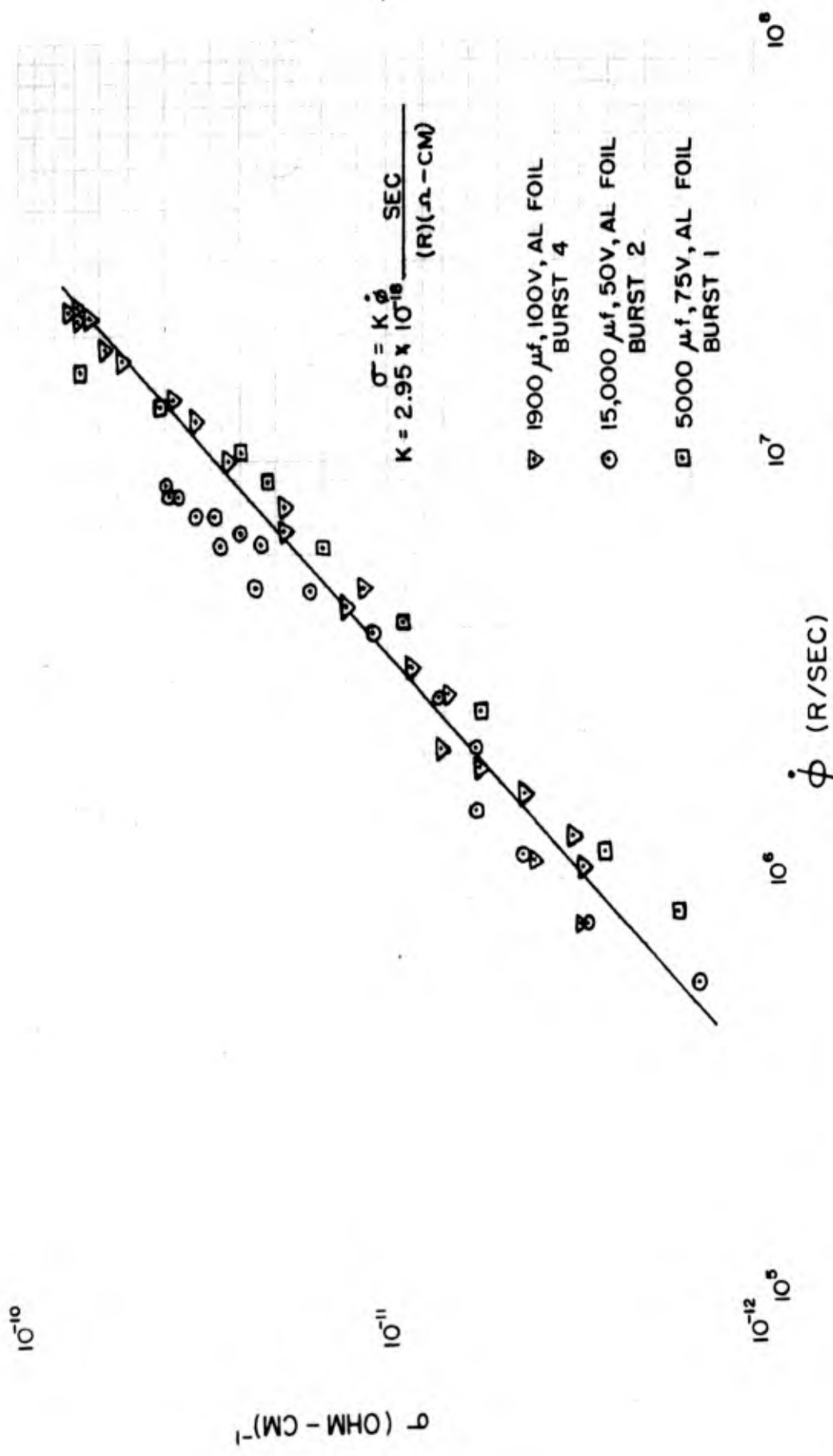


FIGURE 31
RATE DEPENDENCE OF CONDUCTIVITY FOR ALUMINUM OXIDE (AL₂O₃)

considerably throughout the large volume of the aluminum foil capacitors. Geometry and relative variation of radiation levels for the aluminum capacitors is given in Table XIII; dosimetry information is the average of several measurements taken at various positions outside the capacitors. The relative levels at the center of the capacitors are estimated from the $1/r^2$ relation (using the center of the fissionable material as $r = 0$) and absorption factors through the thickest portion of the capacitors as determined from dosimetry measurements (i.e., an absorption coefficient of $-0.12/\text{inch}$ for gammas and $-0.26/\text{inch}$ for neutrons). The true average gamma rate for the aluminum capacitors is a complex function of three-dimensional geometry and three dimensional variation of radiation field around Godiva III. Estimated factors for determining average gamma rate (Table XIII) are based on the relative distribution of radiation levels which are given. The gamma rates used for the three aluminum foil capacitor tests should be accurate within a factor of two.

A comparison of conductivity time variation with gamma rate time variation for tantalum oxide is shown in Figure 32. This comparison suggests a separation of conductivity variation into two parts, each containing a generation and decay term, so that:

$$\delta = (K'_\alpha \dot{\phi} + \alpha \sigma_\alpha) + (K'_\beta \dot{\phi} + \beta \sigma_\beta)$$

where:

δ = time rate of change of conductivity at time t

$\dot{\phi}$ = gamma radiation rate at time t

K'_α, K'_β = constants describing generation of conductivity by gamma dose; $K'_\alpha > K'_\beta$

α, β = constants for exponential decay of conductivity; $\alpha > \beta$

$\sigma_\alpha, \sigma_\beta$ = components of conductivity at time t such that $\sigma_\alpha + \sigma_\beta = \sigma$

TABLE XIII

Geometry and Relative Dosimetry Distribution for Aluminum Foil Capacitors

Capacitor:	5000 μ f, 75V		15,000 μ f, 50V		1900 μ f, 100V	
Diameter:	3"		3"		2"	
Height:	4"		6"		4"	
Distance from Center to Godiva Screen:	1 3/4"		1 3/4"		1 1/4"	
Average Relative Magnitude of Radiation Dose or Rate at Following Location:	<u>nt</u>	<u>Y</u>	<u>nt</u>	<u>Y</u>	<u>nt</u>	<u>Y</u>
Center Front	1.00	1.00	1.00	1.00	1.00	1.00
Center Rear	.138- .181	.206- .271	.138- .181	.206- .271	.226- .306	?-.40
Center Side	~.60	\leq .65	~.60	\leq .65	~.643	\leq .686
Center Top or Bottom	\geq .299	\leq .439	\geq .294	\leq .258	\geq .374	\leq .480
Center(Inside)	.405	.494	.405	.494	.621	.71
Estimated Average Relative Dose or Rate for Capacitor:	0.4	0.5	0.4	0.5	0.6	0.7
Multiply Dosimetry Readings at 5/8" from Screen by:	.364	.455	.364	.455	.545	.636



3 μ f, TA FOIL, NON-POL., PLAIN
BURST 4

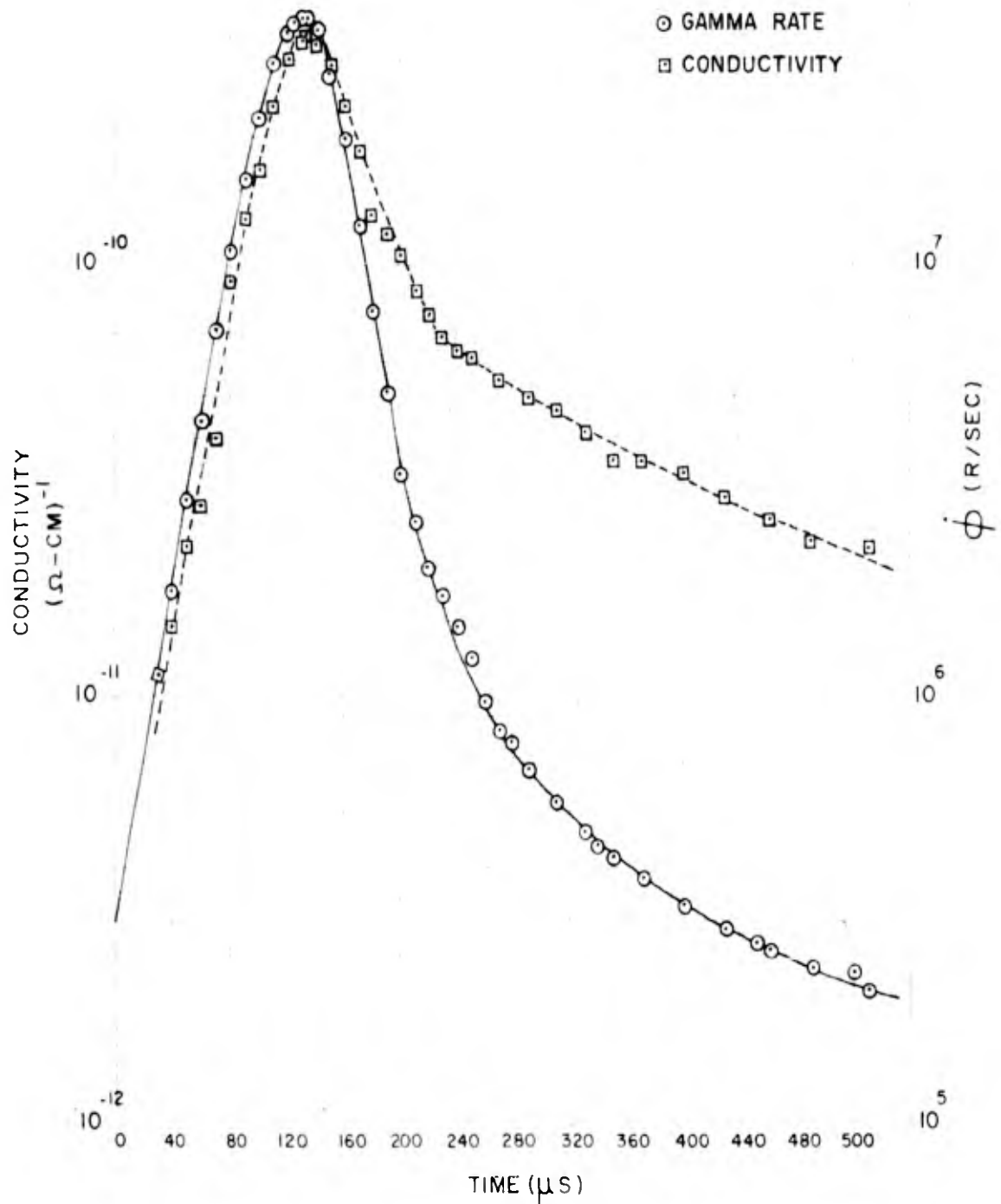


FIGURE 32
 COMPARISON OF CONDUCTIVITY AND GAMMA RATE PULSES
 FOR TANTALUM OXIDE

It was assumed that only the latter portion of the equation contributed to the conductivity after 300 μ s (the first part having decayed to a negligible contribution by that time). Three equations of the form $\dot{\sigma} = K'_\beta \dot{\phi} + \beta \sigma$ were solved simultaneously with values of δ , $\dot{\phi}$ and σ taken from the 300-500 μ s portion of the three most accurate pieces of data [(i.e., the curves for the 3 μ f non-pol. plain foil capacitor (burst 4), the 100 μ f pol. plain foil capacitor (burst 4), and the 480 μ f pol. etched foil capacitor (burst 13))]. It was assumed that $\sigma = \sigma_\beta$ in this time interval. This analysis yielded values of $-3.86 \times 10^3 \text{ sec}^{-1}$, $-4.55 \times 10^3 \text{ sec}^{-1}$, and $-5.30 \times 10^3 \text{ sec}^{-1}$ for β and values of 3.44×10^{-14} , 5.82×10^{-14} , and $1.32 \times 10^{-13} \left[(\Omega - \text{cm})(r) \right]^{-1}$ for K'_β . The average value $\beta = -4.57 \times 10^3 \text{ sec}^{-1}$ (corresponding to a half-life of 151 μ s for the decay) agrees well with four values of half-life between 170 and 200 μ s which were taken directly from extrapolations of the 300-500 μ s portions of conductivity versus time semilog graphs for some of the more accurate data. These direct readings should give a half-life which is higher than the actual, since part of the decay is balanced by the generation term. This method of determining β requires that the value is the same for tantalum oxide in all types of tantalum capacitors.

The β portion of conductivity was obtained by iteration and integration according to the equation:

$$\sigma_\beta = K'_\beta \phi_t + \int_0^t \beta \sigma_\beta dt$$

$$\phi_t = \text{integrated gamma dose (data taken for burst 4) at time } t$$

where:

$$t = \text{time from beginning of dosimetry signal.}$$

$$\beta = -4.57 \times 10^3 \text{ sec}^{-1}$$

The σ_β versus t shape was assumed constant for all bursts and amplitude was

adjusted proportional to $\dot{\phi}_t$ at peak σ_β (180 μ s) for each burst. Then the value of K'_β was adjusted so that the 300-500 μ s portion of the σ_β curve matched the same portion of the total conductivity curve for each tantalum capacitor.

Values of K'_β are given in Table XII.

The values for $\sigma_\alpha = \sigma - \sigma_\beta$ were obtained for each tantalum capacitor using the values of K'_β from above. Graphs of σ_α versus $\dot{\phi}$ from 0 to 220 μ s yielded the relationship $\sigma_\alpha = K'_\alpha \dot{\phi}$, where K'_α is a rate-dependence generation constant. The values obtained for K'_α are given in Table XII.

The relationship describing the conductivity of tantalum oxide when subjected to a pulse of gamma radiation is:

$$\sigma = K'_\alpha \dot{\phi} + K'_\beta \dot{\phi}_t + \int_0^t \beta \sigma_\beta dt$$

where:

$$K'_\alpha = 6.71 \times 10^{-18} \frac{\text{sec}}{(\Omega\text{-cm})(r)} \quad \text{for foil capacitors}$$

$$K'_\alpha = 12.2 \times 10^{-18} \frac{\text{sec}}{(\Omega\text{-cm})(r)} \quad \text{for solid electrolyte capacitors}$$

$$K'_\beta = 1.78 \times 10^{-14} [(\Omega\text{-cm})(r)]^{-1} \quad \text{for foil capacitors}$$

$$K'_\beta = 7.22 \times 10^{-14} [(\Omega\text{-cm})(r)]^{-1} \quad \text{for solid electrolyte capacitors}$$

Figures 33 and 34 show values of σ_α , σ_β and $\sigma_\alpha + \sigma_\beta$ along with experimental values of σ for the 3 μ f non-polarized plain foil capacitor as a function of gamma rate for the first part of the burst and as a function of time during the latter part of the burst.

3 μ f, TA FOIL, NON-POL., PLAIN
BURST 4

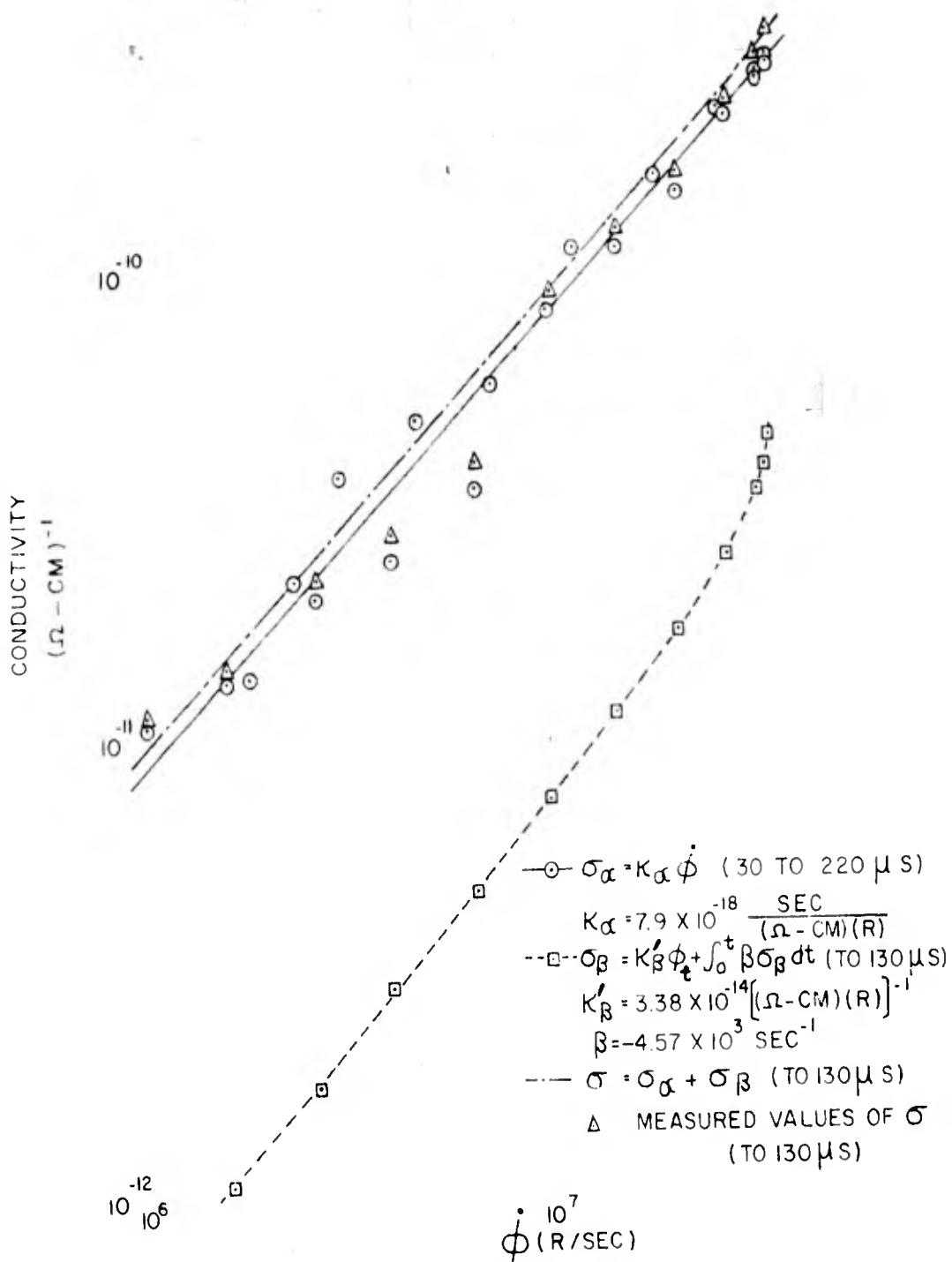


FIGURE 33
BREAKDOWN OF CONDUCTIVITY FOR TANTALUM OXIDE
(0-130 μ S)

3 μf, TA FOIL, NON-POL., PLAIN
BURST 4

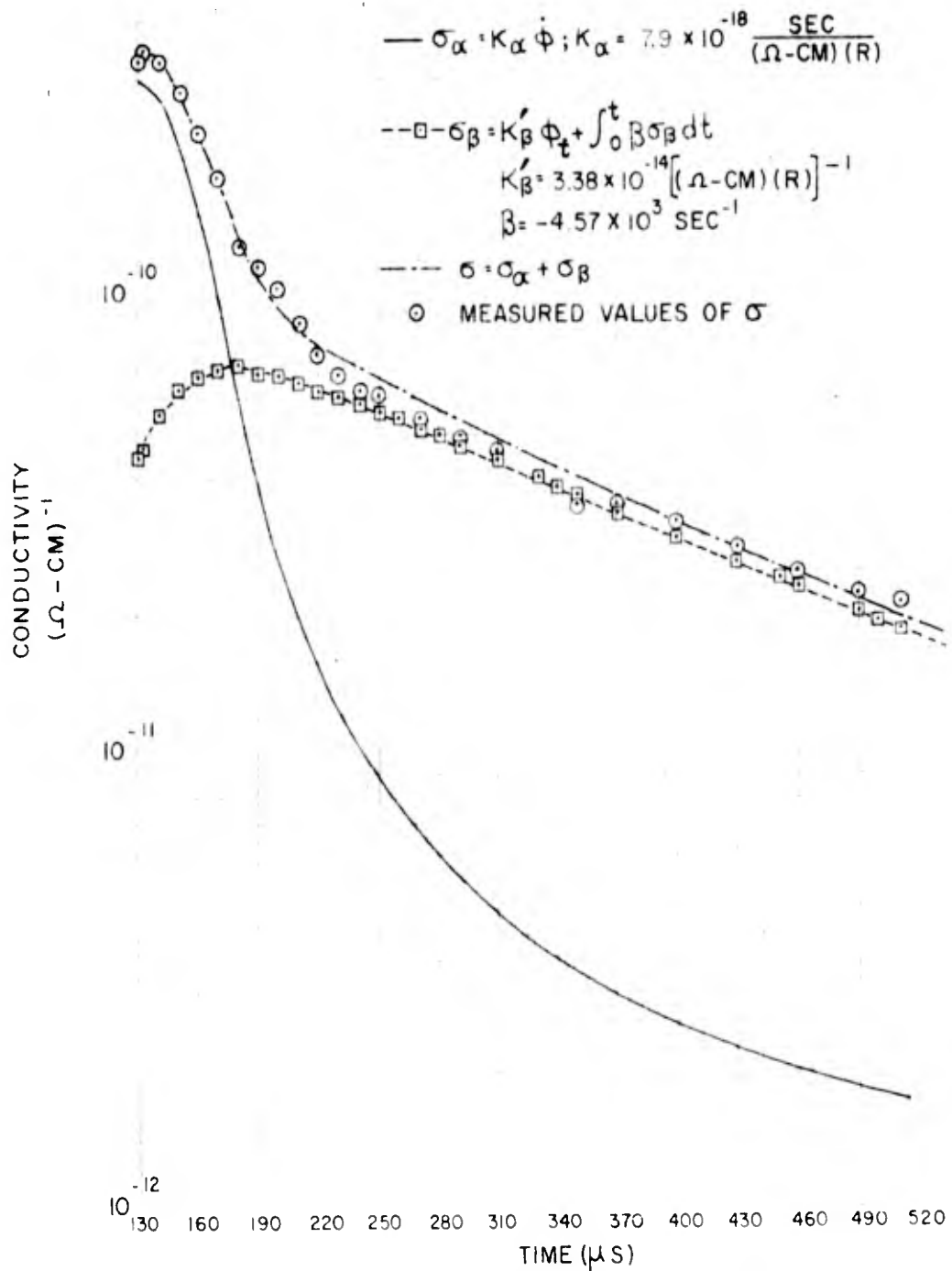


FIGURE 34
BREAKDOWN OF CONDUCTIVITY FOR TANTALUM OXIDE
(130-510 μs)

Permanent Effects Measurements

The measurements of capacitance, leakage resistance and dissipation factor for all capacitors before and after burst indicate no permanent changes in leakage resistance or capacitance within measurement accuracy. Quoted values of initial leakage resistance (R_0) (Table IX) represent minimum values in all cases due to the nature of the measurement technique. Permanent increases of 7 to 27 percent in dissipation factor were noted for the aluminum foil capacitors. Dissipation factor decreases up to 21 percent for 22 μ f tantalum solid, increases up to 12 percent for non-polarized 100 μ f tantalum foil and increases up to 60 percent for polarized 100 μ f tantalum foil capacitors were noted. Other dissipation factor changes varied from +12 percent to -38 percent with no significant trends indicated.

DISCUSSION OF RESULTS

Capacitor Leakage Tests

The gamma-induced conductivity changes in aluminum and tantalum oxide result from excess current carriers which can drift in the presence of an electric field and cause increased conduction. These excess carriers (electrons) are excited from the valence band to the conduction band of the material by the indirect ionizing action of gamma radiation, primarily through the production of Compton-scattered electrons. Recent data (i.e. Ref. 6, 15 and 16) have shown that conductivity for most insulating materials follows the rule:

$$\sigma = K \dot{\phi} \Delta \quad (1)$$

where:

σ = conductivity

K = generation constant

$\dot{\phi}$ = gamma rate

Δ = 0.5 to 1.0



This rate effect (i.e. wholly dependent on radiation rate) indicates that the recombination time of the gamma-induced carriers is very short ((recombination times are probably 10^{-10} sec for typical insulators (Ref. 16)). The recombination of excited electrons from the conduction band to the valence band of the insulating material is occurring at such a high rate that only the immediate production rate of carriers affects the conductivity. This is equivalent to stating that the decay constant for gamma-induced conductivity is very large.

Aluminum oxide conductivity and the large portion (σ_α) of tantalum oxide conductivity both behave according to equation (1) with $\Delta = 1.0$ (i.e. a direct proportion between σ and $\dot{\phi}$). However, the small portion (σ_β) of the tantalum oxide conductivity depends on both radiation rate and dose; the decay time of charge carriers is comparable to the time duration of the Godiva III burst, and the conductivity, σ_β , at a given time depends strongly on the generation and decay which have occurred before. If the excitation pulse of radiation were very short (i.e. $\sim 1 \mu\text{s}$), then the conductivity σ_β would rise to the value $\sigma_{\beta 0} = K'_\beta \dot{\phi}$ at the end of the excitation (ϕ = total integrated gamma dose), and the subsequent decay of conductivity would follow the equation $\sigma_\beta = \sigma_{\beta 0} e^{-\beta t}$ independent of any generation term. Decay would be negligible during the excitation time; this would be a pure dose effect. In the case of a very short radiation pulse, the behavior of σ_α would depend on the carrier lifetime which would no longer be short compared with the excitation pulse duration. In this case, σ_α would obey an equation similar to that quoted for σ_β , i.e. $\sigma_\alpha = K'_\alpha \dot{\phi}_t + \int_0^t \alpha \sigma_\alpha dt$, where K'_α is a dose-dependence generation constant. In the case of a very long excitation pulse (i.e. $\gg 150 \mu\text{s}$ duration), both σ_α and σ_β

would be rate effects (i.e. $\sigma = K_{\alpha} \dot{\phi} + K_{\beta} \dot{\phi}$, where K_{β} is a rate-dependence generation constant).

The gamma-induced conductivity of tantalum oxide apparently is caused by the excitation of electrons from the valance band to the conduction band and a subsequent trapping of some of the excited electrons at a trapping level in the energy gap between the valence and conduction bands. The holes left by the trapped electrons are free to contribute to the conductivity until either the electrons are reionized and recombine or the holes are trapped. The large portion (σ_{α}) of the conductivity can be associated with the excited carriers which recombine directly from the conduction band to the valence band with a very short recombination time; K_{α} is a measure of the efficiency for this process. The small portion (σ_{β}) of the conductivity can be associated with the excess holes which remain after trapping of electrons. The recombination time of the trapped electrons or the trapping time of the holes determines the decay constant (β) for this portion of the conductivity. K_{β} is a measure of the efficiency for the electron trapping process. Additional discussion of electron excitation mechanisms in insulators is presented in Reference 16. Further analysis of the data and the application of conductivity theory for insulators would yield more information concerning excitation processes, number of carriers excited and energy levels in tantalum and aluminum oxide.

The apparent difference between excitation efficiencies for the tantalum oxide in the case of solid electrolyte and foil type capacitors, aside from general measurement and analysis uncertainties, could be associated with:

1. Capacitor geometry effect in calculation of σ .
2. Variation in frequency response of capacitance for the two capacitor types.

3. Variation in physical properties of the tantalum oxide due to differences in capacitor geometry, oxide forming process and electrolyte (i.e. solid versus liquid).

Some considerations in assessing the overall accuracy of the conductivity results are:

1. Measurement accuracy at low radiation rates where observed signals were small and partially obscured by electrical noise. These uncertainties appear for the lowest conductivity portions of data (i.e. at the beginning and end of the measured time interval).
2. Possible distortion of pulse shapes and attenuation due to the transmission lines.
3. Approximately ± 10 percent absolute accuracy of gamma dosimetry.
4. Variations in applied electric field in the capacitor dielectrics due to variations in thickness of the dielectric layer (i.e. for different capacitor rated voltages). No significant trends are noted in the results when capacitor voltage ratings are considered.
5. Certain assumptions made in the fitting of the conductivity curves to the proposed equation, such as the use of a constant pulse shape for σ_p .
6. The use of 60 cps capacitance in the analysis.

There are no significant trends noted in the values of K_u and K'_p due to variation in capacity value for similar capacitor types.

Several considerations must be made in applying the conductivity results to practical problems:

1. Results may vary with applied DC voltage.
2. Results may vary with applied AC frequency.
3. The decay constant α for tantalum oxide will cause pulse shape changes if very short radiation pulses are considered. There will be a similar effect for aluminum oxide.
4. Results may vary considerably with gross changes in radiation energy spectrum.
5. There may be variations due to radiation pulse shape which are not predicted by the conductivity equations. These could arise from frequency response characteristics of the dielectric materials.

Practical use of conductivity results can be made by using the following procedure:

1. Compute conductivity values using gamma rate and dose information for the radiation pulse to be considered. Use $\sigma = K \phi$ for aluminum oxide and

$$\sigma = K_{\alpha} \dot{\phi} + K_{\beta} \phi_t + \int_0^t \beta \sigma_{\beta} dt \text{ for tantalum oxide. The}$$

approximation $\sigma = K_{\alpha} \dot{\phi}$ for tantalum oxide is valid within reasonable accuracy to the peak of the radiation burst.

2. Convert conductivity values into leakage resistance by using the relation

$$R = \frac{k\epsilon_0}{\sigma C}, \text{ using } 60 \text{ cps value for capacitance.}$$

3. Apply this dynamic variation of leakage resistance as a variable shunt resistor to the capacitor in the circuit of interest.

Additional studies of the transient effects caused by gamma radiation in tantalum oxide might include the use of very short radiation pulses (such as linear accelerator or flash X-ray) to verify carrier recombination times, variation of gamma energy spectrum, and variation of applied electric fields.

Cable Tests

The reported cable generation effects due to gamma radiation are similar to those observed by other investigators (Ref. 17 and 18). Current amplitudes and the affect of applied voltage are consistent with work performed by Hughes Aircraft Company on RG-59/U cables. The generated currents have been ascribed to a net scattering of electrons (due to Compton scattering and photoelectric effect) out of the dielectric material. The shield of the cable, by virtue of its large area, acquires more negative charge than the center conductor; hence, a positive potential appears between the center conductor and shield of the cable when there is no applied voltage.



The reduction of generated current by applying a positive voltage could be caused by a leakage current through the cable dielectric which would reduce the observed current. However, this would require a cable leakage resistance of 6.2×10^5 ohms at 10^7 r/sec in order to explain the effect noted in Figure 25. This would indicate that the initial cable leakage resistance is 10^{12} to 10^{13} ohms and that the initial resistivity of polyethylene is $\sim 10^{18}$ ohm-cm. This resistivity is low for polyethylene, and it is suggested that a different effect must be responsible for the observed reduction of generated current.

The reduction in generated current caused by applied cable voltage is probably due to the retarding potential which the applied voltage affords. This retarding potential would reduce the number of scattered electrons which reach the cable shield and increase the number which reach the center conductor. Studies have been made which indicate that this explanation is valid (Ref. 16).

The results in Figure 25 indicate some saturation of the generated current at gamma rates near 10^7 r/sec and above. This effect seems to be enhanced by the applied voltage. It is believed that the current generation is nearly linear with rate up to 10^6 r/sec, and that the saturation effect may be analogous to a space charge effect at the higher rates due to the increasing number of electrons present. The enhancement of the saturation effect by applied voltage is consistent with this belief.

The cable test results are somewhat inaccurate due to the electrical noise pickup at high oscilloscope gain and the small magnitude of signals at the low-rate portions of the radiation burst. The geometrical arrangement of the cable around Godiva III was not constant, and this could cause a large



variation in generated current as noted in Figure 25. The cable extended approximately radially outward from Godiva III, with the dummy terminals at the end nearest the critical assembly.

Cable generation effects could be described quantitatively in a parametric fashion by considering the charge generation per unit of differential surface area between shield and center conductor as a function of gamma rate, cable dielectric and applied electric field. Such a description would result in a factor $Q_{\dot{\phi}} = \frac{\text{coulombs}}{(r) (\text{cm}^2)}$. The charge generation rate \dot{Q} at a given radiation rate $\dot{\phi}$ could be predicted for a known cable geometry, applied voltage and dielectric material by a relation of the form $\dot{Q} = Q_{\dot{\phi}} \Delta A$ where ΔA is the differential area between cable shield and center conductor per unit length of cable. Considerations of cable length and an equivalent cable capacitance would then permit calculation of cable voltages developed due to gamma radiation. Additional analysis would be required to account for charge accumulation and decay. Basic controlled measurements should be made to determine generation constants such as $Q_{\dot{\phi}}$; the results should then be verified by irradiating various types of cables.

Capacitor EMF Tests

The capacitor EMF generation tests show that the capacitor charging current is nearly proportional to gamma rate (Fig. 28) and that the capacitor charge is nearly proportional to integrated gamma dose (Fig. 27) for the polarized capacitors at times up to the peak gamma rate. The long-time signals (Fig. 29) resemble an exponential approach to some final capacitor charge for the polarized capacitors. These effects are generally greater for the larger capacitor values (i.e. larger area of capacitor electrodes).



The observed results in the foil capacitors can be explained by secondary electron processes. The aluminum or tantalum oxide layer ($\sim 10^{-5}$ cm thick) is sandwiched between metallic foil and a liquid electrolyte. The metallic foil forms the anode and is very thin (~ 0.5 mil). The electrolyte forms the cathode and is thicker ($\sim 1-3$ mils) since paper spacers are placed between the oxide layer and a metallic foil which serves as the electrical contact to the electrolyte; the paper spacers are saturated by the electrolyte. Gamma radiation produces a net scattering of secondary electrons (due to Compton and photoelectric processes) from the oxide layer into the metallic foil and the electrolyte. The secondary electrons are distributed throughout the foil and a layer of electrolyte near the oxide layer. This produces an effective charge (and potential) between the anode (foil) and cathode (electrolyte). The effective charge generation rate remains nearly constant while the gamma radiation rate is increasing. As the gamma radiation rate decreases, the production of electrons becomes unimportant, and the electrons which were deposited in the electrolyte diffuse away from the oxide layer. This has the effect of causing the anode to appear more negative (i.e. larger effective capacitor charge), since the cathode charge is becoming distributed throughout the electrolyte. In addition, the added electrons in the liquid electrolyte may cause the number of dissociated electron-ion pairs in the electrolyte to decrease, thus changing the equilibrium state of the electrolyte and reducing the number of charge carriers to a value nearer the initial state. This will also cause the anode to appear more negative with respect to cathode. Similar processes would occur in the solid electrolyte tantalum capacitors.

The generation of an effective charge between anode and cathode causes the increasing or decreasing voltage which is observed up to the radiation peak,

and the diffusion of electrons and the change in disassociation level of the electrolyte cause the slow, exponential decrease of voltage which is observed after the radiation peak. The effective charge during the initial part of the radiation pulse is negative for the tantalum plain foil, tantalum solid electrolytic and aluminum etched foil capacitors; this would indicate that the electrons scattered into the electrolyte are distributed farther from the oxide layer than in the metallic foil. The non-polarized tantalum foil capacitor exhibits little effect, since it consists essentially of two polarized capacitors connected "back-to-back" and the effects cancel. The tantalum etched foil capacitor exhibits an effective positive charge during the initial part of the radiation pulse; it is possible that the unevenness of the etched foil tends to reduce penetration and diffusion rate of scattered electrons in the electrolyte. The fact that the effective charge is negative for the aluminum etched foil capacitor is not necessarily contradictory, since there is a different electrolyte and dielectric involved. The observed effects after the peak of the radiation pulse are similar for all polarized, liquid-electrolyte capacitors and are consistent with the mechanisms described above. The small, long-time effect in the tantalum non-polarized capacitor could be due to small differences in the effective behavior of the electrons in the electrolyte for the two opposing parts of the capacitor.

Basic studies are needed to verify these observed generation effects, to establish the mechanisms which cause the effects and to determine a quantitative description which would allow prediction of the effect for various radiation pulse shapes and energy spectra. It is possible that generation constants and equations of the type proposed to describe cable effects could be used in

the case of the capacitor generation effects. The capacitor generation effects may vary considerably with capacitor geometry, applied voltage, type of electrolyte, and orientation in the radiation field.

CONCLUSIONS

The following results describe the effects of a gamma radiation pulse on tantalum and aluminum electrolytic capacitors which are used in electronic systems:

1. Leakage resistance change factors (R_{\min}/R_0) of 0.36×10^{-7} to 16×10^{-7} for tantalum electrolytic capacitors and 2.6×10^{-7} to 9.1×10^{-7} for aluminum foil electrolytic capacitors were observed for Godiva III radiation bursts with peak gamma rates of 1.9×10^7 to 4.5×10^7 r/sec. Maximum voltage change across the capacitors during these bursts was -0.54 percent to -2 percent for tantalum electrolytic capacitors and -0.8 percent to -0.97 percent for aluminum electrolytic capacitors. The applied capacitor voltage was 9.5 volts DC.
2. Leakage resistance R (ohms) for tantalum and aluminum electrolytic capacitors with 60 cps capacitance C (farads) at gamma rate $\dot{\phi}$ (r/sec) for Godiva-type radiation bursts can be computed with the relationship:

$$R = \frac{G}{\dot{\phi} C}$$

where:

$$\begin{aligned} G &= 2.1 \times 10^5 \text{ for aluminum foil capacitors} \\ &= 3.29 \times 10^5 \text{ for tantalum foil capacitors} \\ &= 1.81 \times 10^5 \text{ for tantalum solid electrolyte} \\ &\quad \text{capacitors.} \end{aligned}$$

The relationship is an approximation for tantalum capacitors and does not apply after the peak of the radiation burst.

3. The capacitance of tantalum capacitors does not vary within ± 1 percent for gamma rates up to 4×10^7 r/sec.
4. Uncharged, polarized tantalum and aluminum electrolytic capacitors exhibit generated positive or negative voltages with approximately linear dependence on dose during the rising portion of a gamma radiation pulse. The amplitudes vary up to ± 10 mv at 1000 r integrated gamma dose for the capacitors tested. The generated voltages all approach a negative value after the peak of the radiation pulse. The amplitudes observed at 500 μ s for the capacitors tested range from -0.7 mv to -8.8 mv. A non-polarized tantalum capacitor exhibited a long-time effect up to 1.8 mv at 900 μ s.
5. No catastrophic effects were observed on tantalum and aluminum electrolytic capacitors due to gamma radiation.

A description of the effects of a gamma radiation burst on conductivity of aluminum oxide and tantalum oxide dielectric materials was obtained as follows:

1. The effect of gamma radiation on the conductivity of aluminum oxide is a rate effect described by:

$$\sigma = K \dot{\phi}$$

where:

σ = conductivity in $(\text{ohm-cm})^{-1}$ at time t

$\dot{\phi}$ = gamma rate in r/sec at time t

K = rate-dependence generation constant = 2.95×10^{18}

$$\frac{\text{SEC}}{(\text{r}) (\Omega - \text{cm})}$$

2. The effect of gamma radiation on the conductivity of tantalum oxide is a combined rate and dose effect for radiation bursts with time duration similar to Godiva III and is described by:

$$\sigma = K_{\alpha} \dot{\phi} + K'_{\beta} \phi_t + \int_0^t \beta \sigma_{\beta} dt$$

where:

σ = conductivity in $(\Omega\text{-cm})^{-1}$ at time t

$\dot{\phi}$ = gamma rate in r/sec at time t

ϕ_t = integrated gamma dose in roentgen at time t

β = exponential decay constant = $-4.57 \times 10^3 \text{ sec}^{-1}$

σ_{β} = component of conductivity associated with decay constant β ; $\sigma_{\beta} = K'_{\beta} \phi_t + \int_0^t \beta \sigma_{\beta} dt$ at time t .

K_{α} = rate-dependence generation constant for short-life portion of conductivity = $6.71 \times 10^{-18} \frac{\text{sec}}{(\Omega\text{-cm})(r)}$ for foil capacitors and $12.2 \times 10^{-18} \frac{\text{sec}}{(\Omega\text{-cm})(r)}$ for solid electrolyte capacitors.

K'_{β} = dose-dependence generation constant for portion of conductivity with decay constant β ;

$K_{\beta} = 1.78 \times 10^{-14} [(\Omega\text{-cm})(r)]^{-1}$ for foil capacitors and $7.22 \times 10^{-14} [(\Omega\text{-cm})(r)]^{-1}$ for solid electrolyte capacitors.

RECOMMENDATIONS:

The test results presented in this report are sufficient for determining the effects of a gamma radiation pulse on tantalum and aluminum electrolytic capacitors in electronic circuits. It is expected that the effects of a gamma pulse on tantalum and aluminum electrolytic capacitors in the Minuteman ground equipment will not be serious for the following reasons:

1. No catastrophic effects occur
2. The expected effects are small compared with capacitor and circuit tolerances.

ACKNOWLEDGMENTS

The following personnel of the Radiation Effects Unit, Applied Physics Section, Aero-Space Division of the Boeing Airplane Company participated in both the preparation and performance of the tests.

Harold B. Almond - Test Coordinator

Henry J. Lubatti and Glenn G. Stevens - SCR and Circuit Tests

Howard W. Wicklein and William R. Chandler - Capacitor Tests

Robin K. Durkee and Richard L. Lander performed the necessary post-test analysis of test dosimetry. Various other personnel of the Applied Physics Section also contributed to these tests.

Many test parts, pre- and post-test measurement and invaluable recommendations were provided by the personnel of the Reliability Unit, Operational Electronic Design Section, Aero-Space Division of the Boeing Airplane Company.

We wish to express our thanks to Mr. R. A. Pederson and other members of the N-2 Division at Los Alamos Scientific Laboratory for their assistance and cooperation during these tests. We appreciate the efforts of Mr. L. J. Zipprich of the Sandia Corporation who coordinated the visit to Los Alamos and also the Sandia Corporation personnel who operated the Godiva III facility during the tests.

In particular we extend our thanks to Mr. G. E. Boyd and the test team from International Business Machines Corp. who provided us with Godiva III pulse shape dosimetry and oscilloscope triggering pulses. The splendid cooperation of the IBM personnel during the tests permitted optimum use of the facility in obtaining thirteen radiation bursts.



REFERENCES

1. Colp, J. L. and O'Brien, P. D., The Sandia Pulsed Reactor Facility (SPRF), Sandia Corporation Monograph, SCR-229, August, 1960.
2. Zipprich, L. J., Radiation Effects Testing at the Los Alamos Godiva II Facility, Sandia Corporation, SCR-76, April, 1959.
3. Cooper, A. E. et al., Pulsed Radiation Effects on Electronic Components, First Triannual Report, International Business Machines Corp., File No. 60-511-11, 20 July, 1960.
4. Foss, F. A. et al., Pulsed Radiation Effects on Electronic Components, Second Triannual Report, International Business Machines Corp., File No. 60-521-10, 31 Oct., 1960.
5. Durkee, R. K., Sulfur Foil Measurements from Los Alamos Test, 27-28 Oct., 1960, Boeing Memo 2-5471-333, Nov. 10, 1960.
6. Keister, G. L. et al., Transient Radiation Effects on Electronics, Part I, Kukla Transient Radiation Tests, Boeing Doc. D2-7899, Sept., 1960 (Preliminary Information).
7. Sayeg, J. A., Revised Neutron Flux Spectrum and Tissue Dose Measurements at the Godiva II Critical Assembly, Los Alamos Scientific Laboratory, LA-2432, April, 1960.
8. Harris, P. S. et al., Dose and Flux Measurements on Godiva Radiation Effects Experiments, Los Alamos Scientific Laboratory, LA-2355, Sept., 1959.
9. Personal communication, Nov., 1960.
10. Stephenson, R., Introduction to Nuclear Engineering, McGraw-Hill Co., 1954, p. 266.
11. Circuit Diagrams for Minuteman (BGS-4) Sequencer and Monitor, Boeing Document D2-6475, May, 1960.
12. BAC Standard Book 30 - Minuteman, Boeing Document D590-30.
13. Weiss, M. M., Fast-Neutron Bombardment of Four-Region Semiconductor Devices, Bell Telephone Laboratories, Inc., Nuclear Electronic Effects Program, First Triannual Technical Note, Appendix H, pp. 121-132, July, 1959.
14. Dummer, G. W. A., and Nordenberg, H. M., Fixed and Variable Capacitors, McGraw-Hill Book Company, Inc., p. 14 (1960).
15. Huth, G. C., Conductivity Induced in Solid Insulating Materials During Gamma Irradiation, General Electric Co. 58-331.
16. Van Lint, V. A. J., Transient Radiation Effects - Physics and Tests, General Atomic GA-1827, Nov., 1960.

17. Perkins, C. W. et al., Third Experiment on Pulsed Neutron Radiation Effects, Hughes Aircraft Co. T.M. No. 623, Oct., 1959.
18. Foss, F. A. et al., Final Report on Some Effects of Pulsed Neutron Radiation on Electronic Components, WADC-TR-60-71, IBM No. 60-911-5, January, 1960.

UNCLASSIFIED

UNCLASSIFIED